THE UNIVERSITY OF CHICAGO

TEMPORAL MECHANISMS OF POPULATION- AND COMMUNITY-LEVEL MICROBIAL ADAPTATION TO SHIFTING RESOURCE LANDSCAPES

A DISSERTATION SUBMITTED TO

THE FACULTY OF THE DIVISION OF THE BIOLOGICAL SCIENCES

AND THE PRITZKER SCHOOL OF MEDICINE

IN CANDIDACY FOR THE DEGREE OF

DOCTOR OF PHILOSOPHY

INTERDISCIPLINARY SCIENTIST TRAINING PROGRAM:

ECOLOGY AND EVOLUTION

BY

MEGAN SUSANNE KENNEDY

CHICAGO, ILLINOIS

DECEMBER 2023

To my family.

TABLE OF CONTENTS

LIST OF FIGURES

LIST OF TABLES

ACKNOWLEDGMENTS

Over the past five years of my PhD work, I have felt excited, disappointed, curious, doubtful, confident, confused, delighted, bored, validated, exhausted, inspired, and everything in between. This scientific journey has carried me through highs and lows, but through it all, I've had an overwhelmingly positive experience thanks to the small army of supportive mentors, advisors, peers, friends, and family who have always had my back. The work presented in this dissertation simply would not have been possible without them, and there are no words that can fully express the depth of my gratitude.

First, I would like to acknowledge my co-advisors, Gene and Joy. In complementary ways, they have each been indispensable to my development as a scientist, and they have shaped my view of what it means to be a good mentor. Joy provided an assiduous attention to detail, an extraordinary intellect that can analyze and understand new information at light speed, and a conversational directness that helped to simplify decision making into its most essential considerations. Gene has always been a nonstop fountain of ideas and enthusiasm for his lab's science. He has an incredible ability to see connections between the disparate projects in our giant lab group, helping us to incorporate interdisciplinary perspectives into our work, and he is an inspiring scientific communicator. Perhaps most importantly, Gene and Joy have exemplified a style of leadership centered around promoting the growth of their trainees. They lead with their ideas and their enthusiasm, and not with their ego. They provide opportunities and give credit where it is due. I have been free to make mistakes, take wrong turns, and fail

experiments in the circuitous scientific trajectory that led me to the finalized work presented here. And all those mistakes have been essential for me to develop resilience, and confidence, and a deeper understanding of how to design, execute, and analyze good and rigorous science. Gene and Joy have made me into the scientist that I am today.

Gene and Joy also share an ability to attract absolutely incredible scientists and people to their lab groups. In Joy's group, Hannah, Caroline, Kat, and Keven have all been essential in ensuring my sense of belonging in the E&E department, especially as a co-advised MSTP whose main lab space was physically distant from the E&E buildings. In Gene's lab, I found so many people who know so much about fields that I know nothing about, and they were willing to share that knowledge with me to help me answer my scientific questions. They have directly shaped my experimental and analytic skills, and have helped me out and filled in on countless occasions so that I could complete far more than I ever could have alone. I feel so privileged and humbled to have shared my training experience with them.

I want to thank my thesis committee, Cathy Pfister, Tim Wootton, and Maureen Coleman, who have given me feedback and advice that has shaped the trajectory of my PhD, as well as the Medical Scientist Training Program and Ecology and Evolution departments, which have each cultivated welcoming academic and social communities that I have been lucky to be a part of.

Next, I have to thank some of the friends to whom I truly owe what's left of my sanity. My MSTP cohort, and especially Alexis Monical, have been with me since the beginning and will

be stuck with me for years of med school to come. My Darwinian squad, especially Will Koval, Laura Cespedes Arias, Paula Fernandez Begne, and Pablo Lechon Alonso, and some of my other past-and-present Chicago friends, including Ale Machado and Mirae Lee, have been foundational to my mental health over the past five years. We made it through a pandemic and more together, and I wouldn't rather do it with anyone else. My Princeton crew, including Julie Aromi, Bryan Jacobowitz, Alex Smith, Emily Bobrick, Ruth Rosenthal, and Nicky Robinson, and my lifelong friends from high school and earlier, Anna Hall, Iulia Gheorghiu, Haley Shoaf, Sarah Gallo, and Asha Bazil, have made sure that I always, always felt supported from both near and far.

Finally, of course, I have to thank my family for making me into me. My brothers Patrick and Michael each inspire me in such distinct ways – Patrick is such an incredible academic, musician, and person, who is so passionate, creative, funny, thoughtful, and analytic. Patrick makes sure that I never mistake intuition for data, and he reminds me that doing research, even if it may be boring to others, can and should feel fun and exciting to me. Michael has always been such a role model to me, and wittingly or not, I have shaped so much of my personality in his image. Michael reminds me not to take myself too seriously, and that the people in my life and the experiences I share with them are what make a life memorable, and that having fun can be a priority too, and isn't mutually exclusive with doing work. Last, I absolutely could not have made it to this stage of my life without the unwavering love and support of my parents. They

have taught me to prioritize kindness, empathy, and generosity towards others, and to always work hard. I am infinitely grateful for them.

INTRODUCTION

When the niche space supporting a population or community changes, its inhabitants must adapt to optimize resource use efficiency, compete within and across species, and maintain the fitness necessary to survive under the new conditions. For microbial taxa in particular, changes in resource availability are extremely common due to the ease and frequency of dispersal into new macro- and microenvironments (Hildebrand et al. 2021). Accordingly, thanks to their fast generation time, remarkable degree of genomic mutability (Lenski 2017; Springael and Top 2004), and the growing arsenal of molecular tools now at our disposal (Q. Wang et al. 2019), microbial eco-evolutionary processes play out rapidly and observably, providing an unprecedented window into the temporal mechanisms of adaptation. In real time, we can evaluate how populations and genomes evolve (Jerison and Desai 2015), and how communities change in response to shifting resource landscapes (David et al. 2014).

The mammalian gut provides a uniquely powerful and clinically relevant opportunity to study dynamic processes of microbial adaptation. First and foremost, the gut is a highly dynamic environment: individuals change their diet, transition between states of sickness and health, are exposed to diverse new microbes from their surroundings, and undergo medical interventions like antibiotic treatment on a fairly regular basis (Schlomann and Parthasarathy 2019). Host factors like tissue oxygenation and O_2 diffusion into the gut lumen, pH, mucus thickness, antimicrobial peptide production, and immune activity fluctuate in a constant homeostatic

balancing act, and these dynamics can directly affect microbial fitness and survival (J.-Y. Lee, Tsolis, and Bäumler 2022).

Second, feedbacks between the host and its microbial symbionts arise that can be either homeostatic or pathogenic, with major consequences for host health (Knights, Lassen, and Xavier 2013; Read and Holmes 2017). For instance, exposure to commensal microbes is essential for the appropriate development of the host immune system, as well as for establishing tolerance to symbiotic or other non-pathogenic microbes (Ivanov et al. 2009; Gensollen et al. 2016). However, the wrong combination of genetic predisposition and environmental conditions can alter the interactions between microbe and host in a way that triggers an inappropriate inflammatory response, precipitating the development of chronic inflammatory bowel diseases (M. Lee and Chang 2021; Miyoshi et al. 2017). Improving our understanding of how gut microbes adapt under changing ecosystem conditions will enable us to better predict and manipulate microbiome dynamics for therapeutic gain.

In spite of the spectacular tractability of microbes for studying adaptation in real time, relatively few studies allow the temporally granular detail necessary for rigorous analysis of dynamic eco-evolutionary processes of the gut microbiome. Specifically, almost all temporally dense *in vivo* studies of gut microbial evolution are limited to the study of *Escherichia coli* populations, usually in monocolonization experiments (Barroso-Batista et al. 2020; Vasquez et al. 2021; Barroso-Batista et al. 2014; Ghalayini et al. 2018; Frazão et al. 2022). Although *E. coli* is a

highly prevalent member of the human gut microbiota, its relative abundance in healthy individuals is estimated at $< 0.1\%$ (Fang et al. 2018). Dense timecourse data on the evolutionary dynamics of more dominant gut-derived taxa are rare (S. Zhao et al. 2019; Garud et al. 2019), and even fewer such studies have been performed in the context of a specific host treatment or phenotype (Dapa et al. 2022; Roodgar et al. 2021). Similarly, temporally dense surveys of community-level microbiome dynamics are occasionally published, often centering around themes of infant gut microbiome acquisition and maturation (Bäckhed et al. 2015), circadian rhythmicity (Leone et al. 2015), or antibiotic response (Palleja et al. 2018; Zmora et al. 2018), but overall, such time series remain fairly uncommon (Schlomann and Parthasarathy 2019).

More typically, for a huge array of clinically-relevant phenotypes, population- and community-level microbial dynamics have been characterized in cross-sectional studies that compare data from a single timepoint across healthy and diseased individuals (Shreiner, Kao, and Young 2015). While such frameworks are effective for identifying long-term selective pressures, they neglect the temporal dynamics that underlie the transitions between states, and therefore assume that the adaptational process is not contingent upon transient or intermediate dynamics *en route* to the endpoint. This dissertation challenges that assumption, instead conceptualizing microbial adaptation as a temporal and iterative feedback-driven process of environmental change and microbial response. With this approach, we are able to improve our understanding of dynamic selective pressures, evaluate instances of historical contingency in population-level

adaptation and community assembly, and identify the predominant selective forces that shape the microbial ecosystem over time. By embracing the temporal dynamics of adaptation in the context of distinct host treatments or phenotypes, we create an opportunity to understand the transitional mechanisms that carry a healthy microbiome to an unhealthy state, or vice versa. In this work, I use two experimental model systems to characterize the ways that microbes adapt to different environments and resource schemes over time: in the first, I assess population-level adaptation to a new host resource landscape, and in the second, I evaluate community-level response to an ecosystem perturbation under different resource conditions.

In Chapter 1, I examine how a human-derived bacterium, *Bacteroides thetaiotaomicron* (*Bt*), adapts to the mouse gut over the course of monocolonization. Using a temporally granular three-pronged approach that includes a functional genetics screen, transcriptomic analysis, and a long-term evolution experiment, I find that *Bt* proceeds through distinct adaptational stages with characteristic patterns of spatial localization, gene expression, and functional requirements, and identify strong selective pressure for efficient metabolism of easily accessible dietary polysaccharides.

In Chapter 2, I evaluate how different dietary resource environments impact gut microbiome robustness and resilience to a brief antibiotic perturbation. Mice on high-fat, low-fiber "Western diet" (WD) exhibit altered microbiome community structure compared to mice on a standard low-fat, high-fiber "regular chow" (RC) diet, and their microbial symbionts experience a distinct

dietary resource environment (Bisanz et al. 2019). Both of these factors could independently impact microbiome robustness, stability, and resilience. In this series of experiments, I compare community-level dynamics of the microbiome across RC and WD treatment groups over a dense timecourse before, during, and after antibiotic perturbation. I perform extensive multi-omics analysis including 16S rRNA sequencing, shotgun metagenomic sequencing, and metabolomics, and find that mice on a high-fat, low-fiber "Western diet" exhibit markedly impaired microbiome recovery after antibiotic perturbation. I then perform intervention experiments to assess the relative contributions of dietary resource environment and microbial re-seeding to recovery, and find that diet plays a greater role in recovery than microbial re-seeding. Finally, I evaluate the consequences of impaired microbiome resilience for host health by performing colonization resistance experiments with *Salmonella enterica* serovar *Typhimurium*, and find that colonization resistance is impaired in antibiotic-treated mice on WD for up to 2 weeks after antibiotic treatment has ended.

Together, these results suggest that by carefully examining the temporal dynamics of microbial population- and community-level adaptation, we can generate powerful insights into the mechanisms that allow microbiomes to adapt and change.

CHAPTER 1

Dynamic genetic adaptation of *Bacteroides thetaiotaomicron* during murine gut colonization

Citation: Kennedy, M.,* Zhang, M.,* DeLeon, O., Bissell, J., Trigodet, F., Lolans, K., Temelkova, S., Carroll, K.T., Fiebig, A., Deutschbauer, A., Sidebottom, A.M., Henry, C., Rice, P.A., Bergelson, J., Chang, E.B. (2023). Dynamic genetic adaptation of *Bacteroides thetaiotaomicron* during murine gut colonization. *Cell Reports.* doi: 10.1101/2022.02.23.481734

*co-first authors

Contributions: Conceptualization, M.S.K., M.Z., E.B.C., and J.B.; Methodology, M.S.K., M.Z., E.B.C.; Formal Analysis, M.S.K., M.Z., O.D., F.T., A.M.S.; Investigation, M.S.K., M.Z., J.B., K.L., S.T., K.T.C., A.M.S., J.L.; Resources, A.D.; Data Curation, M.S.K., M.Z.; Writing – Original Draft, M.S.K, M.Z.; Writing – Review and Editing, M.S.K., M.Z., E.B.C., A.F., J.B., C.H., P.R.; Visualization, M.S.K., M.Z., O.D., F.T.; Funding Acquisition, E.B.C.

1.1 ABSTRACT

To understand how a bacterium ultimately succeeds or fails in adapting to a new host, it is essential to assess the temporal dynamics of its fitness over the course of colonization. Here, we introduce a human-derived commensal organism, *Bacteroides thetaiotaomicron*, into the guts of germ-free mice to determine whether and how the genetic requirements for colonization shift over time. Combining a high-throughput functional genetics assay and transcriptomics, we find that gene usage changes drastically during the first days of colonization, shifting from high expression of amino acid biosynthesis genes to broad upregulation of diverse polysaccharide utilization loci (PULs). Within the first week, metabolism becomes centered around utilization of a predominant dietary oligosaccharide, and these changes are largely sustained through six weeks of colonization. Spontaneous mutations in wildtype *Bt* also evolve around this locus. These findings highlight the importance of considering temporal colonization dynamics in developing more effective microbiome-based therapies.

1.2 INTRODUCTION

Rapid adaptation is paramount to the survival of any species undergoing an environmental transition. For microbial taxa, which are frequently and rapidly dispersed across dramatically different habitats and microenvironments, processes of local adaptation may arise as primary determinants of microbial colonization success and resulting biogeography (O'Malley 2007). The mammalian gut is an environment regularly bombarded with a diverse array of exogenous microorganisms. As such, it represents a biologically and clinically relevant system to explore rapid microbial adaptational processes.

An emerging body of literature has begun probing the evolutionary and selective dynamics of exogenous microbes during colonization of the mammalian gut but has largely neglected early-timepoint or transient dynamics en route to long term persistence. For instance, several studies using TnSeq-based approaches have evaluated the genetic requirements for colonization across various microbes in the guts of conventionally raised, gnotobiotic, and germ-free mice, but have assessed fitness only at a single timepoint after introduction (Goodman et al. 2009; Liu et al. 2021). Wu *et al.* evaluated TnSeq mutant abundances of four *Bacteroides* strains over a 16-day timecourse, but performed only broad characterization of population-level shifts at intermediate timepoints, restricting more rigorous gene-level functional analyses to a single endpoint (Wu et al. 2015). Several recent evolution studies have demonstrated the extent to which carbon limitation and metabolic demands drive the

evolutionary trajectories of commensal and probiotic strains like *B. thetaiotaomicron* (*Bt*) or *E. coli* in the gut (Vasquez et al. 2021; Crook et al. 2019; Dapa et al. 2022; Barroso-Batista et al. 2020). However, in spite of dense timecourse sampling, these studies do not identify genes that are important for fitness specifically at earlier stages of colonization. On shorter adaptive timescales, transcriptomics analyses of commensal microbes like *Bt in vivo* and *in vitro* have demonstrated that gene expression profiles adapt quickly to factors like diet (J. L. Sonnenburg et al. 2005), community membership (J. L. Sonnenburg, Chen, and Gordon 2006; Mahowald et al. 2009), immune activation (Becattini et al. 2021), or spatial localization within the gut (Donaldson et al. 2020). However, no studies have yet comprehensively evaluated the temporal transcriptional profile of a commensal microbe over the course of colonization.

In the following experiments, we introduce a human-derived commensal organism, *Bacteroides thetaiotaomicron* (*Bt*), into the guts of germ-free C57Bl/6 mice to determine whether the genetic requirements for colonization shift over time and, if so, to characterize the biological functions required for microbial survival at different stages of colonization and persistence. Use of a germ-free monocolonization model allows us to reduce the staggering complexity of the gut microbial ecosystem into experimentally tractable and readily interpretable components: here, we rigorously outline population-level microbial colonization dynamics for a widely used model organism and the host-microbe interactions that drive them. Using this

germ-free model as a baseline, future work can evaluate the distinct contributions of microbe-microbe interactions and other emergent community-level properties to community assembly and colonization dynamics.

To identify the microbial genes important for fitness in this context, we combine two complementary unbiased approaches: transcriptomics (RNA-seq), which reveals global gene usage patterns, and a functional genetics approach (BarSeq) (Liu et al. 2021; Wetmore et al. 2015), to assess fitness consequences of gene disruptions at a global scale over the course of gut colonization. We validate these results with both *in vivo* metabolomics analysis and *in vitro* microbial growth experiments. Finally, we evaluate spontaneous evolution of wildtype (WT) *Bt* in the gut to survey natural population-level fitness dynamics. Our results indicate that adaptation to the host gut occurs in distinct stages. During the earliest stage of colonization, genes involved in amino acid and vitamin biosynthesis are upregulated and, in some cases, play essential roles in survival of *Bt*. By colonization D2-4, *Bt* shifts towards upregulation of a diverse array of carbohydrate metabolism genes. This broad survey of available resources continues through D7 before ultimately centering on upregulation of a polysaccharide utilization locus (PUL) responsible for the degradation of raffinose-family oligosaccharides (RFOs) rich in the standard chow diet fed to our mice. This metabolic shift accompanies a change in *Bt* localization from the mucus towards the lumen, where the expression profile remains largely consistent through at least six weeks of colonization.

Spontaneous mutations in WT *Bt* also evolve around the same PUL, highlighting the importance of efficient carbohydrate metabolism for long-term persistence.

These experiments lay the groundwork for future delineation of shifting selective pressures in various host backgrounds and microbiome compositions. We expect that these insights into the temporally dynamic stresses that microbes must overcome to colonize and persist in the gut will prove invaluable to our understanding of microbial adaptation and the development of microbiome-based therapies.

1.3 MATERIALS AND METHODS

Microbial Strains and Growth Conditions

The bacterial strains used in this study, including the RB-TnSeq library, are listed in Table S1 in the supplemental materials. *Bacteroides thetaiotaomicron* VPI-5482 [AMD595, and all its derivatives were cultured anaerobically at 37°C in liquid BHI-S medium or defined Varel-Bryant medium as described in Liu *et al.* (Liu et al. 2021), and Varel and Bryant (Varel and Bryant 1974). Varel-Bryant medium with no carbon source was supplemented with glucose, galactose, sucrose, raffinose, or melibiose to a final concentration of 20 mM. An anaerobic chamber (Coy Laboratory Products) filled from tanks containing 10% CO_2, 7.5% H_2, and 82.5% N_2 was used for all anaerobic microbiology procedures, with working conditions near 2-3% H_2.

Mice

Female 8-12 week-old C57Bl/6J germ-free mice were bred and maintained in plastic gnotobiotic isolators or bioexclusion racks within the University of Chicago Gnotobiotic Core Facility and fed ad libitum autoclaved standard chow diet (LabDiets 5K67). The mice were given a single dose of either wildtype *Bt* VPI-5482 or the *Bt* mutant library (gift from Deutschbauer lab) at 10^6 - 10^8 CFU / 200 µL. All murine experimental procedures were institutionally approved.

In vivo genome-wide mutant fitness assays

Four individual cohorts of mice were used, indicated by the month of the experiment. For each cohort, mice were housed in cages of 2-3 animals either within a gnotobiotic isolator (Dec, Jan) or in hermetically sealed Techniplast IsoCage P Bioexclusion cages on a rack system (Mar, Oct), and allowed to acclimate for 3 days prior to colonization (Fig. S1.1A). The inoculum was prepared by one of two methods: 1) frozen 2 mL aliquots of the *Bt* RB-TnSeq library were thawed and gavaged directly into mice (Dec, Jan), or 2) a thawed 2 mL aliquot of the *Bt* RB-TnSeq library was grown in 150 mL BHI-S medium overnight with 20 µg/mL erythromycin (16 h), and backdiluted to OD600 = 0.05 the next morning to allow for fresh cells to reach mid-log phase (3 h) by the time of inoculation (Mar, Oct). For each experiment, at least 3 cell pellets of the inoculum were collected as Time = 0 references. Each

mouse was colonized by oral gavage with 200 µL of the *Bt* transposon library. Stool samples were collected daily (excluding weekends), up to 14 days post-colonization to assess longitudinal shifts in mutant abundance. Mice were monitored and weighed daily. Genomic DNA was extracted using the DNeasy PowerSoil Kit.

The IsoCage P rack system facilitated sample collection while maintaining gnotobiotic conditions, and although the fresh and frozen inocula exhibited nearly identical coverage of the *Bt* genome (Fig. S1.1B) and harbored statistically indistinguishable levels of diversity (Fig. S1.1C, S1.1D), use of fresh rather than frozen inoculum substantially reduced bottleneck effects, allowing for low-abundance mutants to reach the gut and persist at a much higher rate through at least D1 (Fig. S1.1E), with diversity only beginning to decrease at D4 (Fig. 1.4A). Because of the bottleneck effect in the frozen inoculum cohorts, analysis of early timepoints in the functional genetics experiments is restricted to experiments that used fresh inoculum (Mar, Oct). Results from later timepoints converged across all four runs of the experiment, in spite of differences in protocol (Fig. 1.1D, Fig. 1.4E).

Pipeline for measuring relative abundance and fitness scores of RB-Tn mutants

RB-TnSeq strain and gene fitness scores were calculated as described previously from strain-level count data (Wetmore et al. 2015). For temporal abundance analyses of TnSeq mutants for each run, we first created a feature table with raw counts of strain-level mutants across

each sample. This table was filtered to remove strains with counts of 1, as these are likely produced by sequencing error. Next, counts were normalized by the count of a synthetic spike-in barcode that was introduced at 20 pM into each sample during PCR amplification of the barcodes. Samples where the spike-in represented > 30% of total reads were discarded. The synthetic spike-in barcode was subsequently removed as a feature from the table, and the resulting tables were used for alpha diversity analyses via the R package '*vegan*' (Oksanen et al. 2022). For all other relative abundance analyses, strains were assigned to genes based on previous mapping by Liu *et al.* (Liu et al. 2021), as well as manual mapping performed for this experiment. Strains that had not been mapped here or elsewhere were binned together as "non-mapping" strains, and strain-level counts were then summed for each gene. For all subsequent analyses, we further filtered out genes that mapped to *Bt* plasmids in order to focus on chromosomal gene fitness patterns. The R package '*phyloseq*' was used to calculate Bray-Curtis dissimilarity for all pairwise combinations of samples, which was then used to create PCoA plots (McMurdie and Holmes 2013). Finally, filtered count tables were adjusted to relative abundance based on the total remaining counts, and used to track gene-level relative abundance over time. For linear regression of initial vs final relative abundance of gene mutants, genes with zero-counts were re-assigned a value of $1x10^{-7}$ to perform log-transformation of the data.

In vivo transcriptomic experiments

Mice were sacrificed at 0.5, 1, 2, 4, 7, 14, and 42 days post-colonization. Luminal contents of the mice cecum were immediately snap-frozen in liquid N_2 and stored at -80°C. About 50 mg of the contents were transferred into 2 mL screw-cap tubes, followed by the addition of 1 mL TriZOL reagent for the isolation of RNA. The samples were homogenized by beadbeating with 0.1 mm glass beads in a Mini-BeadBeater-96 for 2 minutes. Total RNA isolation and purification were performed using the TRI reagent protocol and quality checked by BioAnalyzer. All library preparation and sequencing work was performed by MiGS (Pittsburgh, PA). Initial DNAse treatment is performed with Invitrogen DNAse (RNAse free). Library preparation is performed using Illumina's Stranded Total RNA Prep Ligation with Ribo-Zero plus. Custom Ribo-Zero probes were designed for *Bt* and supplemented alongside the standard probe set. Custom probe sequences can be found in Table S2. Sequencing was performed on a NextSeq2000 giving 2x50bp reads. Post sequencing, we use bcl2fastq (v2.20.0.422) to demultiplex and trim adaptors.

Gene Set Enrichment Analysis (GSEA) on transcriptomic data for metabolic pathways, CPS genes, PULs, and stringent response

Metabolism for the *Bt* genome was first estimated using the anvio-v7 program '*anvi-estimate-genome*' that identifies the KEGG Ortholog family (Kofam) annotations for each open reading

frame. Gene calls for each metabolic pathway found within the *Bt* genome were then transferred into a unique GSEA pathway query list in R (*'fgsea')* (Sergushichev 2016). Pathway enrichment was then calculated using the enriched gene lists derived from the RNA-Seq analyses using '*deseq2*' (Love, Huber, and Anders 2014). Pathways were filtered for $q < 0.05$ and the normalized enrichment scores (NES) plotted (GraphPad Prism v9). Other custom gene lists were created to calculate the enrichment of other gene sets including the polysaccharide utilization loci (PULs), capsular polysaccharide loci (CPSs), and genes associated with the *Bt* stringent response.

Isolation of mutants from fecal matter

Mouse feces were collected and immediately homogenized in 500 mL 25% glycerol solution and stored at -80°C. Prior to isolation, glycerol stocks were allowed to thaw on the benchtop for 10 minutes, centrifuged for 30 seconds at 2,000 RPM. On each 150 mm BHI-S plate, 100 µL of 10^{-3}, 10^{-4}, or 10^{-5} dilution of the glycerol stock was spread using 4.5 mm glass beads. The plates were incubated anaerobically at 37°C for two days. Individual colonies were picked into 1 mL 96-well plates containing 750 µL BHI-S in each well. After 16 hours of growth, glycerol was added to a final concentration of 20% and the isolates were stored. The isolate stocks were used as the template in PCR amplifying the barcoded region of the mutants. The PCR products were sent for Sanger sequencing.

In vitro culture and growth measurements

Bt was grown in an anaerobic chamber at 37°C either in Brain Heart Infusion Supplemented (BHI-S) medium or Varel-Bryant (VB) defined medium (Varel and Bryant 1974). The Varel-Bryant medium base was made with no carbon source and was supplemented by 20 mM of the indicated carbon source. For growth measurements, colonies of *Bt* were inoculated into 3 mL of BHI-S in plastic culture tubes and grown overnight at 37°C, for a total of 6 biological replicates. Sealed Hungate tubes containing 10 mL of VB medium and a 20 mL headspace were used for subsequent growth. Immediately before inoculating with the cells, the tubes were inoculated via syringe with autoclaved sugar solution and hemin solution for a final concentration of 20 mM sugar and 5 µg/mL hemin. Overnight cultures were diluted to OD600 = 1, and 100 µL of the diluted culture was inoculated into the prepared media tubes via syringe. Anaerobically sealed cultures were grown outside of the chamber in a 37°C incubator with no shaking. Every 45 minutes, the cultures were taken from the incubator, cells resuspended by shaking, and their OD600 readings measured by a GENSYS 40-Vis spectrophotometer.

Host-associated evolution of spontaneous Bt mutants

Three female mice 8-12 wk-old C57Bl/6J GF mice were co-housed in the same gnotobiotic isolator and fed standard chow diet ad libitum. One week post inoculation of *Bt*, the three

mice were separated into individual cages. A fecal sample was taken six weeks post inoculation. DNA was extracted from the fecal pellets by the phenol-chloroform method, followed by ethanol precipitation, and sent for shotgun sequencing. Individual isolates from each fecal pellet were cultured from the bulk material as outlined in Isolation of mutants from fecal matter. We assayed for isolates with increased growth in VB-melibiose and selected one isolate from each mouse for MinION long-read sequencing.

Isolated genomes sequencing, assembly and polishing

To provide greater context for the delineation of the complex chromosomal rearrangements associated with the BT1872/BT1873 operon, a long-read sequencing strategy was employed. The isolate genomes assessed were wild-type *Bt*, the strain used for the mouse experiments, and three spontaneous mutant cultivars (MZ55, MZ58 and MZ65), which demonstrated enhanced growth rates in the presence of melibiose, recovered from the feces of mice six weeks after initial inoculation. Total genomic HMW DNA was extracted by a standard phenol chloroform protocol on overnight 25 mL BHIS broth cultures (Trigodet et al. 2022). DNA was resuspended in 0.1 mL 10 mM Tris-Cl, pH 8.5.

Slow pipetting, wide bore pipette tips and steps to minimize velocity gradients were implemented throughout to avoid further shearing of DNA molecules. Libraries were prepared with the Rapid Barcoding Kit (SQK-RBK004) and the standard protocols from Oxford

Nanopore Technologies were used with the following modifications. DNA fragmentation was performed on 10 µg DNA using 10 passes through a 22G needle in a 250 µL volume before purification using 0.5% Agencourt AMPure XP beads (A63882, Beckman Coulter). Each elution step of the AMPureXP beads was performed using 10 mM Tris-Cl pH 8.5 instead of water, at 37°C for 5 min. The gDNA inputs into library preparation ranged between 0.5 µg and 1.2 µg (Table S1.3), based on sample availability in a standard 8.5 µl volume, with 1.5 µl Fragmentation mix added to each sample. Barcoded libraries were pooled so each sample contributed an equal input mass (~0.5 µg, Table S1.3). Using MinKNOW (v4.3.4), a single R9.4/FLO-MIN106 flow cell (Oxford Nanopore Technologies) sequenced the final prepared library with a starting voltage of −180 mV and a run time of 72 h. Guppy (v5.0.11) and the sup model were used for post-run basecalling, sample de-multiplexing and the conversion of raw FAST5 files to FASTQ files. For downstream analyses, we only used reads with a minimum quality score of 7. We assembled long-reads contigs with Flye (Kolmogorov et al. 2019). Additional DNA extractions were carried out for every isolate using a standard phenol-chloroform extraction and send for short-read sequencing. We then used the short-reads to polish the long-read assemblies using Pilon v1.23 (Walker et al. 2014).

Metagenomic mapping and coverage visualization

We used anvi'o v7.1 and the metagenomic workflow to compute and visualize metagenomics coverage for each isolate genome (Eren et al. 2020). Briefly, the workflow uses (1) Prodigal v2.6.3 (Hyatt et al. 2010) to identify open-reading frames (ORFs), (2) *'anvi-run-hmm*' to identify single copy core genes from bacteria (n=71) (M. D. Lee 2019) and ribosomal RNAs (n=12) using HMMER v3.3 (Eddy 2011), (3) *'anvi-run-ncbi-cogs'* and *'anvi-run-kegg-kofams'* to annotate ORFs with the NCBI's Clusters of Orthologous Groups (COGs) (Tatusov et al. 2003), and the KOfam HMM database of KEGG orthologs (KOs) (Kanehisa and Goto 2000; Aramaki et al. 2020) respectively. We used Bowtie2 v2.3.5.1 (Langmead and Salzberg 2012) to recruit metagenomic short-reads to the contigs, and samtools v1.11 (H. Li et al. 2009) to convert SAM files to BAM files. We profiled the resulting BAM files with *'anvi-profile'* and used the program *'anvi-merge'* to combine all single profiles into a merged profile for downstream visualization. We used *'anvi-get-split-coverages'* and *'anvi-script-visualize-split-coverages'* to generate the coverage plots. We used *'anvi-export-gene-calls*' and gggenes v0.4.1 to visualize the genomics context around BT1871.

BT1871 copy number

We used blast (Altschul et al. 1990) to compute the number of long-reads with two copies of the BT1871 locus in the MZ65 isolate. We extracted the gene sequence (1989 bp) from the

initial *Bt* genome (AMD595) using anvi'o interactive interface and used blastn v2.5.0 to blast the long-reads from MZ65. Blast hits with an alignment length > 180% of the gene length were flagged as "two copies" and hits with alignment length between 80% and 105% were flagged as "one copy". To visualize long-reads with two copies of *BT*1871, we used minimap2 v2.17 (H. Li 2018) to map the MZ65 long-reads to the MZ65 genome, which had two copies of the BT1871 region. We used samtools v1.11 to extract the reads with two copies as identified above and used IGV v2.11.1 (Robinson et al. 2011) to visualize the mapping and generate a figure.

Metabolite Extraction from Cecal Material

Metabolites were extracted with the addition of extraction solvent (80% methanol spiked with internal standards and stored at -80°C, Table S1.7) to pre-weighed fecal/cecal samples at a ratio of 100 mg of material per mL of extraction solvent in beadruptor tubes (Fisherbrand; 15-340-154). Samples were homogenized at 4°C on a Bead Mill 24 Homogenizer (Fisher; 15-340-163), set at 1.6 m/s with 6 thirty-second cycles, 5 seconds off per cycle. Samples were then centrifuged at -10°C, 20,000 x g for 15 min and the supernatant was used for subsequent metabolomic analysis.

Metabolite Analysis using GC-EI-MS and Methoxyamine and TMS Derivatization

Metabolites were analyzed using gas chromatography mass spectrometry (GCMS) with electron impact ionization. To a mass spectrometry autosampler vial (Microliter; 09-1200), 100 µL of metabolite extract was added and dried down completely under a nitrogen stream at 30 L/min (top) and 1 L/min (bottom) at 30°C (Biotage SPE Dry 96 Dual; 3579M). To dried samples, 50 µL of freshly prepared 20 mg/mL methoxyamine (Sigma; 226904) in pyridine (Sigma; 270970) was added and incubated in a thermomixer C (Eppendorf) for 90 min at 30°C and 1400 rpm. After samples are cooled to room temperature, 80 µL of derivatizing reagent (BSTFA + 1% TMCS; Sigma; B-023) and 70 µL of ethyl acetate (Sigma; 439169) were added and samples were incubated in a thermomixer at 70°C for 1 hour and 1400 rpm. Samples were cooled to RT and 400 µL of Ethyl Acetate was added to dilute samples. Turbid samples were transferred to microcentrifuge tubes and centrifuged at 4°C, 20,000 x g for 15 min. Supernatants were then added to mass spec vials for GCMS analysis. Samples were analyzed using a GC-MS (Agilent 7890A GC system, Agilent 5975C MS detector) operating in electron impact ionization mode, using a HP-5MSUI column (30 m x 0.25 mm, 0.25 µm; Agilent Technologies 19091S-433UI) and 1 µL injection. Oven ramp parameters: 1 min hold at 60°C, 16°C per min up to 300°C with a 7 min hold at 300°C. Inlet temperature was 280°C and transfer line was 300°C. Data analysis was performed using MassHunter Quantitative Analysis software (version B.10, Agilent Technologies) and

confirmed by comparison to authentic standards. Normalized peak areas were calculated by dividing raw peak areas of targeted analytes by averaged raw peak areas of internal standards.

RT-qPCR

Total messenger RNA was isolated from colonic mucosal scrapings with TriZOL reagent according to the same protocol used for cecal RNA isolation. Transcriptor First Strand cDNA Synthesis Kit (Roche Diagnostics Corporation) was used to obtain cDNA. Real-time qPCR was performed using iTaq Universal SYBR Green Supermix with CFX384 Real-Time System (Bio-Rad). The primers were derived from Miyoshi et al, 2017 (Miyoshi et al. 2017); forward (F) and reverse (R) primer sequences are as follows: *Ifng*, F-ATGAACGCTACACACTGCATC; RCCATCCTTTTGCCAGTTCCTC; *Il17a*, F-GGCCCTCAGACTACCTCAAC; R-TCTCGACCCTGAAAGTGAAGG; *Il17f*, F-TGCTACTGTTGATGTTGGGAC; R-AATGCCCTGGTTTTGGTTGAA; *Il1b*, F-GCAACTGTTCCTGAACTCAACT; R-ATCTTTTGGGGTCCGTCAACT; *Il6*, F-TAGTCCTTCCTACCCCAATTTCC; R-TTGGTCCTTAGCCACTCCTTC; *Tnfa*, F-CCCTCACACTCAGATCATCTTCT; R-GCTACGACGTGGGCTACAG; *Gapdh*, F-AGGTCGGTGTGAACGGATTTG; R-TGTAGACCATGTAGTTGAGGTCA.

ELISA

For cecal IgA ELISA, frozen cecal samples were resuspended in 1 mL of ELISA diluent per 100mg of cecal contents and homogenized by bead beating for 1 minute. ELISA was performed using goat polyclonal anti-IgA antibody (capture antibody) (Southern Biotech: 1040-01,) and goat anti-IgA antibody labeled with HRP (secondary antibody) (Bio-Rad: STAR137P). IgG ELISA was performed on frozen serum samples using Invitrogen IgG (Total) Mouse Uncoated ELISA Kit.

Histological Procedures

During sacrifice of mice colonized with WT *Bt* for transcriptomics experiments, distal colonic cross-sections were collected and placed in cassettes. Tissues were fixed by immersion in Carnoy's solution (60% ethanol, 30% chloroform, 10% acetic acid) for 3 hours and were stored in 70% ethanol until tissue sectioning. When ready to process, samples were dehydrated by two successive washes each in methanol for 35 min, ethanol for 30 min, and xylene for 25 min. Tissue samples within cassettes were then submerged in melted paraffin at 68°C for 1hr, removed, and kept at room temperature until sectioning. Paraffin blocks were cut into 4-µm-thick sections and deparaffinized for immunofluorescence.

Immunostaining

After deparaffinization and rehydration, slides were incubated in lysozyme solution at 37°C for 20 minutes, and then in antigen retrieval solution (10 mM sodium citrate [pH 6.0]) at 90°C for 10 minutes. For mucus visualization, a polyclonal rabbit anti-mouse Muc2-specific antibody (Santa Cruz Biotechnology) was diluted 1:100 in blocking buffer (Dako), applied to the slide, and incubated for 2 hours in the dark at room temperature. Slides were washed gently three times in TBS-T. The secondary antibody (Alexa Fluor 488 goat anti-rabbit IgG, Invitrogen) was diluted 1:100 in blocking buffer, applied to the slide, and incubated for 30 minutes in the dark at room temperature. Slides were again washed gently three times in TBS-T, and were then stained with DAPI 10 µg/ml (Sigma), incubated for 1 minute, and washed three times in PBS. Slides were then dried, mounted with ProLong Gold Anti-Fade mounting medium (Invitrogen) and stored at room temperature in the dark until imaging.

Imaging and Image Quantification

Images were acquired on a Leica SP8 laser scanning confocal microscope with the LAS_X Leica software (Leica). All samples were imaged with a 40x oil-immersion objective. Images were acquired at a frame size of 1024 x 1024 with 16-bit depth. For each mouse, a single cross-section was used to generate 6 representative images. Images were masked to split the DAPI signal into an epithelial channel (blue) and a luminal channel (red). The MUC2 channel

was green. To assess proximity of *Bt* to the epithelium, at 10 evenly-spaced points along the epithelium in each frame, a perpendicular line was drawn until it intersected the nearest bacterial cell, and this distance was measured. These measurements were averaged across all frames for each mouse. Average measurements for each mouse were then used to compare *Bt* epithelial proximity across experimental days.

Resource Availability

The data, including DNA and RNA sequencing datasets, that support the findings of this study are available in this article, the Supplemental Information, and BioProject accession PRJNA797447.

1.4 RESULTS

Both transcriptional and genetic fitness determinants shift over the course of Bt colonization and persistence.

To evaluate global transcription during colonization, we introduced WT *Bt* into germ-free (GF) C57Bl/6 mice and collected cecal contents at Days 0.5, 1, 2, 4, 7, 14, and 42 after colonization (Fig. 1.1A, n = 3-4 mice/timepoint). A control cohort of GF mice was gavaged with sterile phosphate-buffered saline (PBS), and *in vitro* control samples were collected from n=4 *Bt* cultures at mid-log phase in BHI-S media. After rRNA and host RNA depletion, the bacterial RNA samples were sequenced and compared across timepoints. In parallel, to assess

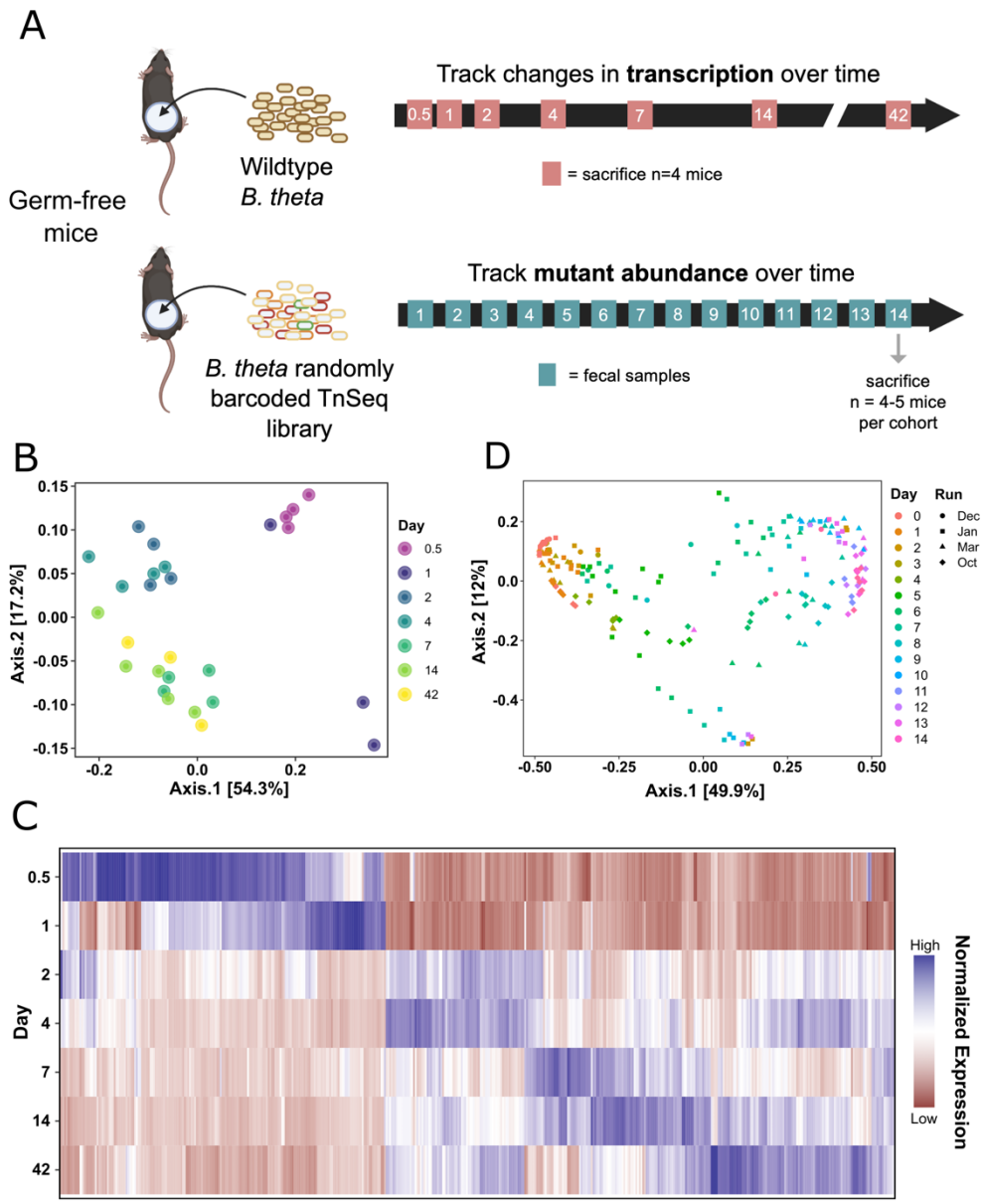

Figure 1.1: *Bt* gene expression and genetic fitness determinants shift over the course of colonization and persistence. (A) Experimental scheme of transcriptomics (top) and functional genetics (bottom) experiments in germ-free mice. **(B)** Principal Coordinates Analysis (PCoA) using Bray-Curtis dissimilarity on the global gene expression profiles of WT *Bt* (circles) and RB-Tn mutant libraries (triangles) at 0.5, 1, 2, 4, 7, 14, and 42 days of colonization (n=4-7 per group). **(C)** Heatmap visualizing all genes that were significantly differentially expressed at any timepoint relative to D1 (criteria: logFDR < -3, $|\log_2 FC| > 2$, and base mean > 50 RPM). Each column represents an individual gene (Table S5); data is normalized across all timepoints for each gene. **(D)** PCoA using Bray-Curtis dissimilarity on the abundances of RB-Tn mutant strains in fecal samples, colored by experimental day, shaped by experimental run. Four different cohorts of mice (n=3-5 per cohort) are represented.

functional genetic requirements during colonization, we introduced a rich library of randomly barcoded Tn insertion (RB-Tn) mutants of *Bt* into four different cohorts of germ-free C57Bl/6 mice (n = 3-5 mice/cohort) and collected near-daily fecal samples (Fig. 1.1A). Amplification and sequencing of the transposon barcodes reveals the relative abundance of each mutant in the library at each timepoint (Wetmore et al. 2015). RB-Tn experiments were carried out according to two slightly different protocols, with adjustments made to optimize experimental logistics and to reduce bottleneck effects (Fig. S1.1, Materials and Methods).

First, we asked whether there are differences in *Bt* gene expression at different times after introduction into the mouse gut. We first performed Principal Coordinates Analysis (PCoA) using Bray-Curtis dissimilarity on all gene expression data (Fig. 1.1B). We performed PERMANOVA analysis including both experimental day and cohort as explanatory factors, and found that only experimental day significantly contributed to clustering, explaining 79% of the variation in the dataset (Table S1.4).

We next performed post-hoc analyses to evaluate clustering by experimental day. We confirmed that the *in vitro* expression profile of *Bt* clustered distinctly from all other timepoints (adj.p < 0.05 for all comparisons, Table S1.5) and excluded *in vitro* samples from further analysis. Examining *in vivo* results, we found that D0.5 and D1 were statistically indistinguishable, as were D2 and D4, and D14 and D42, but that all other timepoints formed significantly distinct clusters (Fig. 1.1B, Table S1.5). Therefore, for all further

analyses, D0.5 and D1 data were combined ("D0.5/D1"), D2 and D4 data were combined ("D2/D4"), and D14 and D14 data were combined ("D14/D42"). The largest changes in gene expression, in which samples traverse PC1, occurred within two days after introduction to the gut. Although D7 and D14/D42 were statistically distinct, these clusters spanned a smaller and overlapping range within PCoA space, and therefore reflect relatively minor changes in global gene expression profile. To further assess overarching gene expression changes in *Bt* over six weeks of gut colonization, all genes that met stringent criteria of differential expression (logFDR < -3, $|\log_2 FC| > 2$, and base mean > 50 RPM) at any timepoint relative to D1 were displayed in a heatmap (Fig. 1.1C, Table S1.10). Even by these stringent criteria, we identified 489 differentially expressed genes (DEGs), which show a temporal pattern of relative peaks in expression at different timepoints.

Consistent with these global changes in gene expression over time, PCoA ordination using the relative abundance profiles of the RB-Tn mutant strains within each mouse in our functional genetics experiment reveals that the mutant pool composition shifted across time in a replicable pattern (Fig. 1.1D) across four independent cohorts of this experiment, despite protocol adjustments. PERMANOVA showed that the data cluster significantly by experimental day ($p = 0.0001$, $R^2 = 0.457$), with less substantial but significant contributions by individual mouse ID ($p = 0.0001$, $R^2 = 0.135$) and experimental run ($p = 0.0001$, $R^2 = 0.092$). The largest shifts across PC1 occurred between D1 and D7, with the mutant pool

changing less dramatically between D7 and D14. Together, these data suggest that different sets of genes mediate colonization and growth immediately upon gut entry and later in the adaptational process.

Amino acid and vitamin biosynthesis are transcriptionally upregulated and functionally significant during early colonization of the gut.

To gain a more comprehensive understanding of the gene pathways expressed during the acute phase of adaptation to the gut, we performed pairwise comparisons of gene expression across sequential timepoints. We identified extensive shifts in the *Bt* transcriptome between D0.5/D1 and D2/D4, with expression of 85 genes relatively enriched on D0.5/D1, and expression of 192 genes enriched at D2/D4 (Fig. 1.2A). The pathways enriched at D0.5/D1 comprised a largely unique set of genes from those that dominate the *Bt* expression profile *in vitro* (Table S1.10). To functionally characterize these DEGs, we mapped them to the Kyoto Encyclopedia of Genes and Genomes (KEGG) catalog (Fig. 1.2B). Although fewer DEGs were upregulated at D0.5/D1 compared to D2/D4, more of these genes mapped to known KEGG pathways, spanning a variety of functions, many of which center around metabolism. In particular, 30 DEGs upregulated at D0.5/D1 mapped to amino acid metabolism functions compared to 10 amino acid genes upregulated at D2/D4.

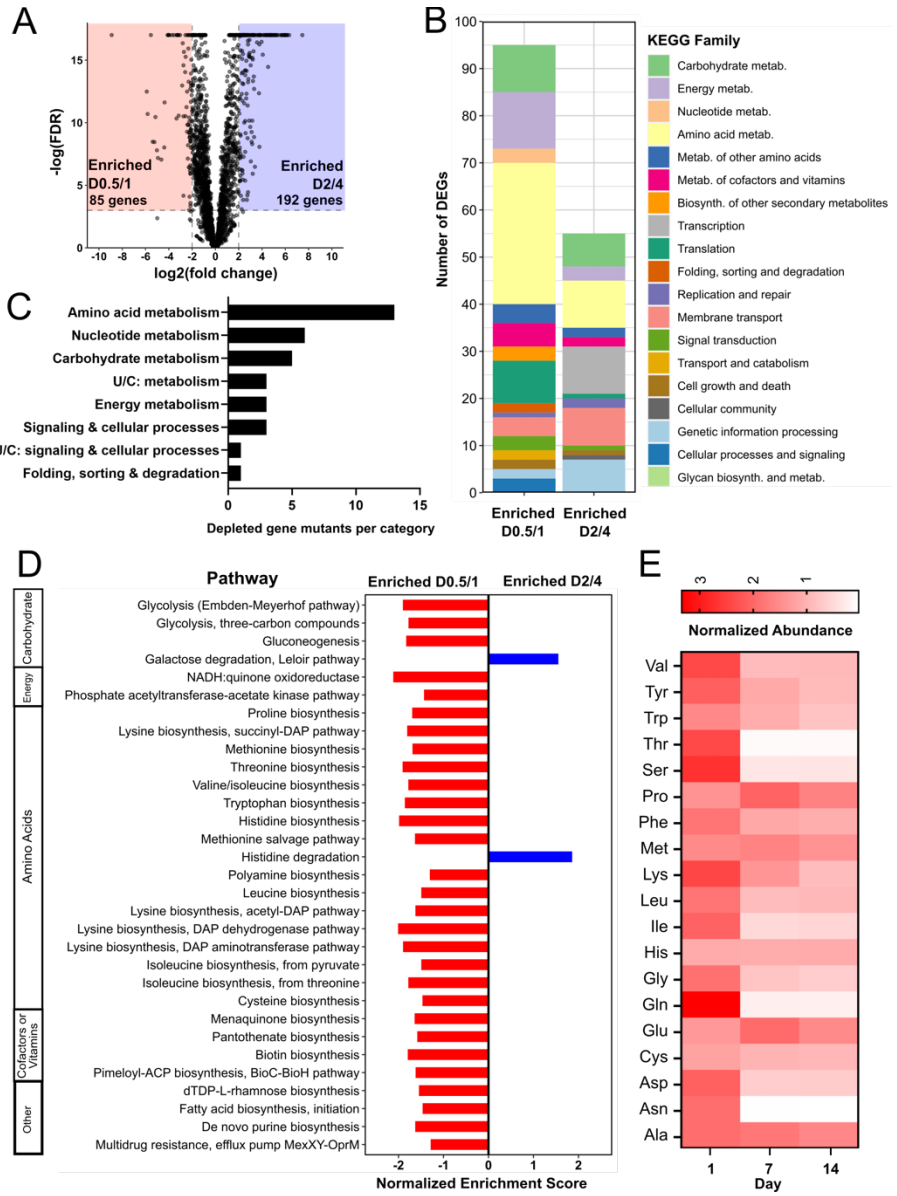

Figure 1.2: The *Bt* transcriptome undergoes dramatic remodeling during the first week after introduction to the murine gut. (A) Volcano plot of significant transcriptional differences between D0.5/D1 and D2/D4. 70 genes had significantly increased expression on D0.5/D1 (red), while 190 had significantly increased expression on D2/D4 (blue) [cut-off: log(FDR-adjusted p-value) < -3, $|\log2(\text{fold change})| > 2$, and max group mean > 50 RPM]. **(B)** DEGs from panel (A) colored by KEGG family. Genes with no KEGG annotations were excluded. **(C)** Number of gene mutants significantly depleted in the RB-Tn experiment (t-statistic $< -3\sigma$) on D1 of the experiment, plotted by KEGG family. **(D)** GSEA using transcriptomics data for all KEGG metabolic modules, comparing D0.5/D1 to D2/D4. Only pathways with significant differential expression ($p<0.05$) are shown. **(E)** Abundances of amino acids in the ceca of ex-germ-free mice at D1, D7, and D14 of colonization measured using GCMS and normalized to internal standards and to GF D0 controls (n=5 mice for GF D0, n=4 for post-colonization samples). See also Table S1.10.

To further explore the metabolic functions characteristic of the early phase of colonization, we performed Gene Set Enrichment Analysis (GSEA) for all KEGG metabolism modules across D0.5/D1 and D2/D4 (Fig. 1.2D). Expression of pathways corresponding to the biosynthesis of many amino acids were enriched specifically at the D0.5/D1 timepoint. Expression of genes involved in the biosynthesis of biotin, a cofactor required for amino acid biosynthesis, was concurrently upregulated at D0.5/D1. These results are supported by RB-TnSeq analysis: by mapping the significantly depleted gene mutants (t-statistic $< -3\sigma$) on the first day of the functional genetics assay using KEGG, we identified amino acid metabolism as the KEGG family with the largest number of significantly depleted mutants (Fig. 1.2C). These genes are identified by gold stars on the amino acid biosynthesis pathway map in Fig. S1.2, which illustrates reactions with upregulated gene expression at D0.5/D1 compared to D2/D4. We observe that biosynthesis of most amino acids involves multiple reactions that are transcriptionally enriched at D0.5/D1, or one step that is functionally essential.

Not only do both our transcriptomics analysis and functional genetics screen support a key role for amino acid biosynthesis early in colonization, but metabolomic analysis of the cecal contents corroborates this finding. We measured the levels of specific amino acids in the cecum of GF mice and compared those to cecal levels in ex-GF mice at D1, D7, and D14 after colonization with WT *Bt*, and found that amino acid levels were generally higher on D1 than D7 or D14 (Fig. 1.2E), as shown previously in an *E. coli* conventionalization model.(Barroso-

Batista et al. 2020) This difference was especially profound and statistically significant for amino acids in the glycine-serine-threonine pathway and for asparagine (Table S1.8, S1.9). By contrast, glutamate and proline reach their highest levels at D7 before being depleted in the second week.

Although upregulation of amino acid and vitamin biosynthesis at D0.5/D1 is reminiscent of the stringent response (SR), in which growth is inhibited under conditions of nutrient limitation to prioritize biosynthesis of essential nutrients,(Irving, Choudhury, and Corrigan 2021) further analysis suggests that early colonization is a distinct transcriptional program. Using a list of *Bt*-specific (p)ppGpp-mediated SR pathways manually curated from transcriptomic analyses by Schofield *et al.*,(Schofield et al. 2018) we performed GSEA to determine if SR transcriptional patterns were better represented at D0.5/D1 or D2/D4. Almost all pathways expected to be downregulated during SR were downregulated at D2/D4 rather than D0.5/D1, but pathways expected to be upregulated during SR were generally upregulated at D0.5/D1 (Table S1.10). Thus, although some pathway targets of the (p)ppGpp-mediated SR transcriptional program may be differentially expressed during gut colonization, these likely represent a distinct but overlapping response to the shifting selective pressures of the gut resource environment.

A shift toward enhanced expression of diverse sugar metabolism genes occurs during the first week of gut colonization.

Of the 192 DEGs upregulated at D2/D4 compared to D0.5/D1, only 50 mapped to known KEGG orthologs (Fig 1.2B, Table S1.10). Among these, we noted specific enrichment of genes involved in transcription, membrane transport, and genetic information processing, which represents *Bt*'s 7 identical IS3-family transposases. In the functional genetics experiment, we found that by D2, amino acid metabolism had been surpassed by carbohydrate metabolism as the KEGG family with the largest number of depleted gene mutants (Fig. 1.3A). This suggests that amino acid metabolism becomes less functionally essential after D1, and efficient carbohydrate metabolism becomes more essential.

Members of the genus *Bacteroides* are well-known for their ability to digest a wide variety of polysaccharides.(Martens, Chiang, and Gordon 2008; Wexler and Goodman 2017; Kaoutari et al. 2013) According to the CAZy database, *Bt* possesses 359 glycoside hydrolases, 87 glycosyl transferases, 15 polysaccharide lyases, and 19 carbohydrate esterases (Drula et al. 2022). To further probe carbohydrate utilization, we performed GSEA on all polysaccharide utilization loci (PULs) in the *Bt* genome in pairwise comparisons across sequential timepoints. Across all timepoints, 49 unique PULs were significantly differentially expressed. We find that from D0.5/D1 to D2/D4, expression of 21 PULs was upregulated compared to only 6 that were downregulated (Fig. 1.3B, 1.3C). From D2/D4 to D7, 12 PULs were upregulated compared to

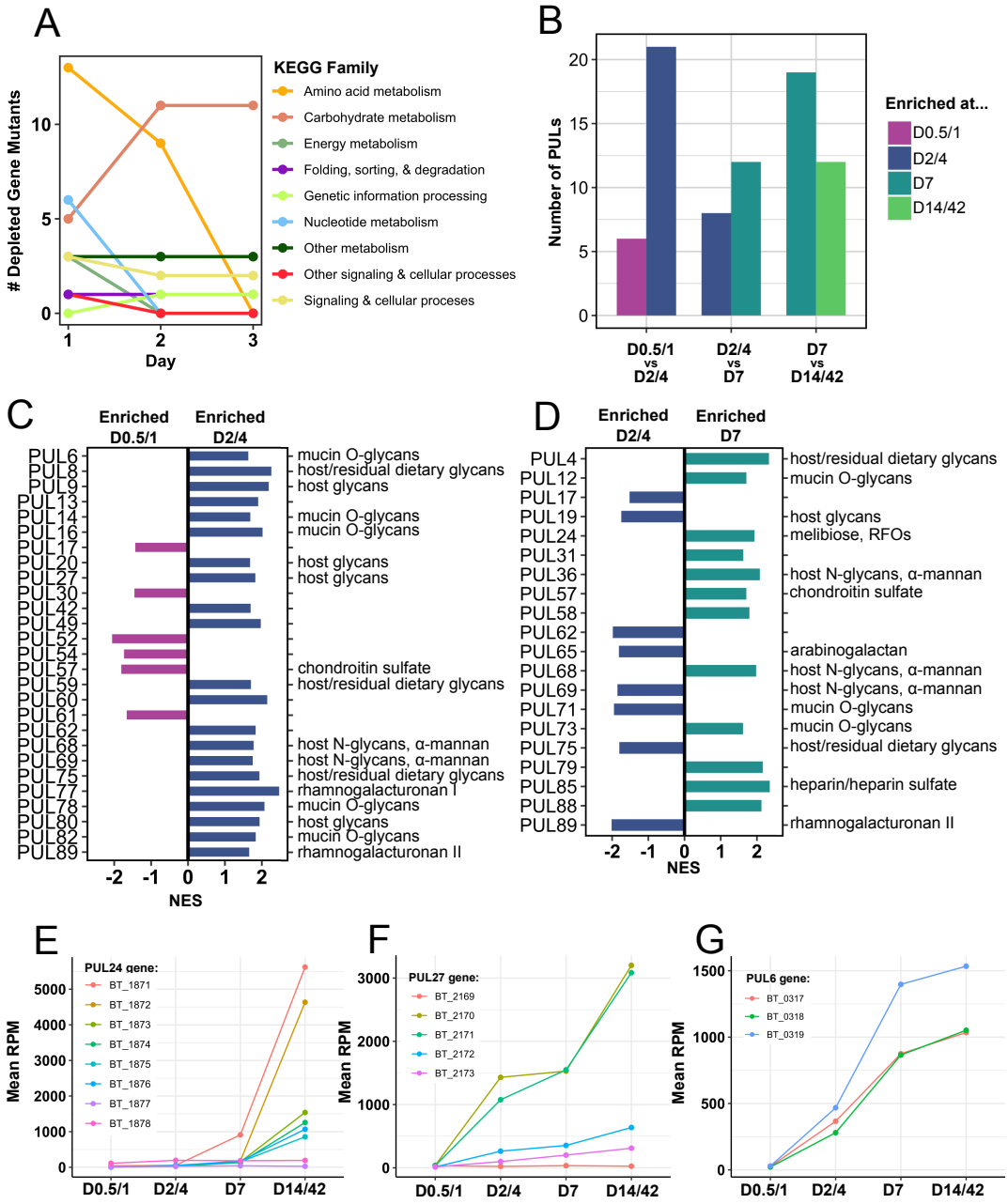

Figure 1.3: A shift toward greater expression of diverse sugar metabolism genes occurs during the first week of gut colonization. **(A)** Number of gene mutants significantly depleted from D1-D3 of the RB-Tn experiment (t-statistic < -3σ), colored by KEGG family. **(B)** Number of PULs significantly differentially expressed (adj. $p < 0.05$) across sequential pairwise comparisons identified via GSEA using transcriptomics data. Specific PULs differentially expressed across **(C)** D0.5/D1 vs D2/D4 and **(D)** D2/D4 vs D7 identified via GSEA. Known PUL substrates are listed on the right. Mean expression levels (reads per million, RPM) for all genes in the **(E)** PUL24, **(F)** PUL27, and **(G)** PUL6 operons. Error bars excluded for visual clarity; statistical comparisons done via GSEA. See also Table S1.10.

8 that were downregulated (Fig. 1.3B, 1.3D), and from D7 to D14/D42, more PULs were downregulated than upregulated (Fig. 1.3B). Collectively, these data show that over the first week of colonization, *Bt* increases expression of a broad array of PULs, but expression of many of these PULs is reduced as time goes on, perhaps to optimize utilization of available resources.

To identify specific PULs that may be particularly central to efficient resource utilization, we searched for PUL genes whose mean expression across mice increased monotonically over all timepoints, and found genes belonging to 21 PULs, including PUL24 and PUL59, both of which are adjacent to IS3-family transposases (Table S1.10). Of these 21 PULs, only PUL24, PUL27 and PUL 6 had expression patterns that were broadly consistent across all genes in the PUL (Fig 1.3E-F). These PULs moreover reached substantially higher levels of expression (~1500-6000 RPM) than any of the other 18 PULs (~200-400 RPM). PUL27 and PUL6 are predicted to enable degradation of host mucosal glycans, suggesting that *Bt* may be foraging for sugars through degradation of the mucus layer (Martens, Chiang, and Gordon 2008). The last gene of PUL24 encodes an α-galactosidase (BT1871), which is predicted to confer the ability to hydrolyze the α-1,6 glycosidic linkage in raffinose family oligosaccharides (RFOs), a major component of the fiber-rich diet that our mice were fed, as well as many standard mouse chows (Vasquez et al. 2021). Though this study focuses on understanding the shifting

genetic determinants of colonization over time, we recognize that the effect of diet is intrinsic to the results of any gut microbiome study.

Global Bt gene expression stabilizes after one week of colonization

In contrast to the 277 DEGs identified between D0.5/D1 and D2/D4, we found only 21 DEGs that met our criteria between D2/D4 and D7, and only 7 between D7 and D14/D42 (Table S1.10). Of the DEGs between D2/D4 and D7, the only one that mapped to any KEGG pathway was in the PUL24 operon, and similarly, 5 of the 7 DEGs between D7 and D14/D42 fell into the PUL24 operon. Thus, we infer that *Bt*'s transcriptional profile has largely stabilized within the first week of colonization and is maintained thereafter, excepting the continued upregulation of certain PUL genes.

Upregulation of α-galactosidase activity confers a significant growth advantage to Bt in GF mice fed a standard RFO-rich diet

Our functional genetics screen confirmed the importance of PUL24: around four days after introduction of the RB-Tn mutant library into GF mice, the diversity of the community begins to collapse due to strong positive selection for a small pool of mutants that seemed to have gained fitness from the Tn insertion (Fig. 1.4A). This could be caused by RB-Tn

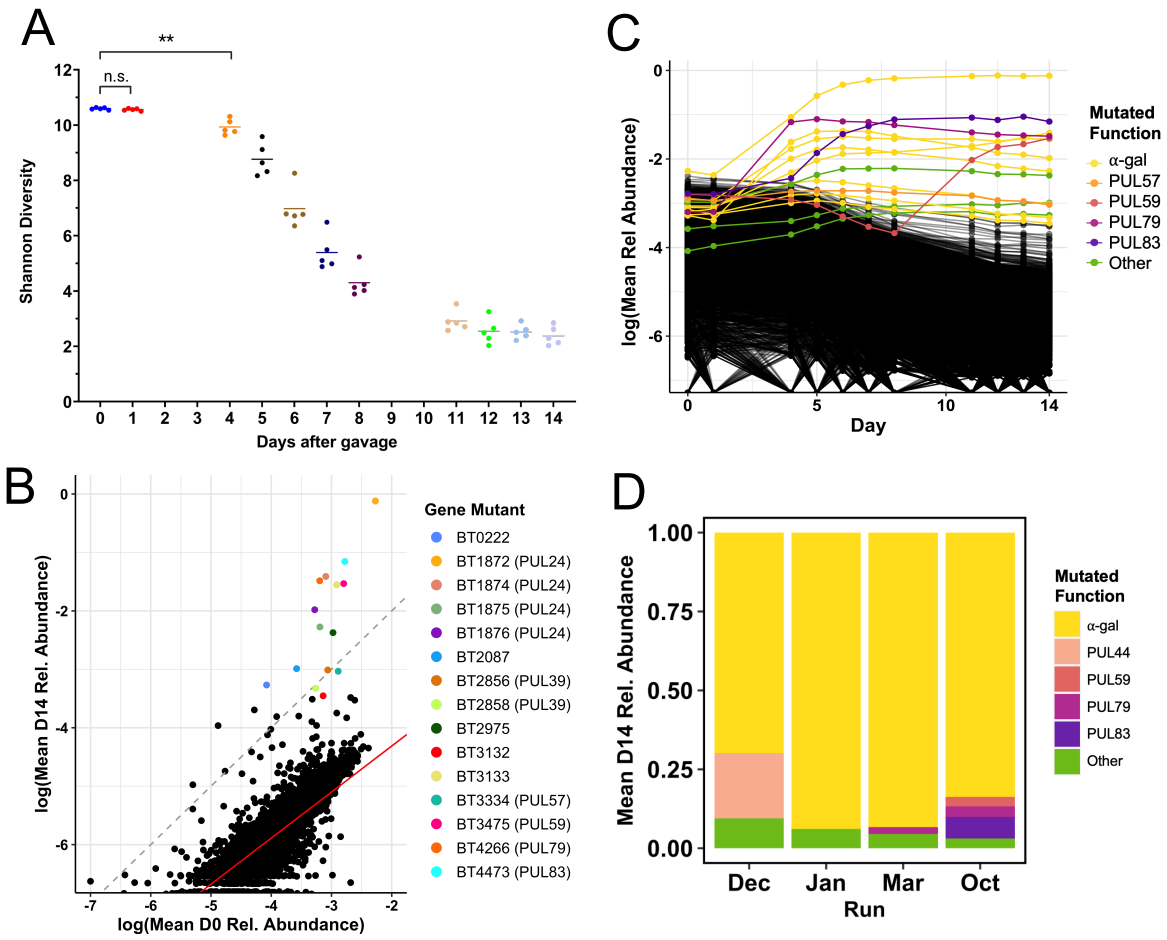

Figure 1.4: Colonization of a complex *Bt* mutant library within GF mice selects for disruptions upstream of α-galactosidase genes. (A, B, D) represent data from a single experimental run (October). **(A)** Shannon diversity of the RB-Tn mutant pool in mice over time. Each point represents the RB-Tn pool within a single mouse on a particular day (**$p < 0.01$). **(B)** Initial (inoculum, D0) versus final (D14) relative abundance of RB-Tn mutant strains. Each point represents the summed relative abundance of all mutant strains that mapped to given gene, averaged across mice. Dashed grey line designates a 1:1 relationship between starting and final abundance; red line represents a linear regression best-fit line generated from the log-transformed data ($p < 2e\text{-}16$, $R^2 = 0.6461$, Methods). **(C)** Relative temporal abundance of RB-Tn mutant strains. Each line represents the summed relative abundance of all mutant strains that mapped to a given gene, averaged across mice. Top 15 most abundant gene mutants at D14 are colored by the PUL to which they mapped; all others are black. **(D)** D14 relative abundance of gene mutants mapping to operons that encode α-galactosidase functions (yellow), known PULs, or other gene functions averaged across mice for each experimental run.

insertions in regulatory elements, or by polar effects on downstream genes driven by readthrough from the antibiotic resistance promoter of the RB-Tn insertion (Liu et al. 2021). RB-Tn mutants with insertions in PUL24 were among the most positively selected mutants at the end of the two-week experiment, exhibiting growth that exceeded a neutral expectation that final abundances would simply reflect initial abundances in the inoculum (Fig. 1.4B). Furthermore, most of the hyperfit mutants had Tn insertions in one of three operons: PUL24 (BT1871-1877), PUL39 (BT2851-2860), or BT3130-3134, all of which encode at least one α-galactosidase, situated at the tail end of the operon. At the end of the RB-Tn selection experiments, the populations were overtaken by mutants carrying Tn insertions upstream of these α-galactosidase genes (Fig 1.4C). This was true for all four independent experimental cohorts, which were performed months apart from one another (Fig 1.4D).

This RB-Tn pool has previously been assayed in over 300 different conditions including distinct carbon or nitrogen sources and specific stress conditions (Liu et al. 2021). The mutants that we identified as hyperfit in GF mice exhibit a phenotype significantly deviant from WT in only two conditions: within GF mice and in defined culture with melibiose—a disaccharide of glucose and galactose, and a breakdown product of the trisaccharide raffinose (Fig. S1.3A)—as the sole carbon source. In both cases, these mutants exhibit a growth advantage. Indeed, when we isolated the most abundant strains from D14 of the RB-Tn

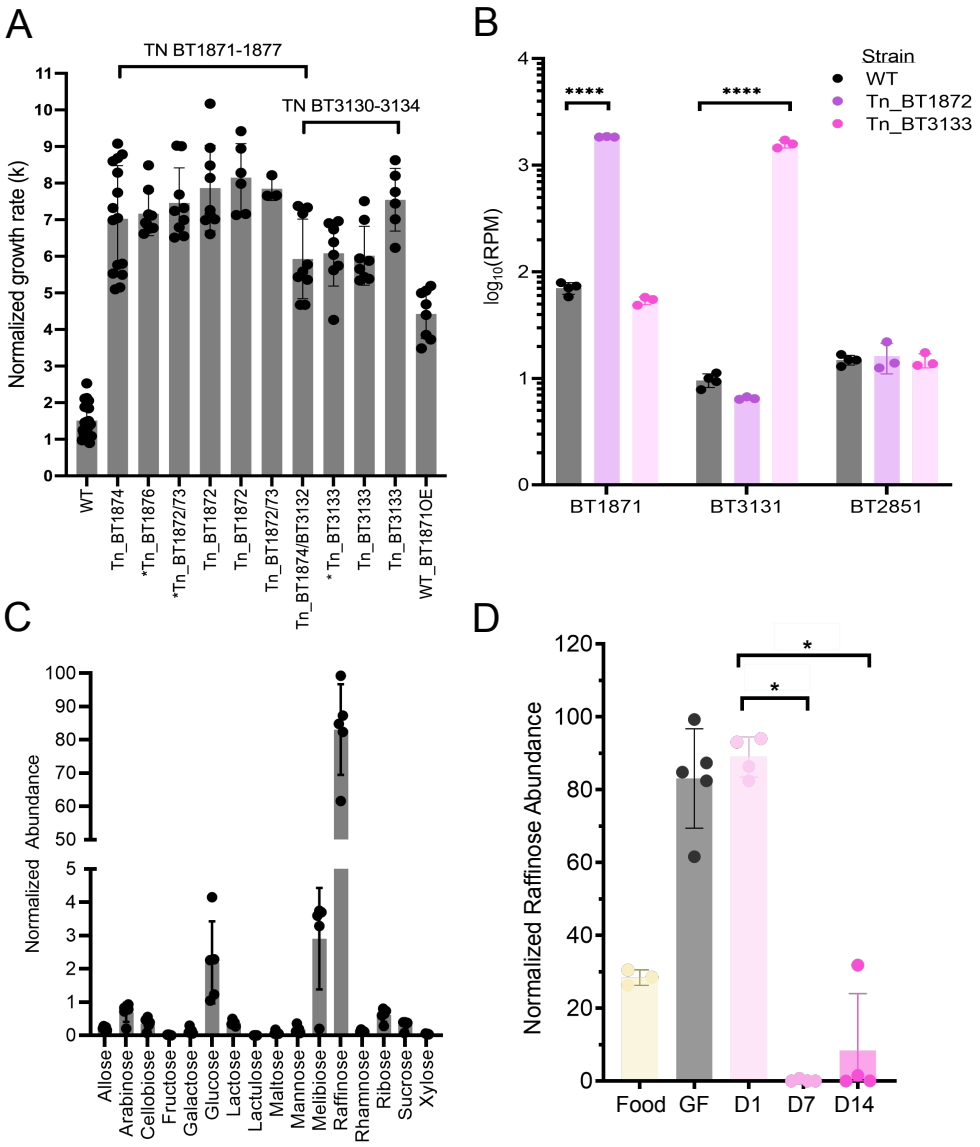

Figure 1.5: Upregulation of α-galactosidase activity confers a significant growth advantage to Bt in GF mice fed a standard RFO-rich diet. (**A**) Log phase growth rates (k) of the most abundant RB-Tn mutant strains isolated from mice and grown in melibiose minimal media. Strains with asterisks carry other mutations in addition to the transposon insertion. The WT + BT1871OE strain carries a plasmid copy of BT1871 expressed from the *rpoD* promoter that was integrated into the WT genome at the attN1 site. All mutant strains grew significantly faster than WT ($p < 0.0001$). (**B**) Normalized abundance of α-galactosidase mRNA (RPM) measured in WT and hyperfit RB-Tn mutants isolated from mice and grown in Varel-Bryant defined medium with 20 mM melibiose as the sole carbon substrate.(Varel and Bryant 1974) (**C**) Abundance of various sugars in the GF mouse cecum as measured using GCMS and normalized to internal standards. (**D**) Abundance of raffinose in the standard chow fed to GF mice, within GF ceca before colonization, or 1, 7, or 14 days post-colonization. (*$p < 0.05$; **$p < 0.01$; ***$p < 0.0001$, ****$p < 0.00001$) See also Table S1.11 – S1.16.

experiment, we found that their growth rate was significantly higher than WT when melibiose is the sole carbon source (Fig. 1.5A, Table S1.11). In this condition, *Bt* must hydrolyze the α-1,6 glycosidic bond to harvest and metabolize the monosaccharide sugars. The competitive advantage of these mutants cannot be attributed to either of the monosaccharides or to hydrolysis of α-1,2 glycosidic bonds, as the mutant growth rates on these carbon substrates (glucose, galactose, and sucrose) are indistinguishable from WT (Fig. S1.3B). In raffinose medium, which contains both α-1,2 and α-1,6 linkages, mutants exhibit an attenuated but still significant growth advantage (Fig. S1.3B, p=3.9e-05, t-test, n=4-6).

Given that release of the monosaccharide sugars of melibiose depends on hydrolysis of an α-1,6 glycosidic bond, we hypothesized that the fitness phenotypes both in mice and *in vitro* did in fact depend on overexpression of the α-galactosidase gene downstream of the Tn insertion site. To test the hypothesis that the transposon insertion enhanced expression of downstream genes, we grew WT and hyperfit mutants in melibiose medium and measured the expression of α-galactosidase genes. For this experiment, we used two mutants, one carrying an insertion in PUL24 and another carrying an insertion in the BT3130—3134 operon. For both mutants, we found $>$ 10-fold overexpression of α-galactosidase downstream of the insertion but within the same operon (Fig. 1.5B, BT1871: p $<$ 1e-6, t-test; BT3131: p=4e-6, n=3-4/group). Meanwhile, expression of an α-galactosidase (BT2851) located outside the operons that carry the insertion was similar between WT and the mutants.

We then overexpressed BT1871 from a strong, constitutively active promoter (P_{rpoD}) in WT *Bt*, and observed a three-fold increase in log phase growth rate relative to WT when melibiose was the sole carbon source (Fig. 1.5A, Table S1.11). We note that even this constitutive-expression mutant did not exhibit as much of growth advantage as the RB-Tn mutant strains. It is possible that the RB-Tn strains may have evolved additional mutations that further promote growth on melibiose media, although we identified no new junctions suggesting genomic rearrangements and no changes in coverage suggesting duplications in whole-genome short-read sequencing of RB-Tn isolates. Alternatively, the promoter used in front of the erythromycin resistance cassette in the RB-Tn mutants may simply be stronger than the P_{rpoD} promoter we used here.

Metabolomic measurements of a carbohydrate panel confirm that raffinose and its constituent sugars are among the most abundant carbohydrate substrates within the ceca of GF mice fed a standard chow (Fig. 1.5C). Although mammals can catalyze hydrolysis at the α-1,2 linkages in raffinose and sucrose, the α-1,6 linkages in raffinose and melibiose can only be hydrolyzed by gut microbes (Fig. S1.3A) (Adamberg et al. 2018). Accordingly, raffinose and melibiose build up in the cecum of our GF mice at high concentrations until *Bt* is introduced. After 7 days, during which time *Bt* has initiated overexpression of α-galactosidase genes, these sugars are depleted (Fig. 1.5D, $p = 0.02857$, Wilcoxon test, n=4, Fig. S1.3C, $p = 0.006193$, t-test,

n=4). In contrast, sucrose is consumed by the host and no significant changes are observed in sucrose concentration following *Bt* colonization (Fig. S1.3D).

Together, we find that when mice are fed standard high-fiber chow, the high concentration of RFOs accumulating in the lower GI tract creates an environment that strongly selects for *Bt* strains that can make efficient use of these sugars through increased expression of α-galactosidases. We infer that efficient carbohydrate metabolism—particularly for abundant dietary fibers—is a major determinant of population-level selective dynamics during the persistence phase of *Bt* engraftment within the gut.

Changes in resource-use strategies coincide with shifts in Bt localization from the mucus towards the lumen

Our previous analyses showed that early in colonization (through ~D7), *Bt* upregulates diverse PULs including many predicted to enable degradation of host-derived mucosal glycans (Martens, Chiang, and Gordon 2008), whereas later on, *Bt* experiences strong positive selection for efficient metabolism of a dietary polysaccharide. We hypothesized that this shift in metabolic preferences from host-derived to dietary resources might reflect differences in microbial localization relative to the colonic mucus layer and lumen. To assess *Bt* localization at D1, D2, D4, D7, and D42 of colonization, we labeled fixed colonic cross-sections with antibodies to MUC2, the predominant colonic mucin (Johansson, Sjövall, and Hansson 2013),

and the DNA stain 4',6-diamidino-2-phenylindole (DAPI), and imaged with a laser-scanning confocal microscope. We then quantified the average epithelial proximity of *Bt* by measuring the distance from the epithelial surface along perpendicular tracts to the nearest bacterial cell (Materials and Methods).

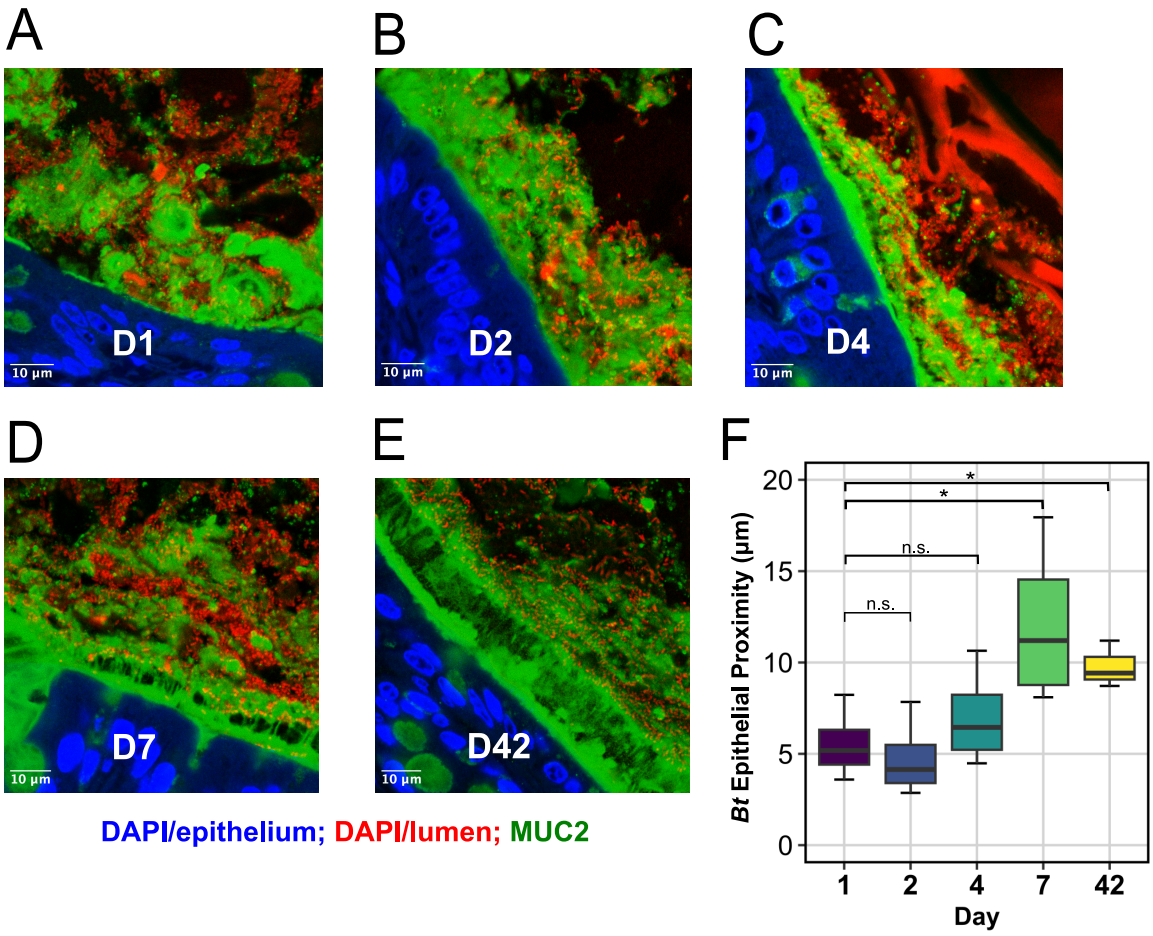

Figure 1.6: *Bt* localization shifts from the mucus towards the luminal space over colonization. Representative cross-sections of distal mouse colon fixed in Carnoy's solution at **(A)** D1, **(B)** D2, **(C)** D4, **(D)** D7, **and (E)** D42 of colonization by *Bt*. Blue, DAPI staining in the epithelium; red, DAPI staining in the lumen of gut, including bacteria, debris, and shed host nuclei; green, antibody staining for MUC2. Scale bars: 10 µm. **(F)** Mean bacterial penetration (µm from epithelium; n=3-4/group, t-test, *p < 0.05).

At D1 and D2, *Bt* was deeply embedded within a largely unstructured mucus layer, often directly adjacent to the epithelium (Fig. 1.6A, 1.6B). By D4, an observable but thin and patchy inner mucus layer began to form (Fig. 1.6C), which expanded in thickness by D7 (Fig. 1.6D). This layer still allowed substantial penetration by *Bt*, although epithelial proximity was significantly reduced compared to D1 (Fig. 1.6F, p=0.037, t-test, n=4/group). At D42, a defined inner mucus layer covered the epithelial surface of each cross-section, effectively excluding *Bt,* which localized primarily to the shedding outer mucus layer and luminal space (Fig. 1.6E, 6F, p=0.024, t-test, n=3-4/group). Thus, we have identified a loose correlation between the timing of shifts in *Bt* resource use strategies and its spatial localization with respect to the mucus layer and luminal space.

Strong selection for efficient RFO metabolism leads to emergence of spontaneous Bt mutants with duplicates of the BT1871 locus through an IS3-family transposable element

The transposon mutants in our functional genetics experiment were able to gain ~10-fold increase in α-galactosidase expression due to readthrough from an extremely strong, synthetic promoter. We wondered if the selective pressure for elevated α-galactosidase activity to utilize the α-1,6-linked sugars abundant in the diet would drive evolution of a spontaneous mutant with enhanced α-galactosidase activity. One week after the initial colonization of GF mice with WT *Bt* in an ongoing transcriptomics experiment, three mice from two cages were separated into individual cages for six weeks of observation, a length of time predicted to be

sufficient for spontaneous mutations to arise and stabilize (Dapa et al. 2022). At the end of six weeks, we performed shotgun metagenomic sequencing on fecal material from all three mice. Assembly of the short-read sequences revealed that there was at least 2x coverage of the BT1871 locus for all samples (Fig. 1.7A). A dip to 1x coverage in the middle of this region mapped to an IS3-family transposase, of which there are six other identical copies in the genome; hence, the corresponding coverage was diluted among the different copies. breseq analysis identified three new junctions in the *Bt* genome indicative of genome rearrangements (Fig. 1.7B). Notably, samples from Mouse A and Mouse C, which were co-housed during the first week of the experiment, shared an identical junction, suggesting that this mutation arose in *Bt* within the first week of colonization and was transmitted across mice. Samples from Mouse B and Mouse C each possessed unique junctions, indicating that these junctions arose independently. In all, three independent junctions spontaneously evolved in this experiment, and all three junctions were formed between either BT1872 or BT1873 and a locus downstream of BT1871, which encodes for rRNAs, tRNAs, and a ribosome recycling factor. All three new junctions occupied a significant portion of the sequencing reads (60-73%), suggesting that the mutants carrying these junctions were competitively dominant in the gut environment.

IS3-family transposases are known to act by a copy-and-paste mechanism (Chandler et al. 2015). We wondered if this transposase, which we had identified as significantly upregulated

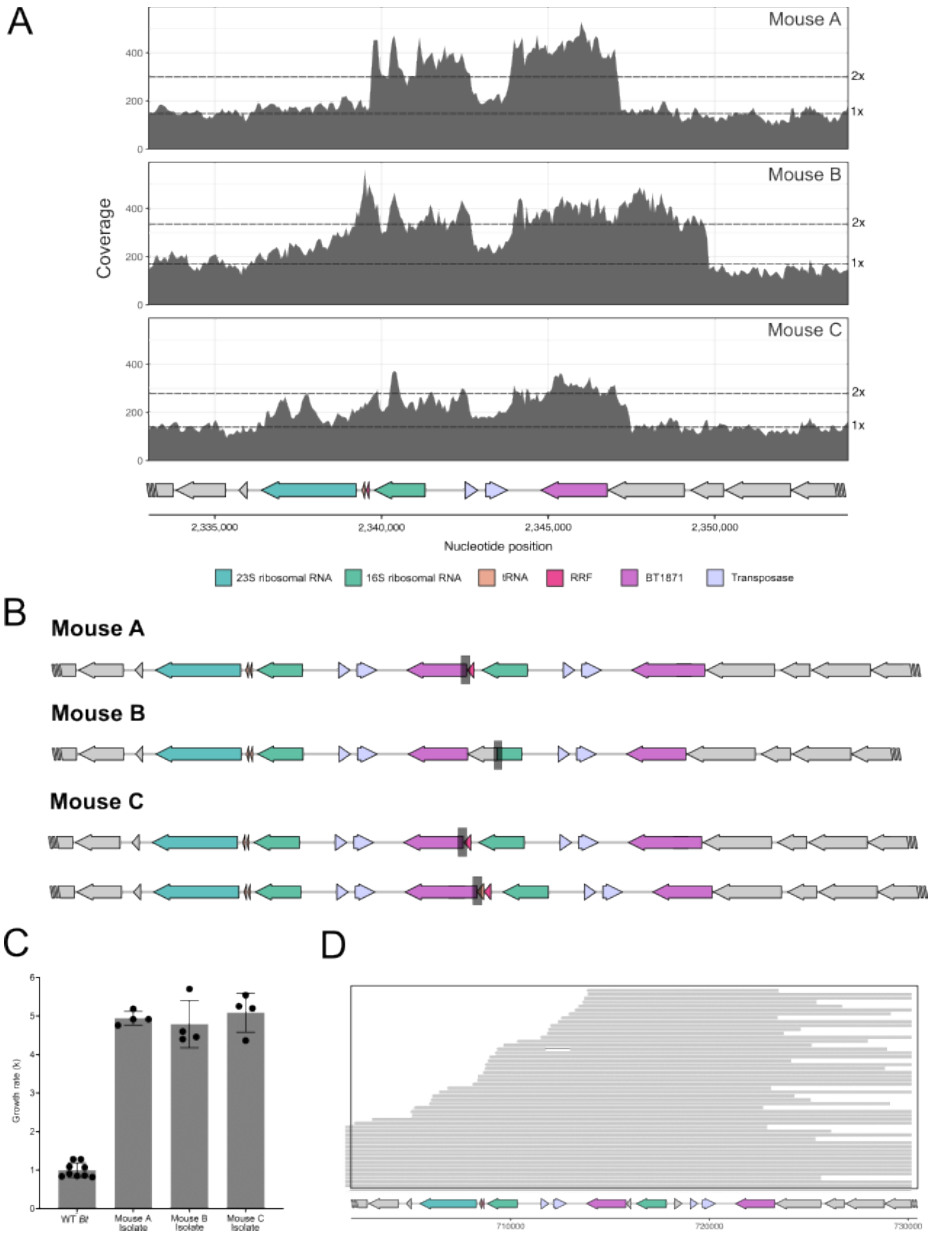

Figure 1.7: Under strong selective pressure, *Bt* duplicates the BT1871 locus with the help of a transposable element. (**A**) Shotgun whole genome sequencing of bulk fecal sample from three mice inoculated with WT Bt shows at least 2x coverage of the BT1871 locus. (**B**) For each mouse, breseq analysis of the shotgun whole genome sequencing identified a new junction joining a segment up- and downstream of BT1871 in 60-70% of the reads. (**C**) Log phase growth rates (k) of 3 mutant strains isolated from feces of mice colonized with WT *Bt* for 6 weeks compared to growth rate of the ancestral WT *Bt* in defined medium supplemented with melibiose (n=4 technical replicates per strain). **(D)** Long-read MinION sequencing of an abundant mutant in Mouse C (MZ65) reveals the duplication of a long segment including the BT1871 gene, which generates a tandem repeat of the locus. Each gray bar represents a single long read, which together span the region containing the tandem repeat.

from D0.5/D1 – D2/D4 (Table S1.10), could have created multiple copies of the BT1871 locus. We isolated individual strains likely to contain these mutations by plating bulk fecal material and then selecting a single strain from each mouse that exhibited a growth advantage compared to WT on melibiose medium (Fig. 1.7C). We then performed long-read sequencing of each strain with MinION. In one of these isolates, we identified a tandem repeat of the BT1871 locus (Fig. 1.7D), which places the original copy of BT1871 downstream of a strong rRNA promoter. Interestingly, the six identical copies of this IS3-family transposase (NCBI gene ID: 60924995) are often found adjacent to PULs in the WT *Bt* genome. This suggests that these transposable elements confer a mechanism to modulate gene expression that may be advantageous in adapting to new metabolic landscapes.

Interactions with the host are relatively consistent throughout colonization

Although the host response to monocolonization is not the focus of this paper and has been thoroughly catalogued elsewhere (Macpherson and Harris 2004; Bunker et al. 2017; Peterson et al. 2007; Hapfelmeier et al. 2010), we assessed levels of cecal IgA and serum IgG, as well as several pro-inflammatory cytokines from colonic mucosal scrapings. We identified no significant or consistent trends in any of these metrics (Fig. S1.4). Previous work has outlined how IgA binding to commensal bacteria like *Bt* may impact gene expression, in some cases affecting dietary polysaccharide usage and microbial localization (Joglekar et al. 2019;

Nakajima et al. 2018; Peterson et al. 2007; Huus et al. 2020). We could not recapitulate these specific changes in our *Bt* gene expression timecourse, which may suggest that *Bt*'s response to IgA binding is sensitive to the specific mouse chow composition and availability of dietary resources.

We then performed targeted GSEA on expression of *Bt*'s capsular polysaccharide (CPS) loci, which encode outer membrane proteins that mediate interaction between *Bacteroides* genera and the host immune system (Mazmanian, Round, and Kasper 2008) and have been shown previously to play a critical role in *Bacteroides* gut colonization (Coyne et al. 2008; Goodman et al. 2009; Porter et al. 2017). We found that CPS loci 1 and 3, and to a lesser extent, 2, 4, and 7, were highly expressed early in colonization, and then downregulated, whereas CPS5 and 6 had increasing relative expression from D7 onward (Fig. S1.5A-D). Only CPS4 mutants showed severe fitness defects during the early days of the functional genetics assay, in line with previous reports (Fig. S1.5E) (Goodman et al. 2009). These data indicate that *Bt* modifies its outer membrane upon entry into the gut and over the course of persistence, which may reflect adaptation to the host immune system, perhaps in parallel to shifts in localization.

1.5 DISCUSSION

Microbial adaptation during colonization is a dynamic process

Bacteroides species are dominant and prevalent in the guts of many human populations (Human Microbiome Project Consortium 2012; Qin et al. 2010). Instrumental to their success is their ability not only to tolerate stress, but to quickly adapt in order to grow under a range of conditions (Kuwahara et al. 2004; Guo, Kitamoto, and Kamada 2020). Although *Bt* has been used as a model organism to understand the genetic drivers of gut colonization for commensal organisms (Goodman et al. 2009; Wu et al. 2015; Townsend et al. 2020), a single representative timepoint has been assessed in most previous investigations, which fail to consider the dynamism of the adaptational process. For example, whereas previous work characterized *Bt* as exhibiting constant, rapid growth in the gut based on gene expression at a single timepoint, our time course data suggest that *Bt* undergoes a temporally dynamic adaptational program (J. L. Sonnenburg et al. 2005). We show that *Bt* prioritizes biosynthesis of amino acids and other essential compounds early in colonization, before ramping up expression of a diverse array of PULs, and ultimately centering metabolism around degradation of a single abundant dietary carbohydrate. This may reflect a transition from an initial stress response during establishment in the gut to a more growth-focused strategy that surveys and optimizes utilization of available environmental resources. We find that the set of genes required for *Bt* to initially establish colonization in the gut are distinct from those

required to persist (Fig. 1.1). The results presented here suggest that because of the rapidly shifting adaptational profile exhibited by microbial populations over the course of colonization, investigators must take care in selecting the appropriate timepoints to address their experimental questions.

Early colonization is a distinct adaptational phase

The process of colonizing a new host presents a diverse array of environmental changes that require physiological adaptation. The largest transcriptomic changes that we observed across six weeks of *Bt* colonization occurred in the first week (Fig. 1.1B), as did the largest shifts in RB-Tn mutant abundances (Fig. 1.1C). Our findings indicate that *Bt* upregulates a broad swath of metabolic processes upon arrival in the lower GI tract during the earliest stage of colonization (Fig. 1.2B). Work from Watson *et al.* examining the qualities of microbes that successfully colonize the gut after fecal microbial transplant suggests that microbes that can be metabolically "self-sufficient" may be better suited to engraft and persist in a new host environment (Watson et al. 2023). We show that, similarly, *Bt* casts a wide metabolic net upon gut entry, upregulating carbohydrate metabolism, energy metabolism, vitamin and cofactor biosynthesis, and especially amino acid biosynthesis. We likewise see that *Bt* upregulates a diverse array of PULs during early colonization (Fig. 1.3). This may better

enable *Bt* to survive conditions of resource scarcity until a more energetically efficient transcriptional program can be fine-tuned to the particulars of its new resource landscape.

Selection for efficient carbohydrate metabolism drives long-term persistence

During the later stages of colonization and persistence, *Bt* re-centers its metabolism around carbohydrate utilization. These results add to a growing body of work identifying metabolic necessity in general, and carbohydrate metabolism in particular, as powerful drivers of microbial fitness and evolution in the gut. For instance, one study showed that *E. coli* evolves mutations to modulate carbohydrate utilization depending on dietary conditions (Crook et al. 2019), while another identified selection for mutations in either amino acid or carbohydrate metabolism depending on the competitive context (Barroso-Batista et al. 2020). Research using *Bt* has demonstrated rapid evolution of divergent metabolic strategies depending on mouse diet (Dapa et al. 2022). One study even showed how microbial competitive fitness in the mouse gut can be promoted by engineering a unique PUL into *Bt* and introducing the strain in combination with its associated carbohydrate substrate (Shepherd et al. 2018). Although microbes mediate competition in a number of ways ranging from direct attack to occupation of physical space to indirect interactions via the host (Hibbing et al. 2010), these findings collectively suggest that competition for scarce metabolic resources is a primary evolutionary battleground within and among microbial species in the gut ecosystem.

In these experiments, we identified strong selective pressure for improved utilization of a specific carbohydrate resource. However, previous work shows that genetic drift and transmission of microbes between hosts can significantly impact the evolution and spread of mutant populations (Vasquez et al. 2021). Therefore, it is important to consider how transmission between hosts may have impacted our results. In our RB-TnSeq experiments, mice were co-housed, facilitating intra-cage transmission. This may have artificially inflated the replicability of our results within cages, although we still saw near-identical trends emerge across 4 independent experiments and 8 independent cages.

Shifts in microbial localization may drive metabolic selective pressures and vice versa

We found that changes in *Bt* resource use over the course of colonization paralleled shifts in its localization from the inner mucus layer towards the luminal space (Fig. 1.6). This aligns with previous work showing that the mucus of GF mice is permeable to bacteria and takes up to 6 weeks of conventionalization to fully mature into the impermeable protective state that excludes *Bt* and most other gut commensals (Johansson et al. 2015; 2008). We hypothesize that this shift in localization may be responsible for the distinct selective pressures that favor PUL24 and RFO metabolism.

Previous *in vivo* mouse studies with *Bt* have demonstrated that dietary microbiota-accessible carbohydrate (MAC) deficiencies select for the upregulation of mucosal glycan foraging and

concomitant localization to and degradation of the mucus layer (J. L. Sonnenburg et al. 2005; Earle et al. 2015; Desai et al. 2016; Hayase et al. 2022; E. D. Sonnenburg and Sonnenburg 2014). Our work suggests the reverse may occur during conventionalization in an environment with abundant dietary MACs: after a brief adjustment period at D0.5/1 to satisfy pressing metabolic demands, *Bt* is gradually excluded from the mucus layer and moves into the lumen, shifting metabolism from broad mucosal glycan foraging while embedded (D2/4) towards hyperutilization of a single abundant dietary resource while excluded (D7-42). Although these results are correlative and require more rigorous follow-up to establish a causal relationship between localization and resource use, they provide preliminary support for the notion that the spatial localization and metabolic profile of *Bt* are deeply intertwined, flexible, and highly responsive to the specific balance of selective pressures like resource availability and energetic efficiency. These factors will doubtless be heavily impacted by the presence of additional community members. Nevertheless, we conclude that resource-use profiling and localization may emerge as particularly informative descriptors of available niche space in the gut.

IS3 transposable elements: a novel mechanism to modulate expression of specific CAZymes?

In GF mice fed a standard RFO-rich diet, the selective pressure for mutants with increased α-galactosidase activity is intense. Mutations in the BT1871 locus were consistently positively selected when WT *Bt* evolved in mice for six weeks. In all three mutant populations, the

downstream side of the duplicated region ends midway through a ribosomal gene, meaning that there are no known transcriptional terminators between the ribosomal promoter and the α-galactosidase gene, BT1871. It is likely that these mutants have increased α-galactosidase activity due to readthrough from the strong ribosomal promoter in the upstream copy of the locus. Though increased α-galactosidase could be simply due to the presence of two copies of BT1871, the growth phenotype that these mutants exhibit, in which log phase growth is 5 times faster than WT, is on par with that of the RB-Tn mutants, for which α-galactosidase expression was more than 10 times greater than in WT.

In *Bt,* identical copies of this IS3 transposable element occur in seven locations, often adjacent to PULs and almost always paired with a ribosomal gene. These genes were upregulated at D2/D4 of our transcriptomics experiment, shortly before we saw extensive upregulation of PUL24 genes. It is well known in both mammals and prokaryotes that transposable elements can modulate the expression of nearby and distant genes (Siguier, Filée, and Chandler 2006). Transposable elements may be selected for because the genetic "cargo" that they shuttle along (such as an antibiotic cassette) is beneficial to the organism or because the position where the insertion occurs results in some downstream effect that is beneficial to fitness. Both reasons may contribute to the selection of the tandem duplication of the BT1871 locus. Future studies will be necessary to investigate whether other IS3 elements in *Bt* perform similar functions in

modulating expression of nearby genes and whether such a mechanism can be found in other families of bacteria.

Limitations of the study

One limitation of this study is that many microbial genes are poorly annotated. At most of our transcriptomic timepoints, only a minority of the DEGs have known annotations, but those un-annotated genes may still serve meaningful adaptive functions. These genes (Table S5B) would be excellent candidates for continued functional characterization through controlled *in vitro* and *in vivo* experiments. We also note the key limitation that this study was performed in a highly simplified monocolonization model. While these results provide evidence of general eco-evolutionary principles and highlight important considerations for understanding microbial GI colonization more broadly – e.g. the dynamism of the adaptational process and the importance of choosing timepoints carefully, the remarkable genetic mutability of bacteria, and the feedback cycles between a microbe and its resource environment – the specific results presented here may not directly apply to scenarios with more complex microbial communities. However, by eventually comparing these results to those from more complex communities, this dataset can provide even greater insight into how host-microbe interactions and inter- and intra-specific microbial interactions each contribute to the adaptational process.

1.6 ACKNOWLEDGMENTS

We thank Hualan Liu for invaluable experimental help with the RB-TnSeq libraries. We thank David Hershey and A. Murat Eren for helpful scientific input. We also thank the Chang lab members for scientific support received. This work was performed with support from NIH T32DK007074 (M.Z., M.S.K.), NIH RC2DK122394 (E.B.C.), NIH T32GM007281 (M.S.K.), and the Host-Microbe and Tissue and Cell Engineering cores of the UChicago DDRCC, Center for Interdisciplinary Study of Inflammatory Intestinal Disorders (C-IID) - (NIDDK P30 DK042086).

CHAPTER 2

Western diet impairs gut microbiome resilience to antibiotic perturbation

Co-authors: Kennedy, M., Cooper, M., St. George, M., DeLeon, O., Kalski, M., Cham, C., Bergelson, J.B., Chang, E.B.

Contributions: Conceptualization, M.S.K., E.B.C., and J.B.; Methodology, M.S.K., E.B.C.; Formal Analysis, M.S.K., O.D.; Investigation, M.S.K., M.C., M.S.; Data Curation, M.S.K.; Writing – Original Draft, M.S.K; Writing – Review and Editing, M.S.K., E.B.C., J.B.; Visualization, M.S.K.; Funding Acquisition, E.B.C.

2.1 ABSTRACT

An extensive body of work shows that high-fat, Western-style diets (WD) induce microbiome "dysbiosis" characterized by reduced taxonomic diversity and metabolic breadth, which in turn increases risk for a wide array of metabolic and immune pathologies like obesity, diabetes, NAFLD, and IBD. A largely unexplored consequence of diet, however, is its effect on the resilience of the microbiome after an acute perturbation like antibiotic treatment in which the native community is severely knocked down. Impaired microbiome resilience could entail either a further loss of diversity or transition to an alternative compositional state that may augment risk for infection or other dysbiosis-associated pathologies. Here, we evaluate the impact of WD versus standard, regular chow ("RC") diet on microbiome resilience to a short course of antibiotics. We find that mice on WD experience more severe ecosystem collapse after antibiotic treatment, and that recovery is slower compared to mice on RC. Although the microbiome of mice on WD retains functional diversity after antibiotic treatment, they lose functional redundancy. Mice on RC appear to undergo a successional process of recovery, traversing intermediate taxonomic and functional stages, whereas mice on WD do not. From intervention experiments in which we control post-antibiotic diet and microbial re-exposure, we find that dietary resource environment plays a more central role in microbiome recovery than microbial re-seeding, subverting common wisdom about the use of microbial transplant for microbiome restoration. Finally, we show that prolonged post-antibiotic dysbiosis in mice on WD renders them susceptible to infection by *Salmonella enterica* serovar Typhimurium for

at least 2 weeks after antibiotic treatment has ended. In sum, these results suggest that diet plays a pivotal role in the restitution of a damaged microbiota.

2.2 INTRODUCTION

The gut microbiome is an essential organ of the human body that functions at the nexus of metabolic (Nieuwdorp et al. 2014; Asnicar et al. 2021; Turnbaugh et al. 2006) and immune (Levy et al. 2017) homeostasis and is increasingly recognized for its contributing role in a wide variety of health and disease states(Shreiner, Kao, and Young 2015). Understanding which qualities define a robust, functionally healthy microbiome and how to transition from an unhealthy "dysbiotic" microbiota towards a healthy state have been longstanding goals of the microbiome field (Eisenstein 2020; Bäckhed et al. 2012; Wong and Levy 2019). However, to date, most therapeutic strategies for microbiome reconstitution have seen only limited success (Suez and Elinav 2017).

The vast majority of microbiome-based therapies that have progressed to clinical trials or public use, such as fecal microbiota transplant (Cohen and Maharshak 2017), probiotics (Ritchie and Romanuk 2012), or other live biotherapeutics (O'Toole, Marchesi, and Hill 2017), center around transplanting exogenous, putatively beneficial microbes into a dysbiotic ecosystem with the hope that these will engraft in the community, shift the ecosystem balance, and restore eubiosis. This approach neglects the basic ecology of the gut microbial ecosystem in many respects: a microbe that is ill-adapted to the specific resource landscape of

a given environment, especially relative to resident competitors, will fail to establish in that community and is unlikely to have lasting therapeutic impact (Xiao et al. 2020; Walter, Maldonado-Gómez, and Martínez 2018; Maldonado-Gómez et al. 2016). This oversight may contribute to the high variability in therapeutic outcomes that has plagued the application of microbiome-based therapies to pathologies like irritable bowel syndrome or inflammatory bowel disease (Ianiro et al. 2022; Reinisch 2017; Thaiss and Elinav 2017; Ford et al. 2018). Efficacious strategies for precision microbiome reconstitution must address both "seed and soil:" not only which microbes are present or introduced into an ecosystem (Wilson et al. 2019; McFarland, Evans, and Goldstein 2018), but also the resource environment that they encounter there, and whether or how that resource environment supports their growth and persistence within the community. In this work, we explicitly address the role of resource environment, in the form of host diet, as a driver of microbiome resilience to perturbation. An extensive body of work shows that Western-style diets (WD) high in fat and refined sugar and low in dietary fiber promote microbiome dysbiosis characterized by reduced taxonomic diversity and altered metagenomic functional capacity, with significant impacts on host metabolic and immune function (Bisanz et al. 2019; Devkota et al. 2012; E. D. Sonnenburg and Sonnenburg 2014). A largely unexplored consequence of WD is its effect on emergent functional properties of the microbiome like robustness to and resilience after perturbation. How does WD dysbiosis, which entails both altered microbiome composition and distinct

dietary resource profile, impact the susceptibility of a microbial community to collapse in the face of perturbation, and the ability of that community to recover afterwards?

Antibiotic treatment is an extremely common perturbation of the gut microbiome that severely reduces bacterial biomass while shifting microbiome composition and functional potential (Francino 2016). Despite substantial literature on microbiome recovery after antibiotic treatment (Chng et al. 2020; Dethlefsen and Relman 2011; Laubitz et al. 2021; Palleja et al. 2018; Raymond et al. 2016) and on microbiome response to diet (Bisanz et al. 2019; Albenberg and Wu 2014; David et al. 2014), little consideration has been given to the confluence of these two stressors. Recent work by Ng *et al.* (Katherine Michelle Ng et al. 2019) and by Tanes *et al.* (Tanes et al. 2021) found that a low-fiber diet promotes gut ecosystem collapse after antibiotic treatment and delays microbiome recovery. Although they draw an association between diet and resilience to perturbation, these works do not differentiate between the contributions of microbial re-seeding and dietary resource availability to recovery, and they do not directly interrogate salient phenotypic outcomes of microbiome dysbiosis for the host.

Here, we use a short course of antibiotics as an experimental perturbation in mice on a standard, low-fat, high-fiber regular chow (RC) diet versus WD to evaluate the robustness and resilience of the microbiome under different dietary regimes, characterize the recovery dynamics of these communities, and evaluate the phenotypic consequences for the host. We find that WD severely reduces microbiome robustness to perturbation, and impairs recovery

thereafter, both taxonomically and functionally. We find that the microbiome on RC undergoes a successional pattern of recovery after antibiotic treatment that never materializes on WD, and that intervention by dietary change is a much more potent predictor of recovery in this model than re-introduction of microbial taxa. Finally, we show that persistent post-antibiotic dysbiosis in mice on WD impairs colonization resistance and facilitates infection by the enteric pathogen *Salmonella enterica* serovar *Typhimurium.* The results of this study suggest that the state of the gut resource environment is an indispensable consideration when developing strategies to achieve more consistent and complete microbiome reconstitution.

2.3 MATERIALS AND METHODS

Mice

C57Bl/6 mice at 5 weeks of age were purchased from The Jackson Laboratory barrier facility EM04 for these experiments. All mice were co-housed in cages of 2-4 mice with pine shavings bedding in standard barrier facilities unless otherwise specified. All mice underwent a two-step microbiome homogenization protocol: 1) bedding was mixed across all cages twice a week from age 5-8 weeks leading up to the beginning of each experiment to reduce intra-cohort cage effects, and 2) mice were gavaged once at 6-weeks with fecal material banked from our SPF colony to reduce inter-cohort differences in microbiome composition (Miyoshi et al. 2018). Mice were fed autoclaved standard RC diet (LabDiets 5K67) during microbiome homogenization. All mouse experiments were conducted in accordance with the University of

Chicago Institutional Biosafety Committee and Institutional Animal Care and Use Committee.

Diet Acclimation and Antibiotic Treatment

Mice at 8 weeks of age were either maintained on RC diet (LabDiets 5K67) or switched to WD (Envigo TD.97222 (Howe et al. 2016)) to acclimate for 4 weeks. This diet was designed to broadly reflect the nutritional intake of a Western population based on the Center for Disease Control and Prevention's National Health and Nutrition Examination Survey (NHANES 2009). During diet acclimation, bedding was mixed across cages within diet treatments twice a week. At 12 weeks of age, mice on each diet were treated with a sterile-filtered triple antibiotic cocktail of vancomycin (0.5 mg/ml), neomycin (1.0 mg/ml), and cefoperazone (0.5mg/ml) or 5% sterile PBS control in the drinking water for 72 hours. Water consumption was monitored during this time to ensure adequate treatment (Fig. S2.1).

Western Diet Microbiome Resilience Experiments

Two female cohorts of mice were used in these experiments, in addition to the pilot cohort (below). After treatment with antibiotics or PBS control, mice were maintained on their respective pre-antibiotic diets, and fecal samples were collected for 4 weeks after cessation of antibiotics on days -31, -3, 0, 1-8, 11, 14, 16, 18, 21, 23, 25, and 28. Cages were changed on days -38, -24, -10, 7, and 21. Subsets of mice were sacrificed at the pre-antibiotic (D-3), post-

antibiotic (D0), week two of recovery (D14), or week four of recovery (D28) timepoints (total n=4/timepoint/treatment group).

Western Diet Microbiome Resilience – Pilot/Long-term Recovery Cohort

One cohort of 8-week old female C57Bl/6 mice (n=6/group, RC-ABX and WD-ABX only) was bred in our animal facility for this experiment. Mice were co-housed in cages of 3 mice with pine shavings bedding in standard barrier facilities and did not undergo the microbiome homogenization protocol. Pilot cohort mice were acclimated to their respective dietary treatment for only 10 days. Although 10-days of diet acclimation was predicted to be sufficient for microbiome stabilization, which can occur within 4 days (Carmody et al. 2015), we lengthened the diet acclimation phase in other cohorts to ensure that host physiological differences across dietary groups had stabilized (Turnbaugh et al. 2008). During diet acclimation, bedding was mixed across cages within diet treatments twice a week. Antibiotic treatment was administered as described above. Fecal samples were collected for 9 weeks after cessation of antibiotics on days -31, -3, 0, 0.5, 1, 1.5, 2-8, 11, 14, 16, 18, 21, 28, 35, 49, and 63, and then all mice were sacrificed. Cage changes were performed on days -10, 7, 21, 35, and 49. Experimental duration was decreased after the pilot cohort as microbiome recovery appeared to stabilize by D28 (Fig. S2.2).

Post-antibiotic Intervention Experiments

Four cohorts of female mice were used in these experiments (n=8/treatment group, n=96 total). For each cohort, 24 mice at 5 weeks of age were split across 4 cages (n=6/cage) in standard barrier facilities for 3 weeks of microbiome homogenization. After microbiome homogenization, mice were transferred into 8 hermetically sealed gnotobiotic Techniplast IsoCage P Bioexclusion cages for diet acclimation and antibiotic treatment as described above (n=3/cage). Immediately following antibiotic treatment (D0), mice were transferred into 12 new sterile gnotobiotic cages and post-antibiotic diet and microbial re-exposure treatments were administered (n=2/treatment group/cohort). For microbial re-exposure treatments, fecal material was collected from all mice on the day before antibiotic treatment (D-1), pooled by dietary treatment, resuspended at 60 mg/ml in 25% glycerol solution, and frozen at -80°C until administration. Microbial re-exposures were administered by oral gavage of 200 µl of the respective fecal solution or sterile PBS at 24 hours after cessation of antibiotics (D1) and were re-administered at D14 of recovery after cage changes were performed to ensure that dispersal limitation did not impair microbiome recovery. Fecal samples were collected on days -31, -3, 0, 7, 14, 21, and 28, and mice were sacrificed at D28 post-antibiotics.

All procedures on the IsoCage P rack system from the time of antibiotic administration onward were performed using a modified sterile technique necessitated by the logistics of handling such a large number of treatment groups: one researcher donned sterile garb including two pairs of sterile gloves, the workspace was covered with a sterile drape, and another team member assisted in manipulation of the outside of the cages. The sterile team

member performed all mouse manipulations without making contact with anything outside of the cage or sterile field. In between treatment groups, the sterile team member donned new sterile gloves, but otherwise continued to use the same garb.

Colonization Resistance Experiments

After diet acclimation and antibiotic or PBS administration, 4 cohorts of female mice (n=3-6/treatment group) and one cohort of male mice (n=6/treatment group, RC-ABX-INF and WD-ABX-INF only) were allowed to recover for 14 days, and were then inoculated by oral gavage with 200 µl of either nalidixic acid-resistant *Salmonella enterica* serovar Typhimurium (*St*, strain IR715 (Diaz-Ochoa et al. 2016)) or PBS control. To prepare the gavage solution, *St* was grown aerobically in Luria Broth (LB) media at 30°C with shaking at 250RPM for 14 hours. Cultures were pelleted by centrifuging for 5 minutes at 4000*xg* and resuspended at 1:100 dilution in PBS (final infection dose: ~7 x 10^7 CFU/mouse). Fecal samples and body weights were collected for 4 days post-infection, and then mice were sacrificed.

Tissue Harvest and Sample Processing

All mice were euthanized by CO_2 asphyxiation and death was confirmed via cervical dislocation. After sacrifice, blood was collected by cardiac puncture and serum was isolated and stored at -80°C. Liver, spleen, mesenteric lymph nodes, and mesenteric, gonadal, inguinal, and retroperitoneal fat deposits were weighed and split across samples that were preserved for

histology, snap-frozen for RNAseq, and homogenized for CFU counts. The GI tract was dissected out, the cecum was weighed, and colon length was measured. Sections of the ileum, cecum, and colon were preserved for histology. Luminal contents from each of these sections were homogenized for CFU counting and snap-frozen for metabolomics/DNA extraction, and mucosal scrapings from each section were snap-frozen for RNAseq and/or RT-qPCR.

CFU Counts

Pre-weighed fecal samples were suspended in 500ml of 25% glycerol solution, homogenized for 1 minute in a Mini-BeadBeater-96 (no beads, 2400 RPM), and serially diluted in PBS. Overall bacterial load was quantified by plating on Brain Heart Infusion-Supplemented (BHI-S) agar and incubating aerobically and anaerobically at 37°C for 24 hours. Measurements of overall bacterial load were collected for the pilot cohort, as well as all Colonization Resistance experiments. Although we do not have bacterial biomass measurements for the two non-pilot cohorts of the Western Diet Resilience experiment, the Colonization Resistance experiments were carried out identically to these experiments through D14 post-ABX, and data from these timepoints may therefore be interpreted in the same manner. These data, collected from 5 separate cohorts and 48 mice, recapitulate the bacterial biomass dynamics of the RC-ABX and WD-ABX treatment groups reported in Figure 2.2A (Fig. S2.3). Moreover, they indicate no significant loss of bacterial biomass over the course of the experiment in RC-PBS or WD-PBS controls.

To evaluate *St* load, pre-weighed fecal or tissue samples were homogenized in 25% glycerol solution as described above, and quantified by plating on LB agar with 25ug/ml nalidixic acid and incubating at room temperature for 24 hours.

DNA Extraction

DNA was extracted using the QIAamp PowerFecal Pro DNA kit (Qiagen). Prior to extraction, samples were subjected to mechanical disruption using a bead beating method. Briefly, samples were suspended in a bead tube (Qiagen) along with lysis buffer and loaded on a bead mill homogenizer (Fisherbrand). Samples were then centrifuged, and supernatant was resuspended in a reagent that effectively removed inhibitors. DNA was then purified routinely using a spin column filter membrane and quantified using Qubit.

16S Sequencing

The V4-V5 region within the 16S rRNA gene was amplified using universal bacterial primers – 563F (5'-nnnnnnnn-NNNNNNNNNNNN-AYTGGGYDTAAA- GNG-3') and 926R (5'-nnnnnnnn-NNNNNNNNNNNN-CCGTCAATTYHT- TTRAGT-3'), where 'N' represents the barcodes, 'n' are additional nucleotides added to offset primer sequencing. Approximately ~412bp region amplicons were then purified using a spin column-based method (Qiagen), quantified, and pooled at equimolar concentrations. Illumina sequencing-compatible Unique Dual Index (UDI) adapters were ligated onto the pools using the QIAseq 1-step amplicon

library kit (Qiagen). Library QC was performed using Qubit and Tapestation and sequenced on Illumina MiSeq platform to generate 2x250bp reads.

Shotgun Metagenomics

Libraries were prepared using 100 ng of genomic DNA using the QIAseq FX DNA library kit (Qiagen). Briefly, DNA was fragmented enzymatically into smaller fragments and desired insert size was achieved by adjusting fragmentation conditions. Fragmented DNA was end repaired and 'A's' were added to the 3'ends to stage inserts for ligation. During ligation step, Illumina-compatible UDI adapters were added to the inserts and the prepared library was PCR amplified. Amplified libraries were cleaned up, and QC was performed using a tapestation. Libraries were sequenced on an Illumina NextSeq 500 to generate 1x150 reads.

Metagenomic Analysis

Raw metagenomics reads were trimmed using Trimmomatic (Bolger, Lohse, and Usadel 2014), and a Minoche quality filter (Eren et al. 2013) was applied. Reads from all samples were co-assembled using megahit (D. Li et al. 2015). We then used the anvi'o v7.1 (Eren et al. 2015) metagenomic workflow to compute coverage for each gene across metagenomes, and to refine metagenome-assembled-genomes (MAGs). Briefly, the workflow uses (1) Prodigal v2.6.3 (Hyatt et al. 2010) to identify open-reading frames (ORFs), (2) *'anvi-run-hmm'* to identify single copy core genes from bacteria (n=71) and ribosomal RNAs (n=12) using HMMER v3.3

(Eddy 2011), (3) '*anvi-run-pfams*', '*anvi-run-kegg-kofams*', and '*anvi-run-cazymes'* to annotate ORFs with EBI's PFAM databse (Bateman et al. 2004), the KOfam HMM database of KEGG orthologs (KOs) (Kanehisa and Goto 2000), and the dbCAN CAZyme HMM database (H. Zhang et al. 2018), respectively. We used Bowtie2 v2.3.5.1 (Langmead and Salzberg 2012) to recruit metagenomic short-reads to the contigs, and samtools v1.11 (H. Li et al. 2009) to convert SAM files to BAM files. We profiled the resulting BAM files with '*anvi-profile'* and used the program '*anvi-merge'* to combine all single profiles into a merged profile for downstream visualization. We used *'anvi-export-gene-coverage-and-detection*' to generate coverage tables for downstream analysis in R. '*deseq2*' was used on the exported count data to identify differentially abundant KOs across time points and treatment groups. To identify CAZyme substrate utilization functions, EC numbers from KEGG annotations were used to map to the dbCAN-sub database (H. Zhang et al. 2018). All plots were generated with the R package '*tidyverse*' (Wickham et al. 2019) or GraphPad Prism (GraphPad Software).

Metabolite Extraction from Fecal/Cecal Material

Metabolites were extracted with the addition of extraction solvent (80% methanol spiked with internal standards and stored at -80°C, Table S2.1) to pre-weighed fecal/cecal samples at a ratio of 100 mg of material per mL of extraction solvent in beadruptor tubes (Fisherbrand; 15-340-154). Samples were homogenized at 4°C on a Bead Mill 24 Homogenizer (Fisher; 15-340-163), set at 1.6 m/s with 6 thirty-second cycles, 5 seconds off per cycle. Samples were then

centrifuged at -10°C, 20,000 x g for 15 min and the supernatant was used for subsequent metabolomic analysis.

Metabolite Analysis using GC-EI-MS and Methoxyamine and TMS Derivatization

Metabolites were analyzed using gas chromatography mass spectrometry (GCMS) with electron impact ionization. To a mass spectrometry autosampler vial (Microliter; 09-1200), 100 µL of metabolite extract was added and dried down completely under a nitrogen stream at 30 L/min (top) and 1 L/min (bottom) at 30°C (Biotage SPE Dry 96 Dual; 3579M). To dried samples, 50 µL of freshly prepared 20 mg/mL methoxyamine (Sigma; 226904) in pyridine (Sigma; 270970) was added and incubated in a thermomixer C (Eppendorf) for 90 min at 30°C and 1400 rpm. After samples are cooled to room temperature, 80 µL of derivatizing reagent (BSTFA + 1% TMCS; Sigma; B-023) and 70 µL of ethyl acetate (Sigma; 439169) were added and samples were incubated in a thermomixer at 70°C for 1 hour and 1400 rpm. Samples were cooled to RT and 400 µL of Ethyl Acetate was added to dilute samples. Turbid samples were transferred to microcentrifuge tubes and centrifuged at 4°C, 20,000 x g for 15 min. Supernatants were then added to mass spec vials for GCMS analysis. Samples were analyzed using a GC-MS (Agilent 7890A GC system, Agilent 5975C MS detector) operating in electron impact ionization mode, using a HP-5MSUI column (30 m x 0.25 mm, 0.25 µm; Agilent Technologies 19091S-433UI) and 1 µL injection. Oven ramp parameters: 1 min hold at 60°C, 16°C per min up to 300°C with a 7 min hold at 300°C. Inlet

temperature was 280°C and transfer line was 300°C. Data analysis was performed using MassHunter Quantitative Analysis software (version B.10, Agilent Technologies) and confirmed by comparison to authentic standards. Normalized peak areas were calculated by dividing raw peak areas of targeted analytes by averaged raw peak areas of internal standards. Bile acid assays for cholic acid also included allocholic acid; assays for lithocholic acid also included allolithocholic acid and isolithocholic acid.

RT-qPCR

Total messenger RNA isolated from colonic mucosal scrapings was used with Transcriptor First Strand cDNA Synthesis Kit (Roche Diagnostics Corporation) to obtain cDNA. Real-time qPCR was performed using iTaq Universal SYBR Green Supermix with CFX384 Real-Time System (Bio-Rad). Primers and cycling conditions were derived from Devlin et al., 2022 (Devlin et al. 2022) (Table S2.2). Expression was calculated via ΔCT relative to the housekeeping gene *actb*.

Resource Availability

The data, including all DNA and RNA sequencing datasets, that support the findings of this study are available in this article, the Supplemental Information, and BioProject accession PRJNA992061.

2.4 RESULTS

To determine whether and how diet impacts gut microbiome resilience to antibiotic treatment, 16 cages of 2-4 specific-pathogen-free (SPF) C57Bl/6 mice (n=64 total) at 5 weeks of age underwent a 3 week microbiome homogenization protocol, and were then acclimated to either a standard, low-fat, high-fiber diet (regular chow, "RC") or a high-fat, low-fiber Western diet ("WD") for 4 weeks. We then treated mice on each diet with either a triple antibiotic cocktail ("ABX") or PBS control in the drinking water for 72 hours, and collected fecal samples through 4 weeks of recovery. To evaluate the impact of microbiome resilience on the host, we sacrificed n=4 mice per treatment group (RC-ABX, RC-PBS, WD-ABX, WD-PBS) at D-3 (pre-ABX), D0 (post-ABX), D14, and D28 of recovery (Figure 2.1A, Materials and Methods). To assess long-term recovery, fecal samples were collected from 4 cages of mice on RC-ABX and WD-ABX (n=6/group) through 9 weeks post-ABX (Materials and Methods).

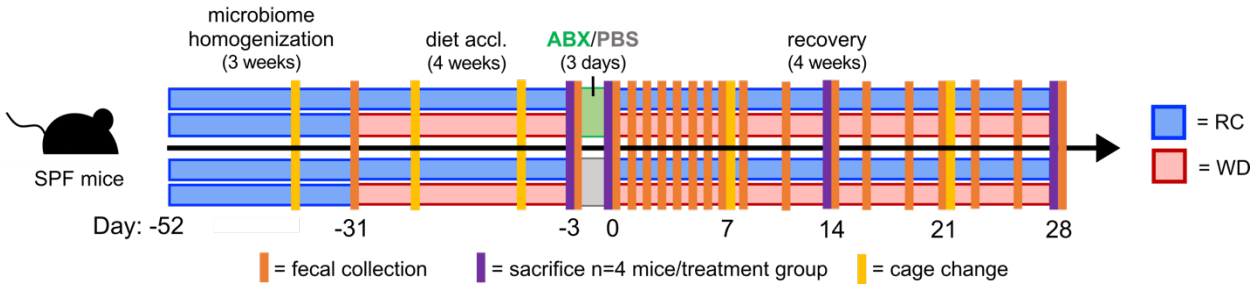

Figure 2.1: Experimental design. Mice on RC or WD were treated with PBS or ABX in the drinking water for 72 hours, and serial fecal samples were collected to assess microbiome recovery (Materials and Methods).

Microbial biomass and taxonomic recovery after antibiotics are impaired in mice on WD

We first assessed gut microbiome resilience to antibiotic treatment across RC and WD in terms of bacterial biomass. We quantified bacterial biomass by counting colony-forming units (CFUs) cultured aerobically and anaerobically on rich media and found that CFU counts dropped precipitously after antibiotic administration for both treatment groups (Figure 2.2A, $q < 0.001$, Figure S2.3, Table S2.3, Materials and Methods). Whereas bacterial load for mice on WD dropped below detectable levels, bacterial load for mice on RC only dropped to ~10^6 CFUs. Moreover, while CFU counts for mice on RC had recovered to baseline levels by D4 post-ABX, CFU counts for mice on WD did not recover to baseline levels through at least D7. Dynamics of aerobes and anaerobes were broadly similar across both treatment groups. Bacterial biomass of PBS-treated controls did not change appreciably over time across either dietary treatment (Fig. S2.3). These results confirm previous findings (Katherine Michelle Ng et al. 2019; Tanes et al. 2021).

We next evaluated the taxonomic recovery of the gut microbiome across treatment groups using 16S sequencing. We first quantified microbiome alpha diversity by ASV richness. We chose richness over other alpha diversity metrics like the Shannon index that weight for relative abundance of different taxa because we expected relative abundances to shift dramatically after antibiotics and over the course of recovery, and were most interested in a simple measure of how many unique taxa were present or absent at different stages of recovery across dietary treatments. Mice on WD exhibited reduced ASV richness compared to

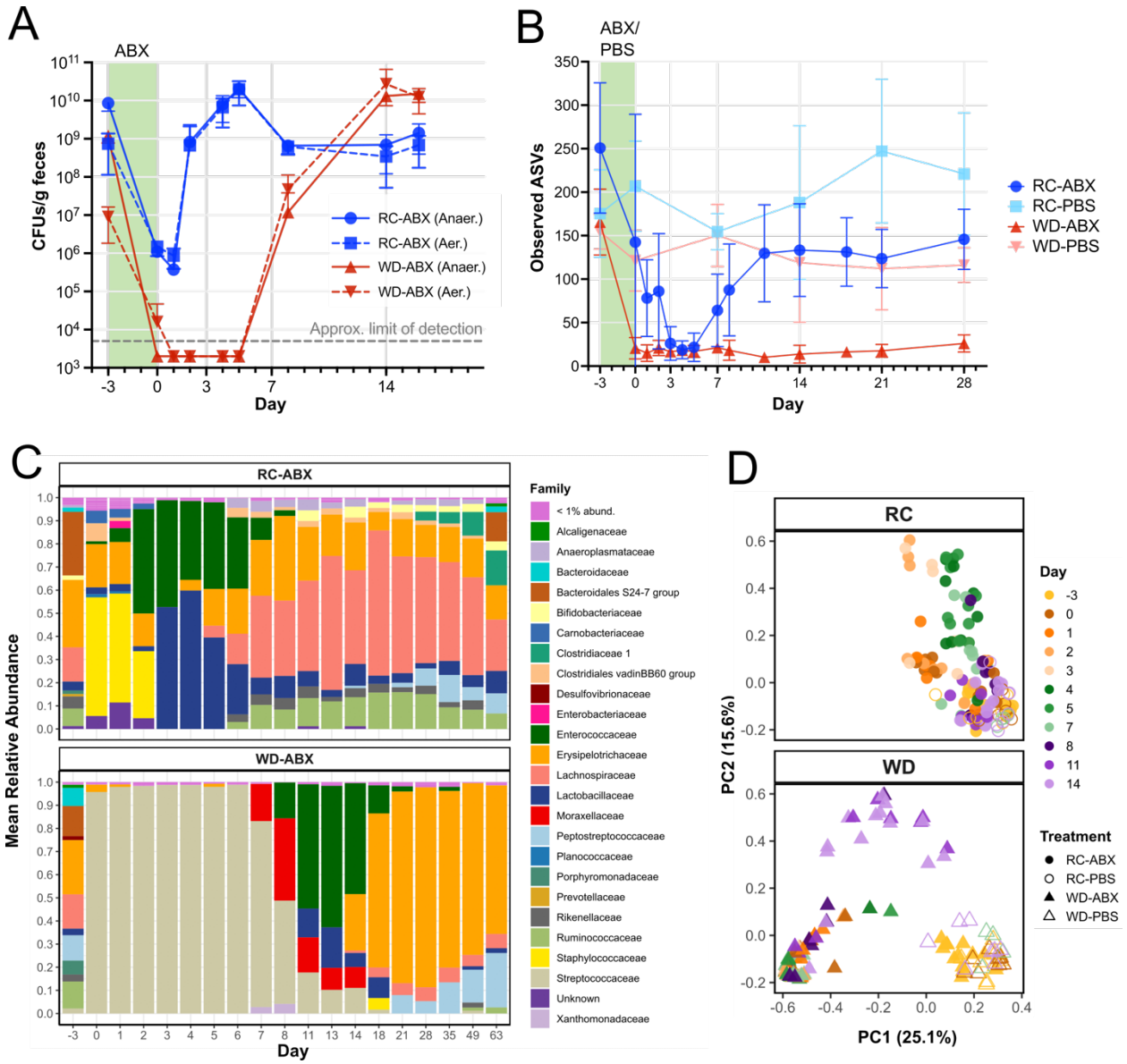

Figure 2.2: Bacterial biomass and taxonomic recovery after antibiotic treatment are impaired in mice on WD. (A) Fecal bacterial biomass in mice on RC-ABX and WD-ABX for mice from Cohort 1 (n=6/group). See also Figure S2.3 and Table S2.3. **(B)** Fecal alpha diversity (ASV richness) of mice across dietary treatments and timepoints (all cohorts, n=6-13/group, Table S2.2). **(C)** Mean relative abundances of different microbial families for n=6 mice/group from Cohort 1. See Fig. S2.4 for other cohorts). **(D)** PCoA of 16S-based microbiome taxonomic composition at the genus level using Bray-Curtis dissimilarity for samples from all treatment groups and cohorts. See Fig. S2.5 for other cohorts.

mice on RC at D-3 before antibiotic treatment (Figure 2.2B, $q = 0.0003$, Table S2.4, Fig. S2.2). ASV richness in PBS-treated controls on both diets wavered, but did not change significantly at any time point. By contrast, antibiotic-treated mice on both diets experienced a sharp decline in ASV richness after antibiotic treatment. For RC-ABX mice, ASV richness began to recover after D5 post-ABX, and recovered only approximately half the taxa that were initially present (mean = 145.7 ASVs pre-ABX, mean = 250.8 at D28, $q = 0.0003$). For WD-ABX mice, ASV richness remained severely diminished through at least D28 in all cohorts, and up to 9 weeks post-ABX (mean = 165.6 ASVs pre-ABX, mean = 26 at D28, $q < 0.0001$).

Correspondingly, relative abundances of different taxa were substantially altered during and after antibiotic treatment for mice on both diets (Figure 2.2C). In RC-ABX mice, the microbiota passed through successive waves of recolonization after antibiotic treatment, marked by early dominance of facultative anaerobes like *Enterococcaceae* and *Lactobaccilaceae*, followed by increasing diversification of stricter anaerobes as biomass recovers. In WD-ABX mice, the minimal, low-biomass post-ABX community was dominated by *Lactococcus* genera until biomass started to recover. Recovery in WD-ABX mice also passed through a successional phase of facultative anaerobes including *Moraxellaceae*, *Enterococcaceae*, and *Lactobacillaceae* around D14 before beginning to recover strict anaerobes at D28. While all specific compositional changes were not precisely replicated across cohorts (Fig. S2.4), certain characteristics, like the early dominance of facultative anaerobes

as biomass recovers, and the post-ABX dominance of Lactococcus in all WD-ABX groups, were common to all cohorts.

By PCoA ordinated using Bray-Curtis dissimilarity, we observe that across all cohorts, microbiome dynamics track a broadly similar trajectory within treatment groups (Figure 2.2D). By D14 or earlier, the microbiome of mice on RC-ABX clustered with their respective pre-ABX community and corresponding RC-PBS controls along PC1 and PC2, while the microbiome of WD-ABX mice remained distinct from their pre-ABX community at D14 (Figure 2.2D). By D28, some, but not all mice on WD-ABX began to approach their initial community structure (Fig. S2.5). Together, these results indicate that mice on WD experience markedly impaired recovery of microbial taxonomic and biomass recovery after antibiotic treatment compared to mice on RC.

Mice on WD exhibit persistently reduced functional redundancy after antibiotic treatment

To determine whether the microbiome of mice with impaired taxonomic recovery also exhibit altered functional capacity after antibiotic treatment, we performed shotgun metagenomic sequencing on fecal samples from a subset of mice on RC-ABX and WD-ABX at key time points throughout recovery (n=1/cohort/treatment, n=6 mice total), as well as n=6 samples from the pre-antibiotic timepoint for WD-ABX and RC-ABX treatment groups. 16S relative abundance data were used to select timepoints at which microbiome taxonomic composition was most distinct over the course of recovery (D-3, D2, D4, D14, and D28; D4 was excluded

for mice on WD as microbiome 16S composition was indistinguishable from D2). Gene calls were annotated with the Kyoto Encyclopedia of Genes and Genomes (KEGG) catalog for functional interpretation.

We first evaluated the functional diversity of the gut microbiome of mice on RC and WD before antibiotics and throughout recovery by calculating functional richness at different hierarchical levels (gene call, KEGG Ortholog (KO), or KEGG Category (KCat) (Figure 2.3A). At the level of gene calls, microbiome functional richness for mice on WD was reduced compared to mice on RC even before antibiotic treatment (RC mean = 412,163 gene calls; WD mean = 306,169 gene calls, $p = 0.0005$, t=4.118, unpaired t-test, n=8/group, Table S2.5). After antibiotics, the functional richness of mice on both dietary treatments collapsed to only 2-3% of their initial pre-antibiotic richness; while mice on RC recovered to ~70% of their initial functional diversity by D28, mice on WD recovered to only 16% of their initial diversity. The extent of these trends, however, differed across hierarchical levels: at the broader KO and KCat levels, mice on RC and WD had statistically indistinguishable levels of diversity at the pre-ABX timepoint (Table S2.5). Moreover, by D28, mice on RC were able to recover up to 90 and 99% of their functional richness at the KO and KCat levels, respectively, and mice on WD were able to recover 65 and 90% of their functional richness at the KO and KCat levels. While this does not mark a "complete" recovery for WD mice at the KO level, it is still a substantial increase from the 16% recovery at the gene call level.

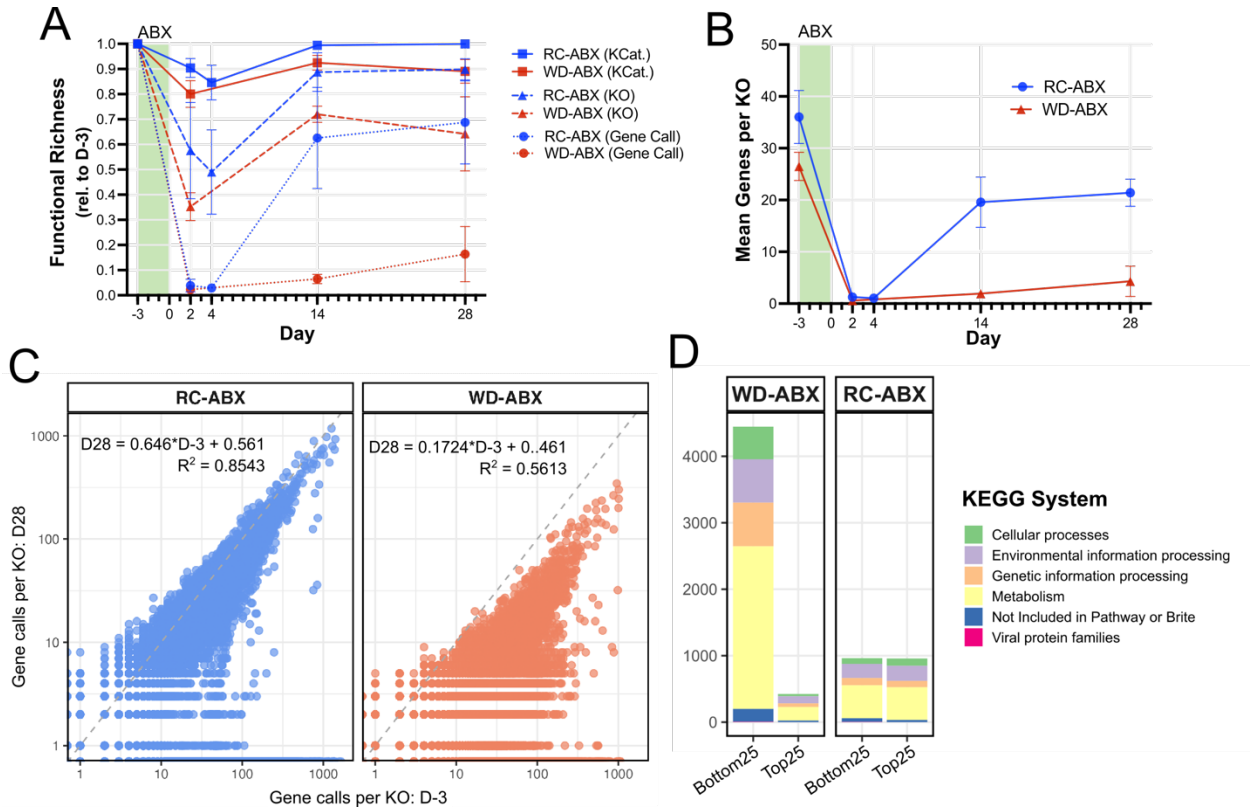

Figure 2.3: Microbiome functional redundancy is lost after antibiotics in mice on WD. **(A)** Metagenomic functional richness in fecal samples from mice on RC-ABX (red) and WD-ABX (blue) at the KEGG Category (KCat), KEGG Ortholog (KO), and gene call level as a percentage of functional richness at D-3 (pre-ABX) (n=3/group, Table S2.5). **(B)** Functional redundancy (mean genes per KO) of mice on RC-ABX and WD-ABX (n=3/group, Table S2.6). **(C)** Initial (D-3) versus final (D28) functional redundancy for mice on RC-ABX (blue) and WD-ABX (red) (Table S2.7). **(D)** KEGG system mapping of KOs that recovered $< 25\%$ of their D-3 FR ("Bottom 25") or $> 75\%$ ("Top 25") across RC-ABX and WD-ABX groups.

We hypothesized that the discrepancy between the failure of mice on WD-ABX to recover at the gene call level and their more robust recovery at the KO and KCat levels could be attributed to a change in functional redundancy (FR), or the number of unique gene calls that map to each KO, before and after antibiotic treatment. High FR before antibiotic treatment could mean that even if many gene calls were persistently lost, the small proportion that did recover may still represent a large proportion of the KOs that were initially present. Indeed,

after calculating the mean number of gene calls per KO for each sample, we observe that mice on RC recover significantly more FR after antibiotics, while mice on WD persistently lose FR (Figure 2.3B, Table S2.6). By plotting initial versus final functional redundancy, we can more precisely characterize this shift: in mice on RC, KOs with even partial recovery recovered a higher proportion of their initial FR (i.e., came closer to approaching the dashed 1:1 line) compared to mice on WD (Figure 2.3C, RC slope = 0.64, WD slope = 0.17, Table S2.7). We also wondered whether KOs that recovered or failed to recover FR shared functional characteristics. To evaluate this possibility, we identified all KOs that recovered $> 75\%$ of their initial FR ("Top25") or $< 25\%$ ("Bottom25"), and categorized them by their corresponding KEGG System (Figure 2.3D). We found that while KOs in the Top25 and Bottom25 were roughly equally distributed across functional categories for mice on RC, KOs in the Bottom25 for mice on WD predominantly carried metabolism annotations. Thus, we conclude that after antibiotic treatment, mice on WD experience a mild loss in functional diversity at the KO level with major losses in functional redundancy, primarily losing metabolic redundancy.

Mice on RC and WD experience distinct temporal functional recovery dynamics

In order to focus on the most functionally interpretable aspects of our data, all further metagenomic analyses were performed at the KO level. We performed pairwise comparisons between the pre-ABX timepoint (D-3) and all post-ABX timepoints for mice on each diet to

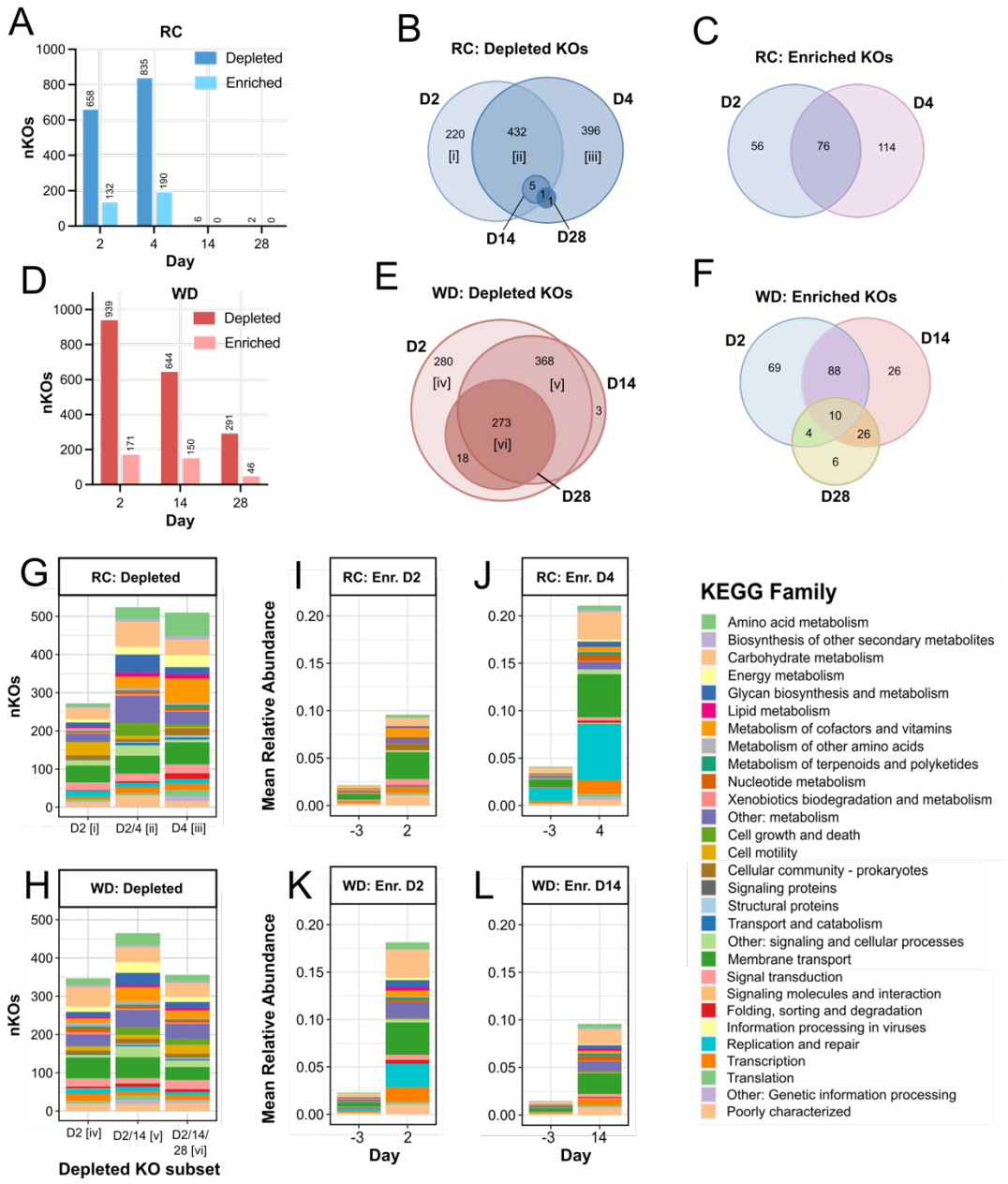

Figure 2.4: Microbiome functional recovery dynamics differ across dietary treatments. Significantly differentially abundant KOs in mice on **(A)** RC-ABX or **(D)** WD-ABX. Venn diagram of significantly depleted KOs in mice on **(B)** RC-ABX or **(E)** WD-ABX. Roman numerals indicate the subset of KOs depicted in panels (G) and (H). Venn diagrams of significantly enriched KOs in mice on **(C)** RC-ABX or **(F)** WD-ABX. KEGG Family mapping of significantly depleted KOs in mice on **(G)** RC-ABX or **(H)** WD-ABX. Roman numerals indicate the subset of KOs depicted in panels (B) and (E). Relative abundances of significantly enriched KOs in mice on RC-ABX at **(I)** D2 and **(J)** D4 relative to D-3. Relative abundances of significantly enriched KOs in mice on WD-ABX at **(K)** D2 and **(L)** D14 relative to D-3.

characterize the functional characteristics of the microbiome throughout recovery and to identify which KOs were significantly differentially abundant (criteria: FDR < 0.05, baseMean > 50, $|\log2\text{FoldChange}| > 2$). Mice on RC had 658 significantly depleted KOs at D2 relative to pre-ABX, and had 835 depleted KOs at D4, but nearly all of these recovered to baseline levels by D14 (Figure 2.4A). Notably, while a large subset (432/658) of the genes depleted at D2 remained depleted at D4, a distinct subset of genes (396) was newly depleted at D4, before recovering almost all differentially abundant KOs by D14 (Figure 2.4B). KOs that were depleted at D2 and D4 collapsed from 28.0% and 34.2% of total mapping reads at D-3 to only 1.1% and 1.3% of reads, respectively (Figure S2.6). Partially overlapping subsets of KOs were enriched at D2 and D4 relative to baseline, all of which returned to pre-ABX levels by D14 (Figure 2.4A, 2.4C). Collectively, these results suggest that for mice on RC, microbiome recovery may proceed through distinct functional phases at D2 and D4, and that functional recovery is largely complete by D14.

Mice on WD had a larger number of significantly depleted KOs than RC counterparts at all timepoints evaluated, and even by D28, still had 291 KOs that had not yet returned to pre-ABX levels (Figure 2.4D). By contrast with mice on RC, the KOs depleted at D14 and D28 were almost all a subset of the KOs depleted at D2 (Figure 2.4E). These KOs collapsed from 33.6% of total mapping reads at D-3 to 0.09% of reads at D2 (Figure S2.6). Mice on WD also had semi-overlapping sets of KOs that were significantly enriched relative to pre-ABX at all timepoints analyzed (Figure 2.4F). Thus, whereas mice on RC appear to pass through distinct

intermediate successional stages with unique sets of KOs depleted and enriched at D2 and D4 before recovering by D14, mice on WD seem to experience a persistent post-ABX dysbiosis that slowly returns to baseline without intermediate successional stages, and which does not fully resolve by D28.

Mice on both diets undergo metabolic and functional switches over the course of recovery

To characterize the functions that were significantly depleted and to identify any broader functional patterns in the order of KO depletion and recovery, we mapped each KO identified in Figures 2.4B and 2.4E to the KEGG Family level and counted the number of depleted KOs in each family (Figures 2.4G and 2.4H). Depleted KOs across both dietary treatments mapped to a wide variety of KEGG families. We note that in RC mice, the subset of KOs that were depleted only at D2 but which had recovered by D4 (section [i] in Figure 2.4B and 2.4G), included relatively few KOs mapping to metabolic functions (~100 KOs), while the KOs that were persistently depleted from D2 through D4 (section [ii]) and the unique subset that became depleted at D4 (section [iii]) each included ~300 unique KOs that mapped to metabolic functions (Figure 2.4G). Thus, in mice on RC, many metabolic functions seem persistently depleted through at least D4, before recovering by D14. For mice on WD, the depleted KEGG family profile was very similar across timepoints, suggesting that there was no single functional category that experienced great shifts in depletion and recovery across different timepoints (Figure 2.4H). Instead, the KOs that recovered from timepoint to

timepoint were scattered across KEGG families, and by D28, KOs from a wide variety of KEGG families were still depleted.

Although the number of significantly enriched KOs relative to pre-ABX was smaller than the number of depleted KOs for both dietary treatments at all timepoints, we wondered whether this limited subset of KOs might still expand substantially in relative abundance. Indeed, for mice on RC, from pre-ABX to D2 the enriched KOs expanded from 2.1% to 9.6% relative abundance, and from pre-ABX to D4, the enriched KOs expanded from 4.1% to 21.1% relative abundance (Figure S2.6). For mice on WD, enriched KOs expanded from ~1% at pre-ABX to 18.1% at D2, 9.5% at D14, and 1.9% at D28.

Next, we examined the functions enriched at each timepoint to learn more about whether and how the microbes that are present at different stages of recovery might respond to and interact with their environment at that time. We mapped all KOs enriched at a given time point to the KEGG Family level and plotted the relative abundances of these families at D-3 and at the indicated timepoint (Figures 2.4I-L). In mice on RC, at D2 the predominant enriched KEGG Family was transporters, along with a limited set of metabolic functions (Figure 2.4I). By D4, transporters were again enriched, as well as replication and repair, and a larger abundance of metabolic functions (Figure 2.4J). In mice on WD, metabolic functions, transporters, and replication and repair were enriched at D2 (Figure 2.4K). Notably, all enriched replication and repair KOs for mice on both diets encoded transposase genes, which

may reflect horizontal gene transfer events, perhaps related to stress response or spread of antibiotic resistance. By D14 for mice on WD, the predominantly enriched KEGG family was once again transporters (Figure 2.4L).

For mice on both diets, many KEGG families, most notably carbohydrate metabolism, other metabolism, and transporters, are highly represented among both depleted and enriched KOs, often at the same time point. Because many different KOs map to each of these broader families, this suggests that the microbial community is not gaining or losing all functional capacity in that family but is instead switching which types of KOs it uses at different timepoints.

Taken together, our functional analysis of depleted and enriched KOs indicates that although the microbial community undergoes severe depletion of many KOs, different KOs, often within the same KEGG Families, are enriched. For mice on RC, metabolic functions stand out as especially depleted at D2, without any clear switch to a distinct set of enriched metabolic KOs. By D4, although many metabolic functions are still/newly depleted, a distinct subset has become enriched and expands in relative abundance. Thus, metabolic recovery appears to begin at D4 in mice on RC. For mice on WD, although they appear to initiate a metabolic switch at D2, as many metabolic functions are depleted and others enriched, this does not seem to change much over the following timepoints. Metabolic shifts across both

diets are often accompanied or even preceded by shifts in transporter abundances, likely reflecting a response to distinct resource environments.

The gut metabolome of mice on RC undergoes faster and more complete recovery after antibiotics than that of mice on WD

To more directly assay the metabolic resource environment of the gut after antibiotic treatment and throughout recovery, we performed a fecal metabolomic screen of microbiome-associated compounds including amino acids, carbohydrates, bile acids (BAs), and more, from mice on RC-ABX and WD-ABX (n=3/group). After normalizing each metabolite to its respective pre-ABX abundance within a given mouse, we first compared values across mice within the same treatment group to characterize the replicability of any changes in the resource environment over the course of recovery (Figure S2.7, S2.8). We found that for mice on both dietary treatments, the metabolomic profile was very consistent across individuals, with the same compounds reaching relatively high or low levels on the same days. We then averaged normalized abundance values across mice within a given treatment (Figure 2.5A).

We found that for mice on RC, the normalized abundances of a variety of compounds were distinct from baseline immediately after antibiotics, but by PCoA, the overall profile clusters with pre-ABX levels by D11 (Figure S2.9, Table S2.8). There appear to be two

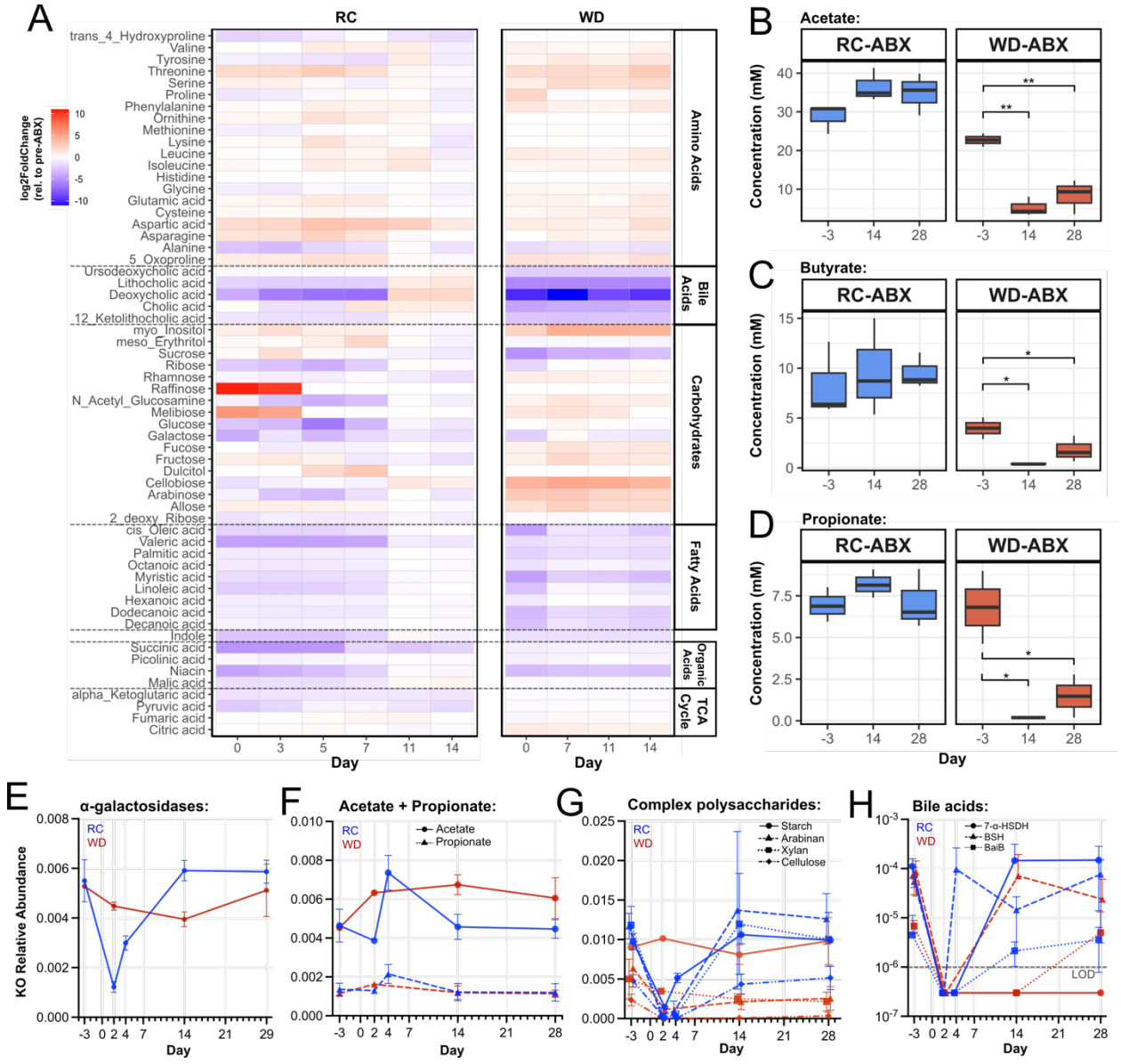

Figure 2.5: Metabolomic recovery is severely impaired in mice on WD. **(A)** Heatmap displaying log2FoldChange in metabolite abundances relative to the pre-ABX timepoint (D-3), averaged across n=3-4 mice/group. **(B – D)** Absolute concentrations of **(B)** acetate, **(C)** butyrate, **(D)** propionate in mice on RC-ABX (blue) and WD-ABX (red) (n=3/group, $*q < 0.05$, $**q < 0.01$). **(E – H)** Relative abundances of KOs mapping to **(E)** α-galactosidases, **(F)** acetate or propionate production, **(G)** starch, arabinan, xylan, and cellulose metabolism, and **(H)** bile acid metabolism in mice on RC-ABX (blue) or WD-ABX (red) (n=3/group, Table S2.10). LOD = limit of detection.

main inflection points for changes in metabolite abundance: first after D3, and then after D7 (Figure S2.9). The first inflection point is driven largely by the dynamics of raffinose and melibiose, two plant-derived α-galactoside compounds that are highly abundant in the RC diet fed to our mice (Figure 2.5A) (M. Zhang et al. 2022). These compounds were found at highly elevated abundances through D3, but then returned to baseline by D5. The second inflection point reflected the dynamics of a wide variety of compounds that were depleted after antibiotics, but which recovered after D7. These included carbohydrate monomers like ribose, glucose, and arabinose, as well as most fatty acids assayed in this panel. The secondary BAs lithocholic acid, deoxycholic acid, and 1,2-ketolithocholic acid, and to a lesser extent, the primary BA cholic acid, were also depleted after antibiotics through D7, but by D11, were relatively more abundant than at baseline.

In stark contrast, the metabolomic profile of mice on WD showed almost no signs of recovery at all through D14 (Figure 2.5A, Figure S2.9). Bile acids stood out as heavily depleted throughout sampling. Sucrose, niacin, and fatty acids, all of which were depleted in mice on RC, but which recovered after D7, remained depleted throughout sampling. Carbohydrates like cellobiose, arabinose, myo-inositol, and allose were over-abundant relative to baseline, and failed to recover to baseline levels.

To further probe the functional outputs of the microbial community, we performed a distinct set of metabolomic analyses to quantify levels of short-chain fatty acids (SCFAs), microbial

products derived from the breakdown of complex polysaccharides, in cecal samples from mice on RC-ABX and WD-ABX at D-3, D14, and D28. Although we did not directly assay the cecal microbiome in these experiments, we were still interested in whether the cecal resource environment showed signs of post-antibiotic dysbiosis across dietary treatments. We found that for acetate, butyrate, and propionate, concentrations at D14 and D28 in mice on RC were statistically indistinguishable from pre-ABX, whereas for mice on WD, they were significantly depleted at D14, and persisted at low levels through D28 (Figures 2.5B-D, Table S2.9).

We wondered if these changes in metabolic resource environment might correlate with changes in microbial gene abundances. To assess this possibility, we plotted the relative abundances of several curated subsets of microbial genes across timepoints for mice on each dietary treatment. First, we hypothesized that the overabundance of raffinose and melibiose after antibiotics in mice on RC diet might correlate with the loss of microbial α-galactosidase genes, which are responsible for the breakdown of these metabolites. Importantly, the host does not have the enzymatic capacity to digest these substrates, and their breakdown is entirely dependent on microbial metabolism. We used the dbCAN-sub database (H. Zhang et al. 2018) to identify all EC numbers predicted to metabolize raffinose, melibiose, or other α-galactoside compounds, and summed the relative abundances of all KOs that mapped to these EC numbers at each time point. As predicted, we found that for mice on RC, α-galactosidase

genes drop sharply in abundance after antibiotic treatment, but recover significantly by D4, correlating with the timing at which raffinose and melibiose abundances return to baseline (Figure 2.5E, Table S2.10).

Next, we evaluated whether genes encoding the production of SCFAs might correlate with levels of acetate, propionate, and butyrate at D-3, D14, and D28. We developed a query list of KOs involved in the metabolism of acetate, propionate, and butyrate based on the work of Zhao *et al.* (C. Zhao et al. 2019). We were only able to identify a single butyrate-producing gene in our dataset at very low abundance due to limitations in sequencing depth, and therefore we excluded butyrate genes from our analysis. We found that while the relative abundances of acetate- and propionate-producing genes peaked at D4 after antibiotic treatment for mice on WD, they returned to baseline levels by D14 (Figure 2.5F, Table S2.10). For mice on WD, however, acetate- and propionate-producing genes did not change significantly in relative abundance at any timepoint, in spite of the observed reduction in acetate and propionate levels.

We hypothesized that the relative depletion of simple sugars in RC mice after antibiotics might correlate with a loss of genes that break complex dietary polysaccharides into simpler monosaccharide byproducts. We again used the db-CAN sub database (H. Zhang et al. 2018) to assemble a list of ECs predicted to encode metabolism of a handful of complex dietary polysaccharides: starch, arabinan, xylan, and cellulose. Notably, only starch and cellulose are

present in our WD formulation. We found that in mice on RC diet, relative abundances of all of these genes were depleted after antibiotics, but had recovered by at least D14 (Figure 2.5G, Table S2.10, not significant for arabinan after correction for multiple hypothesis testing). For mice on WD, relative abundance of cellulose metabolism genes was significantly depleted at all timepoints after antibiotics, but no other assayed genes changed significantly.

Finally, we hypothesized that, as secondary BAs cannot be produced by the host and are exclusively products of microbial metabolism (Ridlon et al. 2014), the observed depletion of secondary BAs after antibiotics may reflect a loss of microbial BA-metabolism genes. Only 3 KOs identified in our samples encoded known BA metabolism functions: a bile salt hydrolase (BSH), a 7-α-hydroxysteroid dehydrogenase (7-α-HSDH), and a bile acid-coenzyme A ligase (BaiB), and all three KOs were detected at very low abundance even before antibiotic treatment (Figure 2.5H). For mice on both diets, all three KOs were undetectable after antibiotic treatment. BSH levels recovered to baseline by at least D14 in mice on both diets. For mice on RC diet, both 7-α-HSDH and BaiB had recovered significantly from D2 levels by D14, correlating with the recovery of BA metabolite levels. In mice on WD, 7-α-HSDH eventually increased in abundance by D28, but BaiB remained undetectable (Table S2.10).

These results show that antibiotic treatment alters the fecal metabolome in mice on both RC and WD. In mice on RC, the metabolome recovers within 2 weeks of antibiotic treatment, whereas in mice on WD, it remains dysbiotic for at least 2-4 weeks after antibiotic treatment

has ended, in spite of the complete recovery of bacterial biomass and the partial recovery of taxonomic and functional diversity within that timespan. This may suggest that although the WD microbiome has the capacity to perform certain metabolic functions, WD may not provide the appropriate resource environment to facilitate those reactions. Although more direct experimental evidence is needed to establish causality, preliminary correlational analyses suggests that at least for mice on RC, changes in certain metabolite levels may reflect the recovery dynamics of microbial populations.

Microbiome recovery dynamics are driven more by dietary resource environment than microbial re-seeding

We next sought to probe the mechanism by which microbiome recovery is impaired in mice on WD. Relative to RC diet, WD changes both the microbial taxonomic composition and the metabolic resource environment of the gut (Albenberg and Wu 2014). WD may therefore change not only which microbial taxa are available to re-seed the gut after antibiotic treatment, but also the specific dietary metabolites that are available to define the gut niche space, and the metabolic preferences of the available taxa under those distinct resource regimes.

To quantify the relative contributions of microbial re-seeding and dietary resource environment to microbiome recovery after antibiotics, we performed intervention experiments

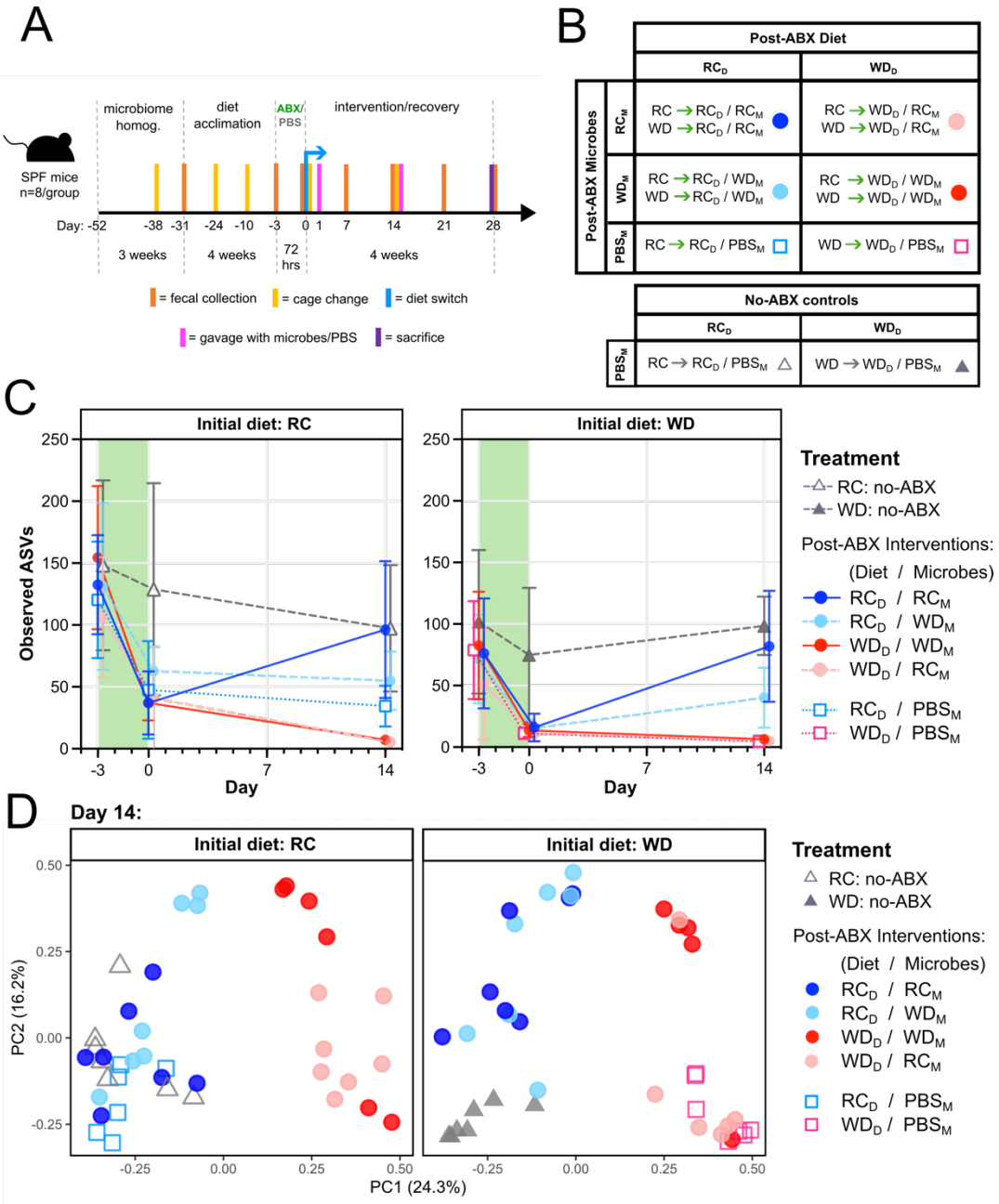

Figure 2.6: Dietary intervention facilitates microbiome recovery from antibiotics. (A) Experimental timeline. After ABX or PBS, post-ABX dietary treatments were provided *ad libitum* from day 0 through the end of the experiment; post-ABX microbial treatments were administered at day 1 and day 14. **(B)** Post-ABX (top) or no-ABX (bottom) treatment groups. Mice on each pre-ABX diet (left of arrow) were split across post-ABX treatment groups as indicated. Green arrow represents ABX treatment; grey arrow represents no-ABX controls. Colored shape represents symbol for treatment group as depicted in panels C and D. **(C)** ASV richness across treatment groups throughout antibiotic treatment and recovery (n=6-8/group). **(D)** PCoA of 16S-based microbiome taxonomic composition at the genus level using Bray-Curtis dissimilarity at D14 of recovery.

in which dietary and microbial re-exposures were controlled after antibiotic treatment (Figure 2.6A, Materials and Methods). These experiments were carried out across 4 cohorts of 24 SPF C57Bl/6 mice (n=96 total, n=8/treatment group). Briefly, after microbiome homogenization, diet acclimation, and antibiotic treatment, mice were transferred into new sterile, hermetically sealed gnotobiotic cages, and post-antibiotic diet ("RC_D", "WD_D") and microbial re-exposures ("RC_M", "WD_M") were administered in a factorial manner (i.e., for mice on each pre-antibiotic diet, we changed either microbial re-exposure, diet, both, or neither, Figure 2.6B). Microbial re-exposure was performed by pooling fecal material from mice on each diet at 24 hours before antibiotic treatment, homogenizing at 60mg/ml in 25% glycerol solution, and gavaging into the respective treatment groups at 24 hours post-antibiotics. We included controls that remained on their respective pre-antibiotic diet and were gavaged with PBS instead of any microbial re-exposure ("PBS_M"), as well as no-antibiotic controls that were treated with PBS instead of antibiotics, remained on their pre-antibiotic diet, and were gavaged with PBS instead of any microbial re-exposure ("no-ABX"). Fecal samples were collected before and after antibiotic treatment, and every 7 days through 4 weeks of recovery, when mice were sacrificed and dissected for tissue harvest. 16S rRNA sequencing was performed on samples from days -3, 0, 14, and 28 from all treatment groups.

Based on the previous set of experiments, we identified D14 as the most salient timepoint to evaluate the distinct recovery dynamics of mice on RC and WD, as mice on RC had broadly

recovered in terms of microbiome taxonomic composition, functional capacity, and metabolome by D14, whereas mice on WD had not (Figures 2.2-2.5). We first evaluated ASV richness across treatment groups from pre-antibiotics through D14 (Figure 2.6C). Relative to pre-ABX, we observed no significant loss in ASV richness for no-ABX controls on either diet throughout the sampling period, while mice from all other treatment groups lost ASV richness after antibiotic treatment (Table S2.11). However, irrespective of initial dietary treatment, mice fed WD_D after antibiotics continued to lose diversity through D14 regardless of microbial re-exposure, whereas mice fed RC_D after antibiotics either plateaued in ASV richness or recovered to baseline (Table S2.11). At D14, irrespective of initial dietary treatment, mice on RC_D/RC_M recovered the most ASV richness, followed by mice on RC_D/WD_M and RC_D/PBS_M (Table S2.11 Thus, post-ABX diet appears to be a more important predictor of ASV richness recovery than microbial re-exposure, although for mice fed RC_D after antibiotics, microbial re-exposure may determine the extent to which ASV richness recovers.

We next performed PCoA using Bray-Curtis dissimilarity on D14 data from all treatment groups, with no-ABX controls on each diet serving as a reference point for "recovery" (Figure 2.6D). First, to assess whether this experimental model recapitulates the RC-ABX and WD-ABX phenotypes observed in our first series of experiments, we evaluated the recovery dynamics of the treatment groups for which all post-antibiotic treatments matched their initial dietary treatment (RC → RC_D/RC_M and WD → WD_D/WD_M). The primary distinction

between these treatment groups and the initial experiments is that in the first series of experiments, microbial re-exposure was passively mediated by coprophagy, whereas in these experiments, it was actively controlled by gavage. We observe that the RC → RC_D/RC_M group clustered indistinguishably from the RC/no-ABX controls, whereas the WD → WD_D/WD_M group remained distinct from the WD/no-ABX controls at D14 (Table S2.12). Thus, as in the initial experiments, the RC group recovered, whereas the WD group did not. This confirms that despite the distinct microbial re-exposure protocol, this experimental model captures the phenotypes outlined in Figure 2.2, validating our use of this model.

We observe several broad trends across dietary and microbial treatment groups (Figure 2.6D). First, irrespective of initial diet, recovery across PC1 appears to be driven by post-ABX diet, with mice on RC_D (blue tones) generally falling lower on PC1 and closer to the no-ABX controls (triangles) than mice on WD_D (red tones). The effect of microbial re-exposure was more variable, but most notably, it was insufficient to promote full recovery in mice on WD_D, and unnecessary to promote recovery in mice on RC_D.

In more detail, PBS_M controls (open squares) on each diet were roughly aligned with respective no-ABX controls (triangles) along PC2. Thus, any divergence along PC2 is likely driven by microbial re-exposure, although the specific effect of any treatment group was variable. Qualitatively, for mice initially on RC (left panel), RC_M mice (royal blue, light pink) tended to cluster lower on PC2 closer to the no-ABX controls irrespective of post-ABX diet,

while WD_M mice (red, light blue) were more variable along PC2, and had more individuals with higher PC2 values. This could suggest that WD_M may actively impair microbiome recovery. Among mice initially on WD (right panel) that switched to RC_D (blue tones), RC_M and WD_M were indistinguishable (Table S2.12). Among mice initially on WD that stayed on WD_D, RC_M mice (light pink) clustered lower on PC2, closer to recovery, while WD_M mice (red) clustered higher, farther from recovery. Thus, microbial re-exposure of any variety was at best unimpactful relative to PBS_M controls, and at worst, shifted community composition further from recovery.

To quantify contributions of initial diet, ABX treatment, post-ABX diet, post-ABX microbial treatment, and the interactions between these factors, we performed PERMANOVA analysis on our Bray-Curtis dissimilarity matrix, and after model reduction based on AIC, found that ABX treatment, pre-ABX diet, post-ABX diet, post-ABX microbial exposure, and the interaction between ABX, post-ABX diet, and post-ABX microbes significantly contributed to microbiome compositional clustering (Table S2.12, $R^2 = 0.41$). Post-ABX diet explained the most variation in composition ($R^2 = 0.15$).

In sum, dietary resource availability is a primary driver of microbiome taxonomic recovery in this model, while microbial re-exposure can have a variable secondary effect that is impacted by initial and post-ABX diet. While RC_M does not have a large impact on overall microbiome composition based on PCoA, diversity analysis shows that it may facilitate recovery of ASV

richness in mice on RC_D. By contrast, WD_M fails to promote compositional recovery, and more often than not, shifts composition even further from recovery than PBS_M controls.

Prolonged post-antibiotic dysbiosis on WD impairs colonization resistance to Salmonella Typhimurium

Under healthy conditions, the microbiome protects the host against opportunistic pathogens in a phenomenon known as "colonization resistance" (Buffie and Pamer 2013). In particular, previous work has shown that the pathogen *Salmonella enterica* serovar *Typhimurium* (*St*) is unable to establish lower GI infection or cause colitis in SPF mice unless they have been pre-treated with streptomycin (Barthel et al. 2003). Established models of *St* colonization resistance and infection pre-treat with antibiotics for 24 hours immediately leading up to *St* challenge. We wondered if the prolonged post-antibiotic dysbiosis experienced by mice on WD might render them more susceptible to opportunistic infection by *St* as late as 14 days after antibiotic treatment has ended.

To evaluate this possibility, we performed a new series of experiments including 4 cohorts of female mice and one cohort of male mice in standard, non-gnotobiotic cages (Materials and Methods). After microbiome homogenization, diet acclimation, and antibiotic or PBS administration as in other experiments, mice were allowed to recover for 14 days, and then each dietary and antibiotic treatment group was split into infection and non-infection

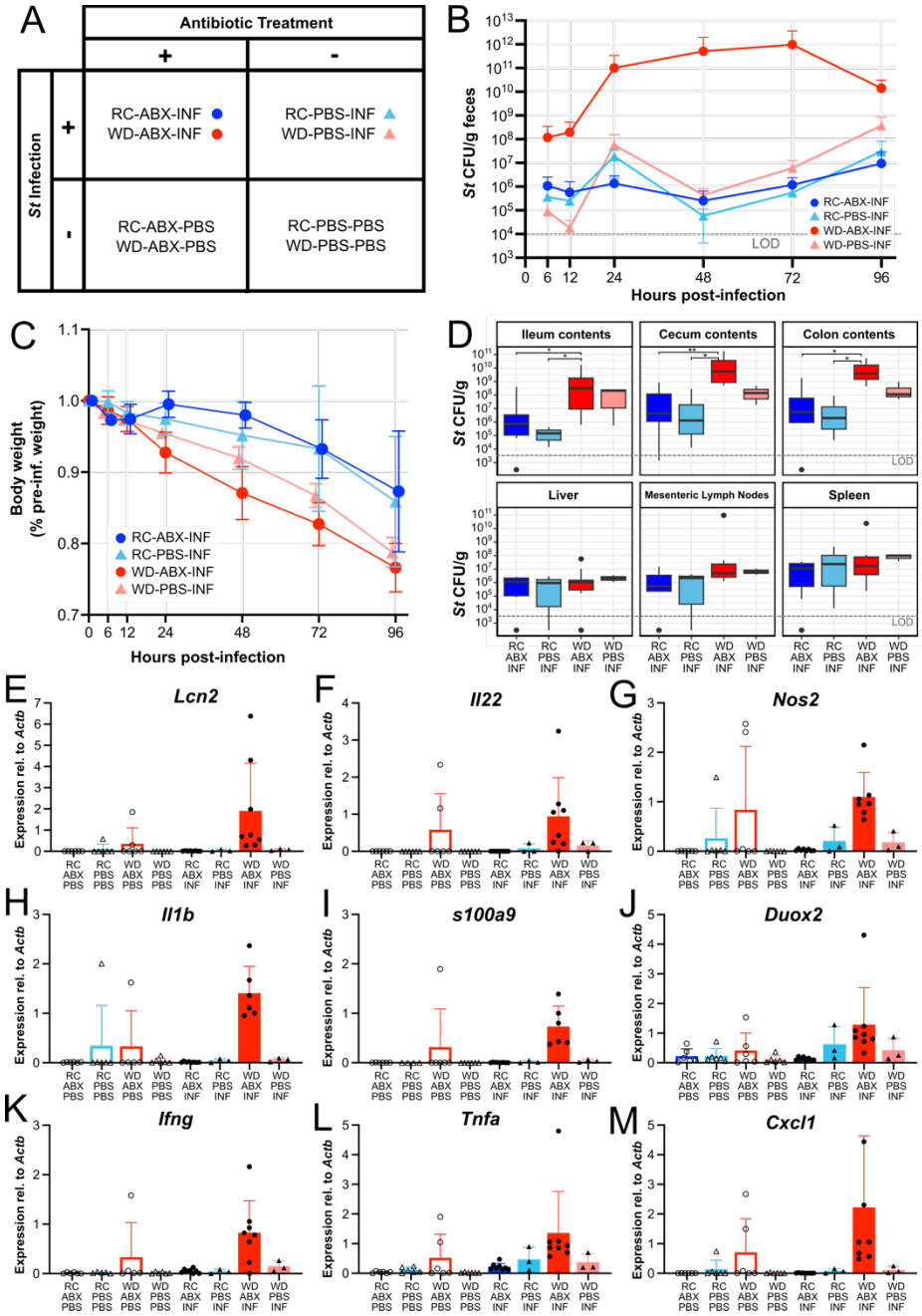

Figure 2.7: Prolonged post-antibiotic dysbiosis in mice on WD impairs colonization resistance to *St*. **(A)** Experimental treatment groups. **(B)** Fecal *St* load (CFU/g) among infected treatment groups. Uninfected controls had no detectable *St* and are therefore not depicted. **(C)** Body weight during infection as a percentage of pre-infection weight. Uninfected controls did not change body weight (Figure S2.10, Table S2.14). **(D)** *St* load in different GI regions and tissues at t=96 hpi (CFU/g) among infected treatment groups. Uninfected controls had no detectable *St*. $*p < 0.05$; $**p < 0.01$; $***p < 0.001$; Table S2.15. **(E – M)** mRNA expression of immune genes in cecal mucosal scrapings at t=96 hpi based on RT-qPCR. Expression is normalized to the housekeeping gene *Actb*. N=3-9/group for all analyses; see Table S2.16 for statistical analyses.

treatment groups (Figure 2.7A). WD on its own has previously been shown to facilitate *St* infection relative to RC even without antibiotic pre-treatment (Wotzka et al. 2019), but by comparing between ABX and no-ABX PBS control groups on each diet, we are able to isolate the specific effects of diet and diet-induced post-antibiotic dysbiosis. Infection treatment groups were challenged with ~7 x 10^7 CFU of *St* by oral gavage, and non-infection groups were gavaged with 200 µl sterile PBS. Fecal samples and body weights were collected at t=6, 12, 24, 48, 72, and 96 hours post-infection (hpi). At t=96 hpi or when mice lost >15% of their pre-infection body weight, they were sacrificed and dissected for tissue harvest. Fecal and tissue samples were homogenized and plated aerobically on selective LB agar with nalidixic acid to enumerate *St* load. As trends were consistent across male and female cohorts (Figure S2.10), all data were combined for the following analyses.

We first evaluated *St* load at each timepoint after infection (Figure 2.7B). Uninfected controls had undetectable levels of *St*, confirming that they were not contaminated. As hypothesized, mice on WD-ABX-INF were the most susceptible to infection, exhibiting persistently higher *St* loads than all other treatment groups from as early as t=6 hpi, and reaching up to 10^6-fold higher mean infection loads than the WD-PBS-INF group. Although *St* loads for the WD-ABX-INF group were not statistically significantly higher than the WD-PBS-INF group at most timepoints due to limitations in sample size and statistical power with noisy CFU data, the mean area under the curve (AUC), which accounts for persistently elevated *St* load across

all timepoints, was significantly higher for the WD-ABX-INF group relative to all other treatment groups (Figure S2.10, Table S2.13). Recapitulating previous work, the WD-PBS-INF group also had significantly greater AUC than the RC-ABX-INF group, although it was not statistically higher than the RC-PBS-INF group after correction for multiple hypothesis testing, likely indicating insufficient statistical power due to small sample sizes in these treatment groups.

We next evaluated weight loss after infection across treatment groups as a high-level measure of host pathology (Figure 2.7C). Mice that were not infected did not exhibit any significant changes in body weight through t=96 hpi (Figure S2.10C, Table S2.14). At t=96 hpi, all infected treatment groups lost significantly more weight than all uninfected control groups. Among infected treatment groups, WD-ABX-INF lost significantly more weight than the RC-ABX-INF group by t=96, but not more than RC-PBS-INF or WD-PBS-INF, and all other infected groups were statistically indistinguishable from each other (Table S2.14).

We hypothesized that the substantial weight loss across all infected treatment groups including those with substantially lower *St* loads may reflect systemic infection rather than localized lower GI infection. There are two established models of *St* infection: in the "typhoid model," sufficient doses of *St* in mice that are not pre-treated with antibiotics establish systemic infection by invading the epithelial tissues of the ileum, disseminating to other tissues, and inducing a typhoid-like response (Santos et al. 2001). In the "colonization

resistance" model, even low doses of *St* in antibiotic pre-treated mice establish a persistent luminal lower-GI tract infection, inducing acute inflammation of the cecum and colon, diarrhea, weight loss, and severe host pathology (Barthel et al. 2003). Tissue dissemination is, in theory, specific to the typhoid model, whereas lower GI enteritis is specific to the colonization resistance model. Thus, we examined dissemination of *St* to the liver, mesenteric lymph nodes, and spleen, as well as cecal mucosal mRNA levels of several inflammatory markers of *St*-induced enteritis (Devlin et al. 2022).

We observed detectable levels of *St* in all treatment groups for all GI regions and tissues assayed, confirming dissemination of *St* beyond the gut (Figure 2.7D). The colonization resistance phenotype in which the WD-ABX-INF group experienced greater infection loads than other treatment groups, however, was specific to the three GI regions (Table S2.15). From our panel of inflammatory markers (Figure 2.7E-M), we observed that, generally, only two treatment groups exhibited any signs of inflammation: the WD-ABX-PBS uninfected controls, and the WD-ABX-INF group. Levels of all markers were significantly higher for the WD-ABX-INF group than all other groups except for occasionally the WD-ABX-PBS group (Table S2.16). Within the WD-ABX-PBS group, only two mice consistently showed any expression of inflammatory markers, while all other mice had undetectable levels of expression for these genes. This suggests that antibiotic treatment in mice on WD may itself contribute

to a baseline level of inflammation even without *St* challenge, albeit variably across individuals.

Together, these results suggest that mice in the WD-ABX-INF treatment group may have experienced both systemic infection and acute lower-GI infection, exhibiting both dissemination of *St* to other tissues and cecal inflammation. However, the lower-GI infection and enteritis phenotype was specific to the WD-ABX-INF group, supporting the hypothesis that prolonged post-antibiotic dysbiosis in mice on WD impairs colonization resistance in the lower GI tract relative to mice that were not pre-treated with antibiotics, or that were on RC diet.

2.5 DISCUSSION

WD predisposes the microbiome to ecosystem collapse after antibiotic perturbation

We show that the double-hit of WD and antibiotic treatment, each of which independently cause distinct forms of dysbiosis, have a synergistically negative impact on the microbiome, causing a more severe and prolonged ecosystem collapse than observed for either factor on its own (Figures 2.2-2.5). This collapse entails extreme loss of taxonomic diversity, as previously reported (Katherine Michelle Ng et al. 2019; Tanes et al. 2021), as well as reduced functional redundancy and a distinct skewing of the gut metabolome. Given that our WD formulation is designed to reflect typical American consumption patterns (NHANES 2009) and that

antibiotics are prescribed liberally for an enormous array of pathologies for which they may or may not be indicated (J. Wang et al. 2014; Bell 2014), this finding bears great clinical relevance.

Although more mechanistic follow-up experiments are needed to explain exactly why the WD microbiome is more prone to collapse, one testable hypothesis is that the dominant microbes under WD are more sensitive to antibiotics. This seems unlikely though, as taxa that overlap between mice on RC and WD were more severely diminished in mice on WD than in their RC counterparts (Figure 2.2D). Alternatively, susceptibility could arise from the metabolic network structure of the WD microbiome: we observed that the WD community has reduced functional diversity even before antibiotics (Table S2.11). Especially under WD resource conditions in which the substrates for many reactions are absent, the realized network of metabolic crossfeeding interactions between microbes may be only sparsely connected. Ecological network theory suggests that networks with poor connectivity and redundancy may be less robust to perturbation (Vieira and Almeida-Neto 2015; Allesina, Bodini, and Pascual 2009), and therefore this network structure may render the WD community particularly vulnerable to collapse. A final hypothesis is that hysteresis effects might allow taxa that were supported under RC during the pre-experimental microbiome homogenization phase to persist in their niche after the WD switch (Carmody et al. 2015), but these microbes, which were never particularly well-adapted to WD, fail to re-establish after antibiotic treatment.

Diet is more essential to microbiome recovery than microbial re-seeding

We demonstrate that diet plays a critical role in restoring successional dynamics and allowing the endogenous microbiome to naturally rebuild after antibiotic treatment. Variability in antibiotic response and recovery remains poorly understood. One landmark study by Dethlefsen and Relman (Dethlefsen and Relman 2011) showed that microbiome resilience to antibiotic treatment varies from person to person, but provided no experimental evidence to explain this phenomenon. Analysis from Shaw et al. (Shaw et al. 2019) using published datasets (Zaura et al. 2015; Palleja et al. 2018) similarly identify individualized responses to antibiotic treatment, as do Chng et al. in a separate study (Chng et al. 2020). Chng et al. go on to hypothesize that microbes capable of breaking down complex fibers are able to open up niche space that permits the growth of more specialized taxa later on, enabling diversification and recovery. However, like most studies of the microbiome response to antibiotic treatment, their analyses failed to explicitly track or consider diet during or after antibiotic treatment: if those complex fibers are absent from the diet, no fiber-breakdown niche space can be opened. Our data collectively suggest that diet may be a key explanatory factor in antibiotic recovery dynamics, carrying the immediate translational implication that post-antibiotic dietary interventions, such as prescribing a fiber supplement, may help to promote recovery.

Additional experimentation to identify which specific resources best promote recovery, as well as the optimal timing and duration of such dietary interventions, are needed.

Of course, many studies have documented that microbial re-seeding additionally plays a significant role in antibiotic recovery (Katherine Michelle Ng et al. 2019; Taur et al. 2018; Tropini et al. 2018). Consistent with this, our intervention experiments showed that re-exposure to RC microbes in mice on RC diet improved the recovery of microbial diversity relative to antibiotic-treated mice that received PBS control (Figure 2.6C). However, in mice that were fed WD after antibiotics, neither RC nor WD microbes were sufficient to promote recovery. Even under controlled lab conditions using autologous FMT of a complex, diverse community in genetically matched, diet-controlled individuals, the outcomes of microbial transplant are variable, difficult to predict, and ultimately dependent upon a permissive post-antibiotic diet.

It is also worth noting that the microbiome was only briefly perturbed in our experiment and that internal microbial reservoirs likely remained for re-seeding and diversification. This is supported by the substantial microbiome recovery of mice on RC diet that received only PBS without any microbial re-exposure treatment (Figure 2.6D). In clinical settings, the extent to which microbial populations are driven fully extinct after antibiotic treatment likely varies by therapeutic regimen. Thus, in cases with more prolonged or intensive antibiotic treatment, it may be necessary to reintroduce both microbes and dietary resources.

We hypothesized that WD impairs microbiome recovery by changing the resource environment of the gut, and therefore changing the ecological niche space available to the present microbial taxa. An alternative explanation for the failure of mice on WD to recover from antibiotics could be that our antibiotic cocktail lingers in the gut for a longer time in mice on WD than on RC. GI transit is slower in mice on WD (Anitha et al. 2016). Antibiotics may therefore take longer to clear the system, although this difference should be on the scale of hours rather than weeks as observed in our experiments. Even if diet does interact with our antibiotics to alter their pharmacokinetics, this would itself be a novel finding, carrying the same clinical implication that diet must be more explicitly and carefully considered when administering antibiotic therapies.

Western diet-antibiotic induced dysbiosis is long-lasting and has consequences for the host

Few published studies on the interaction between diet and antibiotic treatment have examined the duration of dysbiosis, or the long-term consequences of dysbiosis for the host (J. Y. Lee et al. 2020). We find that the post-antibiotic dysbiosis experienced by mice on WD can be extremely long-lasting. In our long-term experiment, mice on WD showed few signs of recovery over the course of 9 weeks (Figure S2.2), or roughly 10% of the mouse's lifespan (The Jackson Laboratory 2017). Among humans, which are not coprophagic like mice, stronger microbial dispersal limitation and consistent WD could compound the dysbiosis over

time, allowing more taxa to go extinct from individual hosts if interventions are not introduced in a timely manner (E. D. Sonnenburg et al. 2016). These effects might be further exacerbated in individuals that undergo multiple courses of antibiotics without complete recovery in between.

Although the host metabolic and inflammatory consequences of prolonged post-antibiotic dysbiosis remain to be evaluated for our study, our experiments with *St* challenge show that lingering post-antibiotic dysbiosis may precipitate the emergence of acute pathology at later timepoints (Figure 2.7). The pathogenesis of *St* colitis relies on 1) inducing or aggravating inflammation in the host and 2) circumventing the competitively dominant endogenous microbiome (A. D. Palmer and Slauch 2017; Winter et al. 2010). In other experimental models, this has been achieved by streptomycin pre-treatment immediately before *St* challenge, which both induces a baseline level of inflammation and depletes the microbiome (Barthel et al. 2003). Related to our model, Lee et al. have shown that antibiotic treatment in mice on WD produces persistent low-grade colonic inflammation (J. Y. Lee et al. 2020), and although bacterial biomass was restored by D14 in our WD-ABX mice, we found that functional redundancy of the WD-ABX microbiome remained diminished (Figure 2.3B). This may act to temper the intensity of competition for resources like sialic acids in the gut, thereby facilitating *St* infection (Katharine M. Ng et al. 2013). Thus, our data establish that emergent community-wide functions like colonization resistance remain compromised well

after antibiotic treatment has ended in mice on WD. Given the widespread concurrence of WD and antibiotic treatment in US human populations, impaired colonization resistance could have serious ramifications for susceptibility and resistance to a wide range of opportunistic pathogens.

Ecological succession as a framework for approaching microbiome restoration

The conceptual framework of ecological succession has been widely applied to the maturation of the infant gut microbiome (Bäckhed et al. 2015; Stewart et al. 2018; C. Palmer et al. 2007; Koenig et al. 2011), but we argue that this framework is a particularly helpful tool for understanding microbiome restoration in contexts of perturbation, including and extending beyond the antibiotic scenario presented here. Under this model, both the taxa present and their surrounding resource environment interact in an iterative feedback process to guide the progression of the community from one stage to the next (Gilbert and Lynch 2019; Prach and Walker 2011). Early arriving microbes may either facilitate the arrival of later arriving microbes by producing metabolic byproducts for cross-feeding (Douglas 2020) or by more generally changing the resource environment (e.g. oxygen levels (J.-Y. Lee, Tsolis, and Bäumler 2022), pH (Van Herreweghen et al. 2018), bile acid pool (Ridlon et al. 2014)) in a favorable way, or they may inhibit the re-growth or colonization of certain organisms (Baumgartner, Pfrunder-Cardozo, and Hall 2021). Fundamentally, the transition of the

ecosystem towards a mature "climax community" is driven by the dynamic microbial response to their current resource environment: the community cannot proceed to the next stage if it is missing either the right taxa with the capacity to survive and change their environment, or if the taxa do not have access to the right resources or conditions to perform those reactions.

In our experimental model, we hypothesize that under RC conditions, fast-growing facultative anaerobes initiate the transition from a more oxygenated post-antibiotic state (Reese et al. 2018) back to the typical anaerobic state, which allows strictly anaerobic fiber-degrading taxa to re-colonize. These taxa then break down dietary fibers, as inferred from our metabolomics data in Figure 2.5, opening up niche space to support the growth of diverse taxa that specialize on the array of newly liberated carbohydrate monomers, in line with predictions from Chng *et al* (Chng et al. 2020). Under WD, epithelial oxygenation spikes after antibiotic treatment (J. Y. Lee et al. 2020). The few taxa that remain after antibiotic treatment seem to have the genomic capacity to break down dietary fibers (Figure 2.4), but their diet does not provide any fiber to break down, and therefore levels of fiber-derived SCFAs like butyrate remain depressed (Figure 2.5). Reduced butyrate availability has been documented to increase epithelial oxygenation (Rivera-Chávez et al. 2016), further preventing strictly anaerobic fiber-degraders from re-colonizing. Niche space remains limited to fierce competition for a handful of simple dietary carbohydrate resources, and the community does not diversify or proceed

towards recovery. These hypotheses require more rigorous experimental support but are testable by administration or removal of specific resources or microbes from the ecosystem.

An important corollary of the ecological succession framework that is supported by our results is that recovery does not necessarily occur as the reverse of disturbance: in RC mice, recovery proceeds through taxonomically and functionally distinct intermediate stages and returns back to baseline much faster than in WD, where functionally, the community slowly reverts towards baseline, but ultimately fails to change the resource environment in a way that permits diversification or complete recovery (Figures 2.2-2.5). In approaching microbiome restoration, we should think about ecological succession in a more deliberate way. Perhaps strategies will arise that entail introducing pioneer taxa with the resources required to thrive and allowing the ecosystem to naturally evolve from there - start with grasses, rather than trying to transplant a mature forest. By providing the right taxa with the right resources at the right time, this may pave the way for an individualized, endogenous recovery process to unfold.

2.6 ACKNOWLEDGMENTS

We thank the Chang lab members for scientific support received. This work was performed with support from NIH T32DK007074 (M.S.K.), NIH RC2DK122394 (E.B.C.), NIH T32GM007281 (M.S.K.), and the Host-Microbe and Tissue and Cell Engineering cores of the

UChicago DDRCC, Center for Interdisciplinary Study of Inflammatory Intestinal Disorders (C-IID) - (NIDDK P30 DK042086).

CONCLUSIONS

More complete understanding of microbial adaptational processes will be critically important for the development of better strategies for promoting the engraftment of exogenously administered live biotherapeutics, as well as for more effective methods of endogenous microbiome restoration. This dissertation uses two experimental models to explore adaptation at the level of strain abundance dynamics, phenotypic plasticity, and genetic evolution within a population, as well as broader sense community-scale adaptation defined by shifts in both abundances of community members and the overall metagenome of the community. These approaches arrive at overlapping conclusions about the essential importance of the metabolic resource environment as a driver of selection and adaptation.

In Chapter 1, we showed that *Bt* adapts to its environment in distinct stages, with different functional requirements, transcriptional responses, and selective pressures at each stage. We found that during the first day of colonization, *Bt* upregulated a broad array of biosynthesis genes, including many amino acid genes, and our functional genetics screen revealed that genes for the biosynthesis of amino acids were particularly essential to fitness and survival. This early stage, when *Bt* is at relatively low abundance, could be a particularly vulnerable period in the engraftment process, and perhaps exogenous supplementation of AAs or other substrates that must otherwise be synthesized by *Bt* could promote survival. Recently published work has shown that the capacity to perform biosynthesis of essential compounds is

important for engraftment and survival of a broad array of microbes under stressful conditions (i.e. after FMT, in IBD, etc) (Watson et al. 2022; Veseli et al. 2023). This brand of early-phase resource supplementation to help exogenous microbes establish a foothold in the community could be a novel intervention to improve engraftment of live biotherapeutics.

In the same experiments, we also identified extremely strong dietary selective pressure that acted to enhance metabolism of raffinose family oligosaccharides (RFOs) that were abundant in our mouse chow. We found that an upregulated IS3-family transposable element acted to duplicate a region of the genome in at least 3 independent instances. The resultant evolutionary innovations involved an alpha-galactosidase gene that enables improved RFO metabolism, while also placing a strong promoter upstream of the original copy of that gene, ultimately producing a ~5-fold growth advantage over wild-type Bt. The role of IS elements in expanding the dynamic range of phenotypic plasticity in microbial genomes has only very recently begun to be characterized (Tempel, Bedo, and Talla 2022; Vandecraen et al. 2017). Our finding that this form of genomic regulation can play a role in colonization suggest that IS elements could be useful tools for improving the fitness of exogenous strains, perhaps in combination with a specific resource substrate.

These results hint at a broader strategy for improving the adaptational fit of an exogenous microbe to a new host environment by harnessing strong, directed dietary selective pressure. Under such selective conditions *in vivo*, we identified convergent evolution for metabolic

adaptations that greatly improved *Bt* fitness. To improve exogenous microbial engraftment in a community context, perhaps we could first condition microbes with strong, directed selective pressure, and then introduce that microbe with its associated substrate. In innovative work from Shepherd *et al., Bt* was engineered to express a PUL for metabolism of a seaweed polysaccharide that is not typically present in Western host diets, and for which other members of the host microbiome had no metabolic pathways (Shepherd et al. 2018). Introduced in combination with the seaweed substrate, *Bt* was able to invade and engraft in a community context, and its abundance was fine-tunable by controlling the amount of metabolic substrate supplied. The authors posit that this specific PUL could be introduced into other strains to promote their engraftment, and therefore sidestep the issue of metabolic competition with the native microbiota. However, many exogenous microbes that we may want to introduce into a community are not as genetically tractable as *Bt,* and may not be amenable to the engineered introduction of the seaweed PUL. Instead, we could potentially use genomic and metagenomic comparisons to identify metabolic niche space that is exclusive to the microbe that we would like to introduce, and then introduce it in combination with the appropriate resource after applying strong dietary selective pressure to improve microbial fitness on that substrate.

In Chapter 2, we document the strong negative impact of Western diet (WD) on gut microbiome resilience to antibiotic perturbation. Our dense time series data reveals that mice

on regular chow (RC) diet undergo a rapid successional process of recovery that passes through distinct intermediate stages before returning to baseline. In mice on WD, the inappropriate dietary resource environment inhibits any recovery process from unfolding, in spite of the metagenomic capacity of the remaining microbes to perform more complex metabolic functions. Diet emerges from these studies as an agent of historical contingency after antibiotic treatment: depending on the dietary resources available, the same community can take vastly different trajectories that may or may not lead to recovery.

Given the widespread consumption of Western diet and the liberal use and misuse of antibiotics in clinical settings, this work has unsettling implications. Although we have not yet delved into the metabolic and immune consequences of prolonged post-antibiotic dysbiosis for the host, our colonization resistance studies provide evidence that emergent symbiotic functions of the microbiome may be lost or weakened, and for long periods of time.

The primary importance of dietary resource environment for microbiome restoration is broadly underappreciated. We show that under the right dietary conditions, microbial transplant may help to promote recovery of microbial diversity, but under the wrong conditions, it has variable and potentially even damaging effects on microbiome recovery. To date, the current standard of clinically adopted microbiome-based therapies and live biotherapeutics has been almost exclusively based on brute-force strategies of microbial transplantation with little consideration of the adaptational fit between the microbes that are

being introduced, the environment that they will encounter, and how that environment and their ecological niche will change as they establish, adapt, and grow. In clinical scenarios where the native microbiota has not been completely obliterated by heavy use of antibiotics or other long-term dysbiosis, a microbiome *restoration* approach that centers on providing the right resource environment for recovery of endogenous microbes may be a safer and more effective approach than transplant of exogenous microbes. This could entail provision of specific resources and/or microbes at specific stages of recovery to ensure that the ecosystem is maturing along a healthy successional trajectory.

More generally, these studies show that the mechanistic insight to be gained from cross-sectional studies in diseased and healthy conditions is limited compared to what can be learned by evaluating the time course of adaptational events that lead a population or community from state to state. We provided evidence that intermediate dynamics play an important role in shaping adaptational trajectories, and we suggest that these may be attractive new opportunities for intervention strategies to better facilitate the transition towards a healthy microbiome. In order to fulfill the promise of the microbiome as an agent of therapeutic impact, we must apply a more thoughtful and scientific strategy that requires a stronger understanding of the dynamic eco-evolutionary forces that guide engraftment, adaptation, and persistence.

APPENDIX 1: SUPPLEMENTAL FIGURES AND TABLES FOR CHAPTER 1

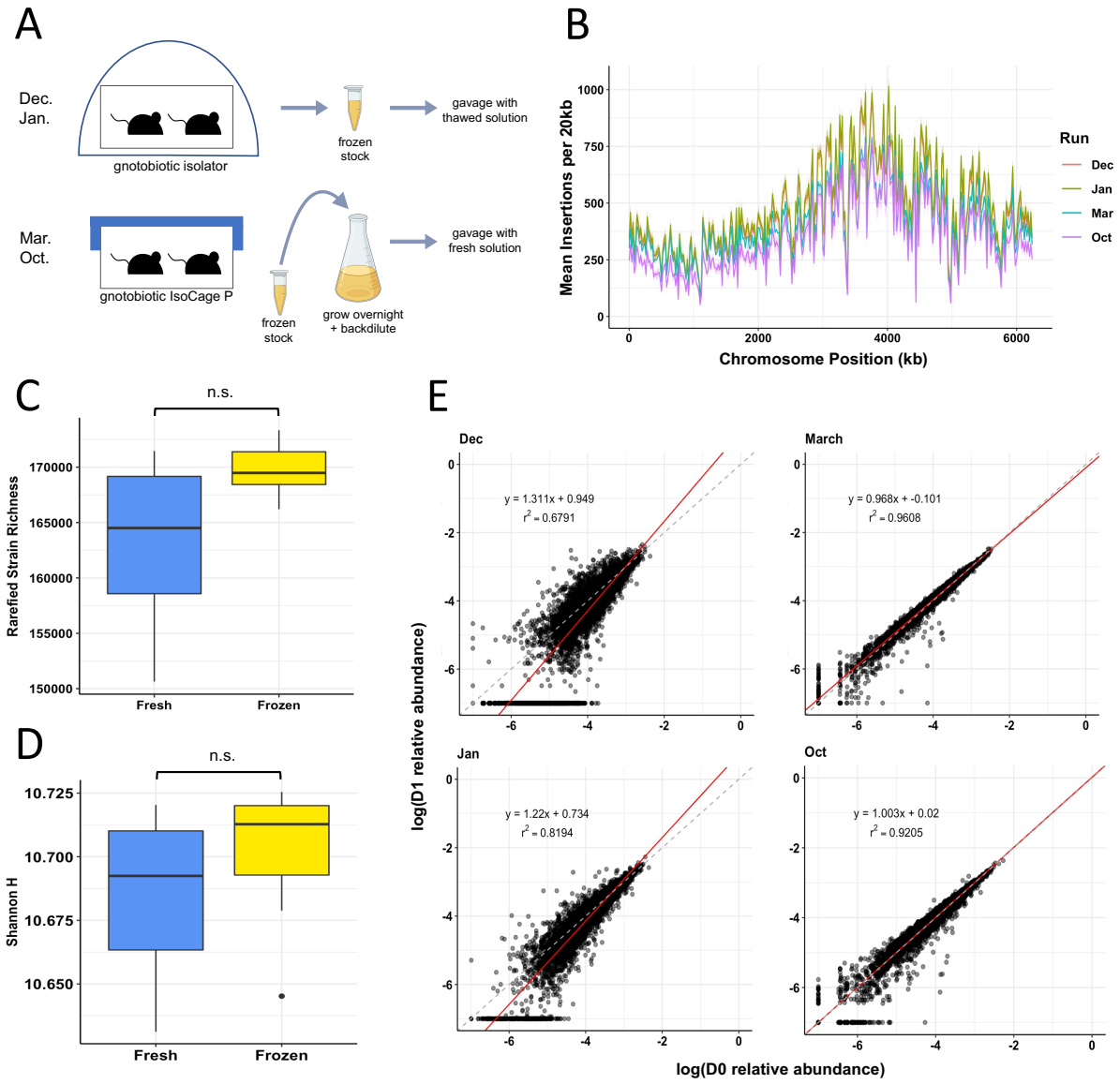

Figure S1.1: Comparison of functional genetics experimental protocols and outcomes. A) Schematic representation of protocol differences across experimental cohorts. In Dec. and Jan. runs, mice were housed in cages of 2-3 animals within gnotobiotic isolators and gavaged with thawed stocks; in Mar. and Oct. runs, mice were housed in gnotobiotic cages of 2-3 animals on an IsoCage P Bioexclusion rack system and gavaged with stocks that had been grown overnight in fresh media. B) Mean number of unique mutant strains with RB-Tn insertions identified per 20kb region in inoculum samples from each experimental cohort. C) Rarefied strain richness is not significantly different across fresh and frozen inocula (two-sided Wilcoxon rank sum test, p = 0.09, n= 8–13 per group). Samples were rarefied due to uneven sequencing depth across experimental cohorts.

Figure S1.1 (cont.): D) Shannon diversity is not significantly different across fresh and frozen inocula (two-sided Wilcoxon rank sum test, p = 0.1774). E) Comparison of inoculum (D0) versus D1 relative abundance of each RB-Tn gene mutant. Dashed line represents 1:1, red line and equation represent linear regression best-fit line. Runs with frozen inoculum (Dec, Jan) experienced greater loss of mutants with low D0 relative abundance (< 0.0001) compared to runs with fresh inoculum (Mar, Oct).

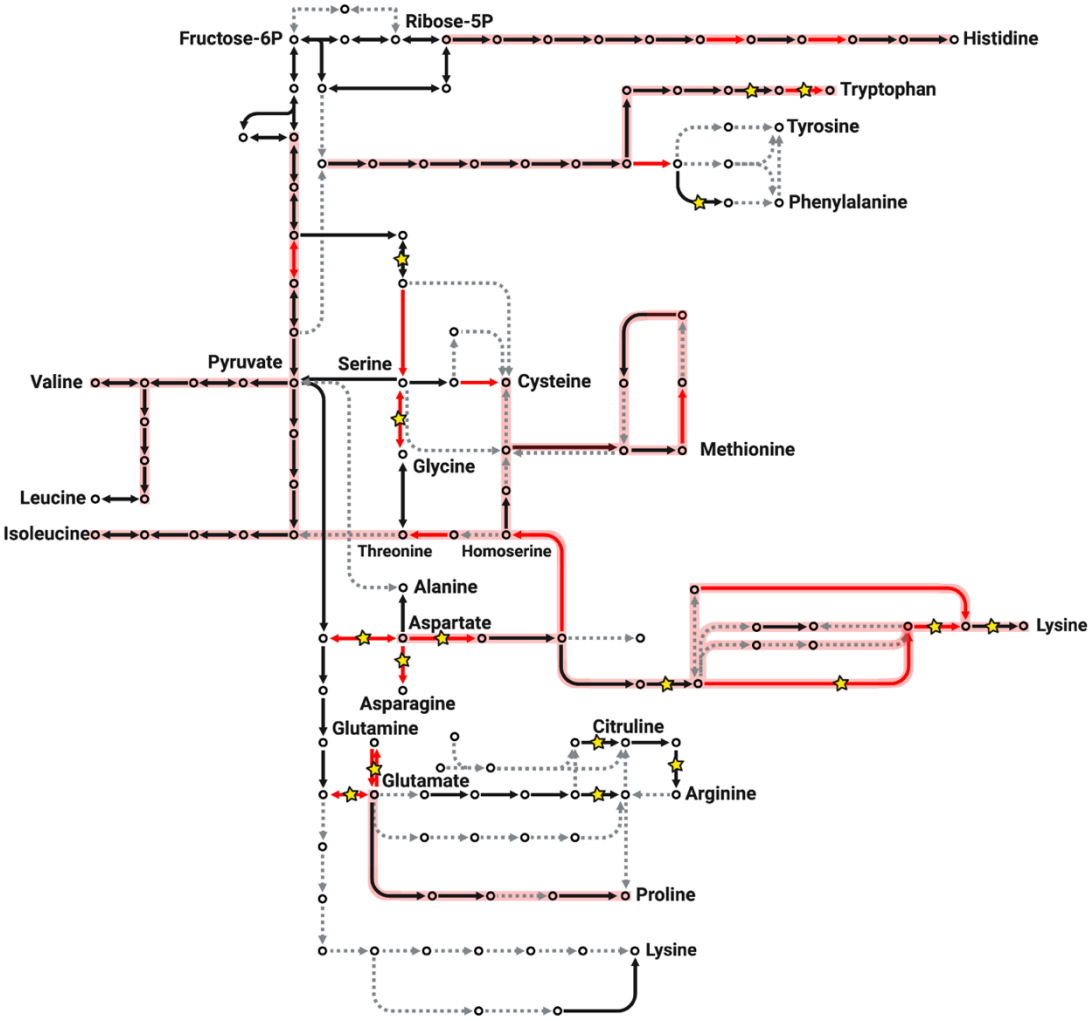

Figure S1.2: Pathway map of reactions related to amino acid biosynthesis. Red arrows represent specific genes whose transcript is significantly enriched on D0.5/1 relative to D2/4 (logFDR < -3, $|\log_2 FC| > 2$, and base mean > 50 RPM), and red highlight represents pathways that were overall enriched on D0.5/1 relative to D2/4 (padj < 0.05). No genes or pathways on this map were relatively more expressed at D2/D4 than D0.5/D1. Genes whose transcript level did not differ significantly between D0.5/1 and D2/4 are colored in black. Grey dashed arrows represent reactions for which the associated gene is unknown in the *Bt* genome. Gold stars represent gene disruptions that were depleted in the RB-Tn assay, as in Fig. 2C. See also Table S6.

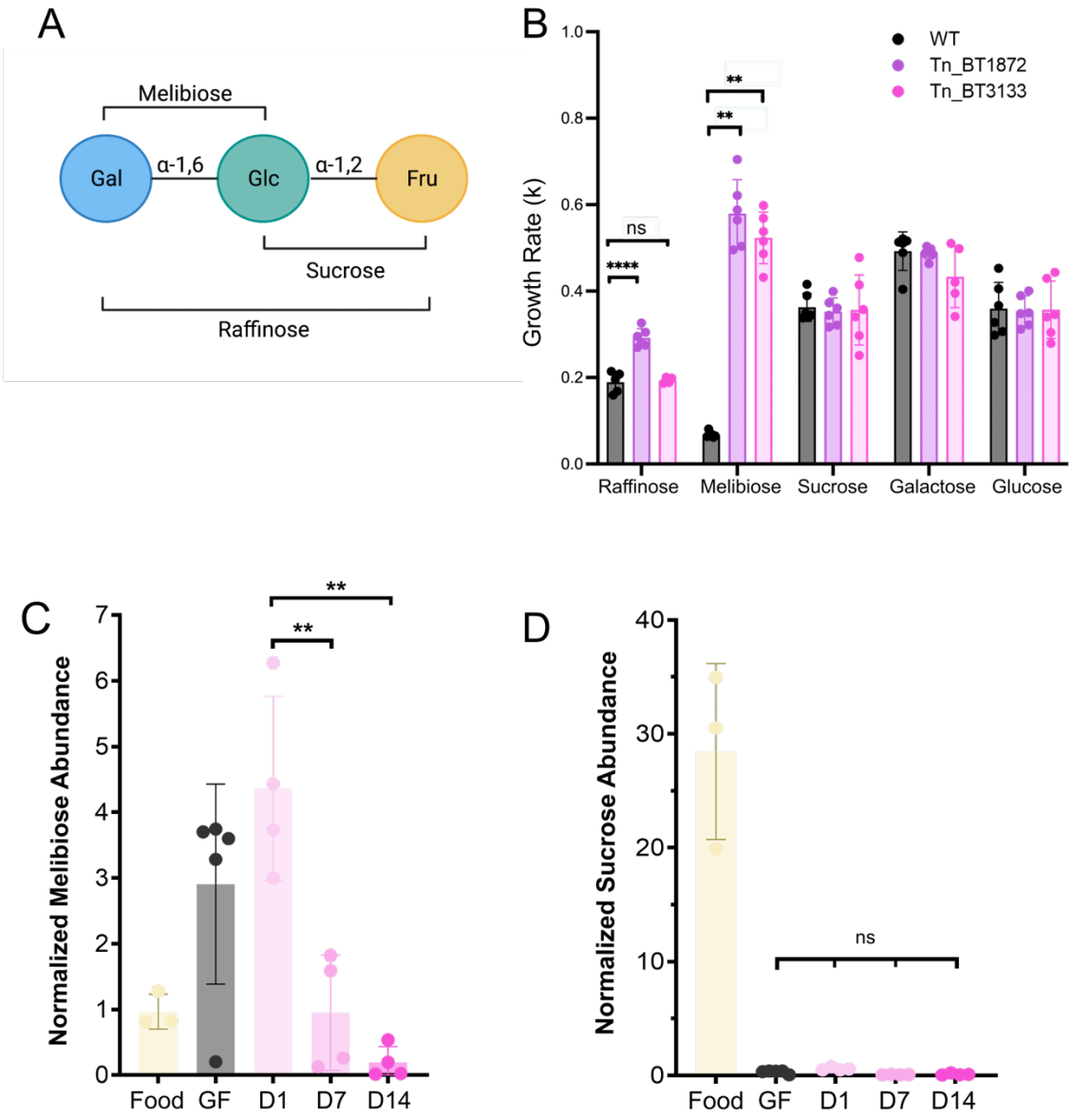

Figure S1.3: *Bt* adapts to the GF gut specifically by increasing efficiency of metabolizing α-1,6 bonded sugars. A) Structure of the trisaccharide raffinose. B) The log phase doubling times of Tn_BT3133 and Tn_BT1872 were measured in Varel-Bryant medium with 20 mM raffinose, melibiose, sucrose, galactose, or glucose as the sole carbon substrate. Abundance of C) melibiose or D) sucrose in the standard chow fed to GF mice, within GF ceca before colonization, or 1, 7, or 14 days post-colonization. See also Table S1.14.

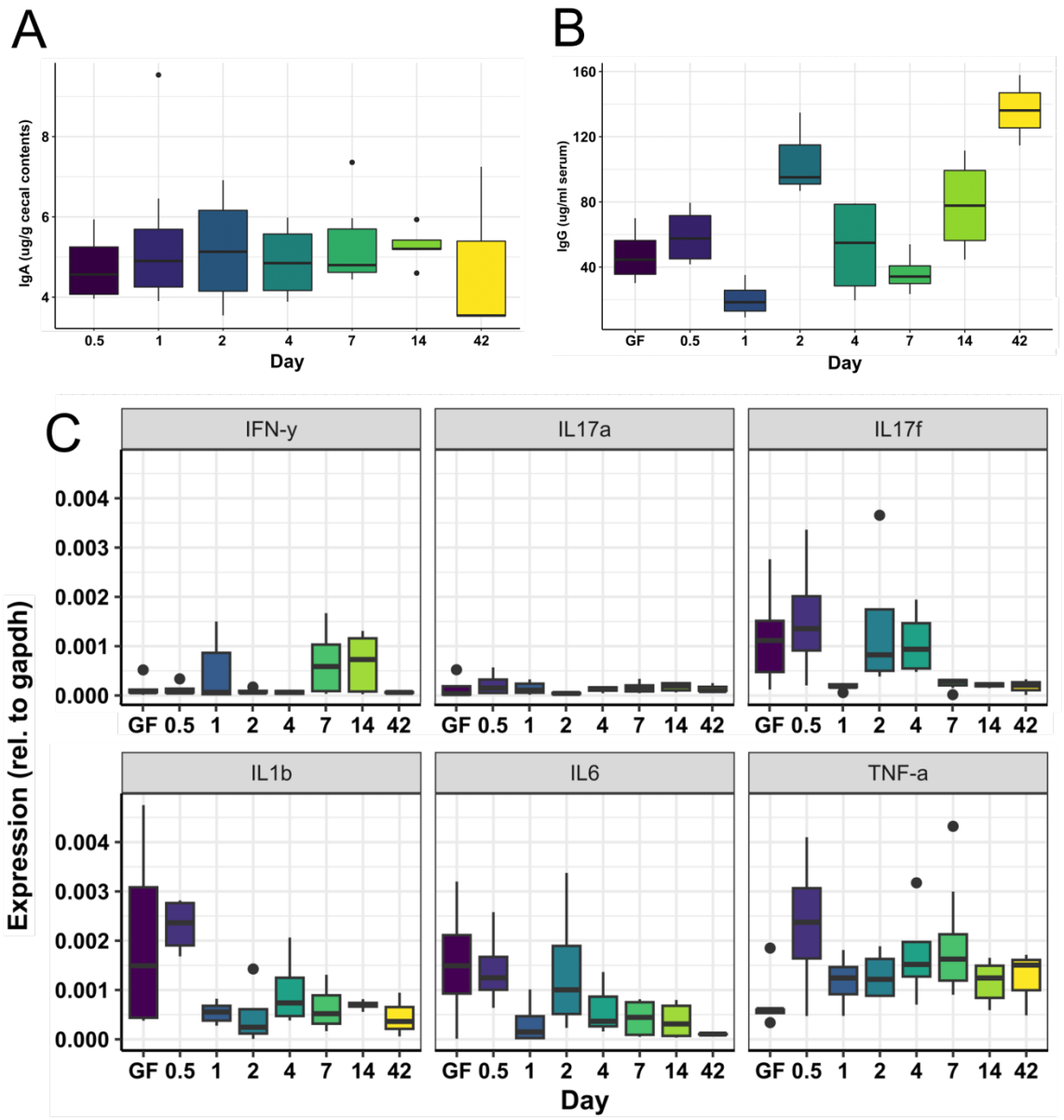

Figure S1.4: *Bt* does not elicit a strong temporal host response. A) Cecal IgA and B) serum IgG levels from mice sacrificed at different timepoints after colonization (n=3-4/timepoint). C) Cytokine expression relative to gapdh in colonic mucosal scrapings at different timepoints after colonization (n=4-6/timepoint).

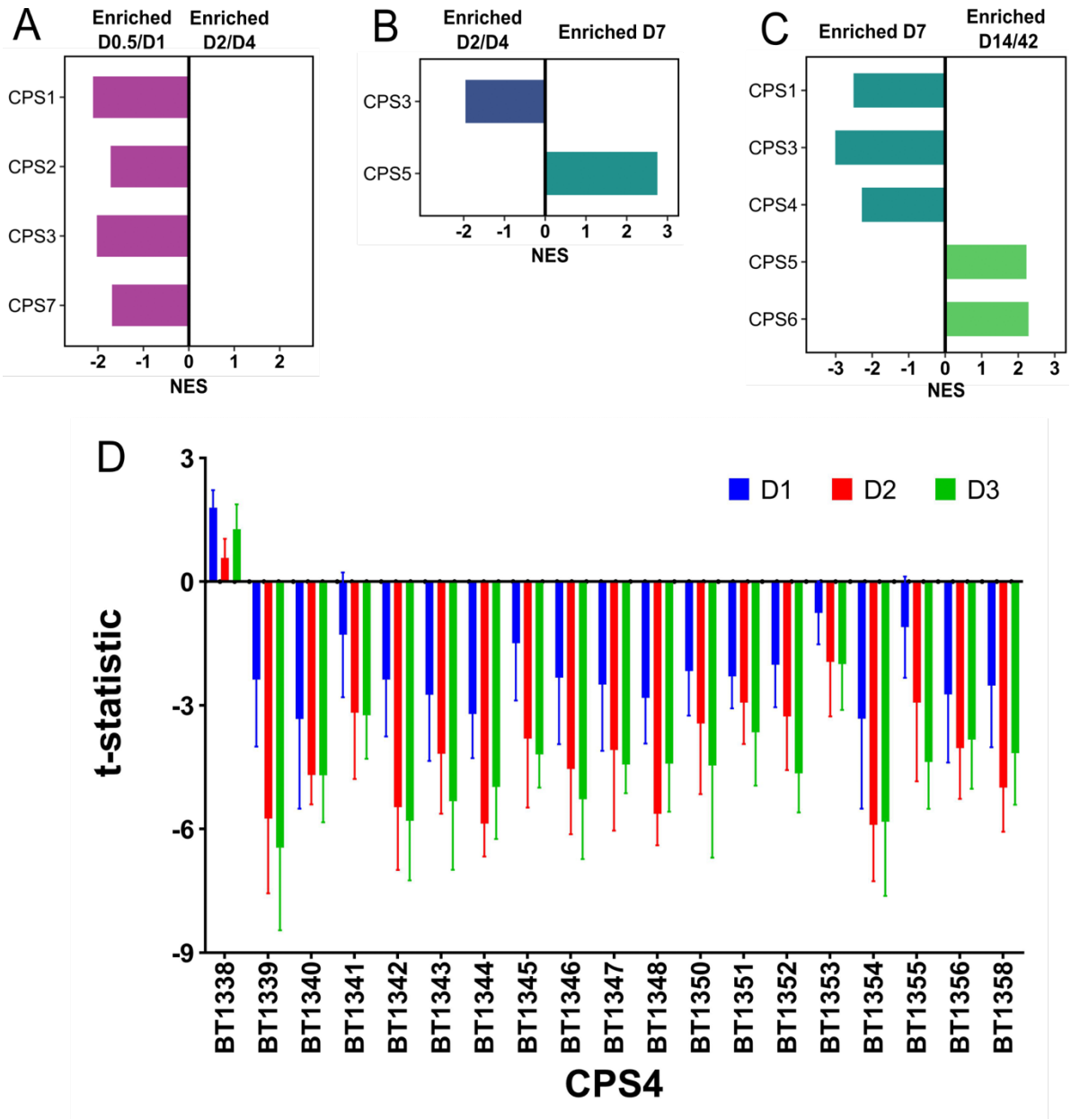

Figure S1.5: Capsular polysaccharide biosynthesis operons are significantly associated with different stages of colonization. (A – D) Gene set enrichment analysis (GSEA) using transcriptomics data for capsular polysaccharide biosynthesis operons, comparing sequential timepoints. Only statistically significant (adj. $p < 0.05$) scores are shown. E) Measurement of the adjusted t-statistic (12) in the RB-Tn assay on all days where fitness score was measurable (D1-3) shows that gene insertions in CPS4 consistently result in significant declines in mutant fitness for all genes within the CPS4 locus except for BT1338. See also Table S5.

Table S1.1: Strains used in this study.

Identifier	Genotype	Source
AMD595	Bacteroides thetaiotaomicron VPI-5482 wildtype	Gift from Deutschbauer lab
AMD790	AMD595-derived RB-Tn library	Gift from Deutschbauer lab
Tn_BT1874	RB-Tn mutant isolated from monocolonized mice with barcoded transposon insertion in BT1874	This work
Tn_BT1876	RB-Tn mutant isolated from monocolonized mice with barcoded transposon insertion in BT1876	This work
Tn_BT1872-83	RB-Tn mutant isolated from monocolonized mice with barcoded transposon insertion in the intergenic region between BT1872 and BT1873	This work
Tn_BT1872	RB-Tn mutant isolated from monocolonized mice with barcoded transposon insertion in BT1872	This work
Tn_BT1874/BT3132	RB-Tn mutant isolated from monocolonized mice with barcoded transposon insertion in BT1874 and BT3132	This work
Tn_BT3133	RB-Tn mutant isolated from monocolonized mice with barcoded transposon insertion in BT3133	This work
WT+BT1871OE	WT Bt with a copy of BT1871 integrated into the Bt genome at the attN1 site under the BT1311 (rpoD) constitutive promoter.	This work
MZ65	Bt mutant isolated from feces after 6-week monoassociation of Bt; carries a tandem repeat of the BT1871 locus (see Fig. 7).	This work

Table S1.2: Custom Ribo-Zero Plus probes

Pool name	Sequence
Supp. Probe Pool	ATCAACGTCATCGTCTTTAACGACCCTAAGAAATCTAATCTTGTGGCTGG
Supp. Probe Pool	ACAGTGTCCTCGCAACTACGAGTTAGAACTCAAATAATCAAAGGGCCGTA
Supp. Probe Pool	CACAAATACTGGCGTACCTGCTTCAAAGTCTCCGGCCTATCCTACACATC
Supp. Probe Pool	AGAAAGGAGGTGTTCCAGCCGCACCTTCCGGTACGGCTACCTTGTTACGA
Supp. Probe Pool	AGCCAGTATCAACTGCAATTTTACGGTTGAGCCGCAAACTTTCACAACTG
Supp. Probe Pool	TATTTGGGGACCTTAGCTGATGGTCTGGATTCTTCTCCTTTAGGACATGG
Supp. Probe Pool	CCTCGCATCTTATCAGTCGCTCTACCTCACATTAGTAACTCACAAGGCTG
Supp. Probe Pool	GCACGGAGTTAGCCGATCCTTATTCATATGGTACATACAAAATTCCACAC
Supp. Probe Pool	CGCTCGTTATGGCACTTAAGCCGACACCTCACGGCACGAGCTGACGACAA
Supp. Probe Pool	TTGTTAGTCTCCCAGTCAAGCGCCCTTATGCCATTACACTCTACGGACGG
Supp. Probe Pool	TACGCTCCCTTTAAACCCAATAAATCCGGATAACGCTCGGATCCTCCGTA
Supp. Probe Pool	CCAGCGGTCAGTCCAACACGGTCCTCTCGTACTAGTGTCAGAGCCACGCA
Supp. Probe Pool	ATCTTACGACGGCAGTCTCTCTAGAGTCCTCAGCATGACCTGTTAGTAAC
Supp. Probe Pool	GCTGCACATCTCAAGATGCTTAACCTTGCCGGAAAAAGTAACTCGTAGGT
Supp. Probe Pool	ATACCACTACGCTTAATTTGACTTCGTATACCGGACTATCACCGTCTATG
Supp. Probe Pool	AGGGCACCTTTAGAAGCCTCCGTTACTATTTTGGAGGCGACCACCCCAGT
Supp. Probe Pool	CCTTTATCGTTACTTATACCTACATTTGCTTTTCCACACGCTCCAGCAAA
Supp. Probe Pool	CGACTTGCATGTGTTAAGCCTGTAGCTAGCGTTCATCCTGAGCCAGGATC
Supp. Probe Pool	ACGTGTTACTCACCCGTGCGCCGGTCGCCATCTCCAGTTTGCAAGCAAAC
Supp. Probe Pool	GGATTCTACTCATCAAATGTCTTGCGACATCGTGGTCCTACAACCCCACA
Supp. Probe Pool	CCCATATAAAAGAAGTTTACAACCCATAGGGCAGTCATCCTTCACGCTAC
Supp. Probe Pool	CAATGTGGGGGACCTTCCTCTCAGAACCCCTATCCATCGAAGGTTTGGTG
Supp. Probe Pool	TAAGGATTAAGTTTAGCGGATTTTCTTGGGAGTATGCTTACACGCACTAT
Supp. Probe Pool	GAACAGCCCAACCCTTGGGACCTTCTCCAGCCCCAGGATGTGACGAGCCG
Supp. Probe Pool	TATATCGCAAACAGCGAGTATTCATCGTTTACTGTGTGGACTACCAGGGT
Supp. Probe Pool	ACATTTGCCTTACGGCTATACTGTTTCCAATATATTCAAATGCAATTTAA
Supp. Probe Pool	GATTATACCATCGGGTATTAATCTTTCTTTCGAAAGGCTATCCCCGAGTT
Supp. Probe Pool	AAAGAAAGTGAACGGGCAATTAGTAATGCTCGGCTTTGATGTTACCACCT
Supp. Probe Pool	CTTTTCAACGCTTATCGGTTCGGTCCTCCAGTTAGTGTTACCTAACCTTC
Supp. Probe Pool	CCCTCACTCCTGTGATAGAACTAATGCGCATTCGGAGTTTATCAAGACTT
Supp. Probe Pool	CACGCCGTCACTGCTTAAGCAGCTCCGACCGCTTGTAGGCGCACGGTTTC
Supp. Probe Pool	CTAACCCTGATCCGATTAGCGTTGATCAGGAAACCTTAGTCTTTCGGCGA

Table S1.2 (cont.): Custom Ribo-Zero Plus probes

Supp. Probe Pool	TCGACGCAGAGTGGAATGCTCCCCTACCGATCATTACTGATCCCATAGCT
Supp. Probe Pool	TTGAGCGATGTCCCTTCCATACGGAAACACCGGATCACTATGCTCTAGTT
Supp. Probe Pool	ATTTAGCCTTACCGGATGGTCCCGGCAGATTCACGCAAGATTTCTCGTGT
Supp. Probe Pool	ATACCCACACTTTCGAGCATCAGTGTCAGTTGCAGTCCAGTGAGCTGCCT
Supp. Probe Pool	GTGGTTTGGGCTATTCCCCGTTCGCTCGCCACTACTAGGGGAATCATTAT
Supp. Probe Pool	CGATAGATAGAGACCGAACTGTCTCACGACGTTCTGAACCCAGCTCGCGT
Supp. Probe Pool	ATGCCGGGTTGTCCCATTCGGAAATCTCTGGATCAAAGGTTATTTGCACC
Supp. Probe Pool	GCCATGGCTGATGCGCGATTACTAGCGAATCCAGCTTCACGAAGTCGGGT
Supp. Probe Pool	CAGTTTTACCCTAGGACGCTCCTTGCGGTTACGTACTTCAGGTACCCCCG
Supp. Probe Pool	GCAGCTTATCACGTCCTTCATCGCCTCCGAGAGCCAAGGCATCCGCCATG
Supp. Probe Pool	GTAATCTTTCAATTTGGCACAGCCCTGTGTTTTTGTTAAACAGTTGCCTG
Supp. Probe Pool	CTTCTATTCGAAGTGCTTTTCACCTTTCCTTCACAGTACTGGTTCGCTAT
Supp. Probe Pool	AGTTTCACCGTTGCCGGCGTACTCCCCAGGTGGAATACTTAATGCTTTCG
Supp. Probe Pool	CGGGGAGTACGAGCTATCTCCAAGTTTGATTAGCCTTTCACCCCCACCCT
Supp. Probe Pool	AGATCACTTGGTTTCGCGTCTACTCCTTCCGACTCGACGCCCTGTTCAGA
Supp. Probe Pool	ATGTTAAGCTATAGTAAAGGTTCACGGGGTCTTTTCGTCCCATCGCGGGT
Supp. Probe Pool	CTTTCAGCACTTATCCAATCCCGACTTAGATACCCAGCAATGCACCTGGC
Supp. Probe Pool	ATGCTTCTCTTGCGATGACATCTCCTCTTAACCTTCCAGCACCGGGCAGG
Supp. Probe Pool	CAGGTACTAAGATGTTTCAGTTCCCTGCGTTAGCTTCCATCAAAGATGGA
Supp. Probe Pool	GGCTGCTTCCAAGCCAACATCCTAGCTGTCTTAGCAATCTGACTTCGTTA
Supp. Probe Pool	ATGCCCGATTATTATCCACGCCAAACTCCTCGACTAGTGAGCTGTTACGC
Supp. Probe Pool	CTTCAACGGACTATTCCGTCAGTCCGCGGCGCTGTCACTGCTCCGTCTCC
Supp. Probe Pool	TTCGTGATATCTAAGCATTTCACCGCTACACCACGAATTCCGCCCACCTC
Supp. Probe Pool	GAATCACTCAAGCGCCTTAGTATATTCAACCCGACTACGTGTGTCCGTTT
Supp. Probe Pool	GTAGTACAGGAATATTAACCTGTTCTGCCATCGGCCTCACCGTTCGGCTG
Supp. Probe Pool	AACGCTCCATACTATCAGGTTCGACTCTCATCCCGGATTTGCCTGGGATG
Supp. Probe Pool	GAACTGAGAGAGGCTTTTGGGATTAGCATCCTGTCACCAGGTAGCTGCCT
Supp. Probe Pool	AACTGCCTAATGGAACGCATCCCCATCGATAACCGAAATTCTTTAATAAC
Supp. Probe Pool	ACCCCTCCGTCGATATGAGCTCTTGGGAGGGATCAGCCTGTTATCCCCGG
Supp. Probe Pool	GTAACACGTGTGTAGCCCCGGACGTAAGGGCCGTGCTGATTTGACGTCAT
Supp. Probe Pool	CCCAACTCTCGTTGGGACCCTTTATCCCGAAGTTACAGGGTCAATTTGCC
Supp. Probe Pool	CTGCGCCCATTGACCAATATTCCTCACTGCTGCCTCCCGTAGGAGTTTGG
Supp. Probe Pool	CGATACTACAATTTCACTGAGCTCACGGTTGAGACAGTGTCCAGATCATT

Table S1.3: MinION Sequencing Attributes

	AMD595	MZ55	MZ58	MZ65
Library Kit	SQK-RBK004	SQK-RBK004	SQK-RBK004	SQK-RBK004
Flowcell ID	FAQ98839	FAQ98839	FAQ98839	FAQ98839
Pore Type	R9.4.1 (FLO-MIN106)	R9.4.1 (FLO-MIN106)	R9.4.1 (FLO-MIN106)	R9.4.1 (FLO-MIN106)
Start Materials (ng)	10,000	10,000	10,000	10,000
DNA Shearing	22G needle 10X, 250ul	22G needle 10X, 250ul	22G needle 10X, 250ul	22G needle 10X, 250ul
Barcoding Input (ng)	994.5	792.2	494.7	1249.5
Pool Volume (ul)	5	6	10	4
Pool DNA Input (ng)	497.3	475.3	494.7	499.8
Total Pool Volume (ul)	25	25	25	25
Total Reads	~1,510,000			
Total Pass Reads (%)	1,343,227 (88.95)			
Total Pass Reads per Barcode	344,988	298,543	445,074	113,979
Average length (bp)	7,226	8,857	7,882	8,266
Max. length (bp)	108,747	141,745	114,845	109,375
N50 (bp)	12,596	16,820	14,970	15,675
Top 25% Templates (bp)	9,643	11,730	10,532	11,037
Total Called bases	2,493,077,325	2,644,475,924	3,508,117,512	942,158,294
Base Calling	Guppy v5.0.11	Guppy v5.0.11	Guppy v5.0.11	Guppy v5.0.11
MinKNOW version	4.3.4	4.3.4	4.3.4	4.3.4

Table S1.4: RNAseq PERMANOVA Analysis

Factor	Df	SumOfSqs	R2	F	Pr(>F)
Experimental Day	7	1.4155123	0.7989091	13.05374	0.0001
Residual	23	0.3562941	0.2010909	NA	NA
Total	30	1.7718064	1	NA	NA

Table S1.5: RNAseq PERMANOVA post-hoc analyses

pairs	Df	SumsOfSqs	F.Model	R2	p.value	p.adjusted
IV vs 0.5	1	0.3363126	54.3571139	0.9005917	0.033	0.04454545
IV vs 1	1	0.36414389	14.2263602	0.7399404	0.033	0.04454545
IV vs 2	1	0.33830191	69.1004526	0.920107	0.034	0.04454545
IV vs 4	1	0.40338568	44.330188	0.8807873	0.034	0.04454545
IV vs 7	1	0.39487113	72.0813667	0.9231571	0.035	0.04454545
IV vs 14	1	0.4582011	47.5005038	0.8715608	0.007	0.04454545
IV vs 42	1	0.396247	50.3418962	0.9096525	0.027	0.04454545
7 vs 14	1	0.036523	3.17603916	0.17473769	0.023	0.03054545
7 vs 1	1	0.17683643	5.8942621	0.5410428	0.029	0.04454545
7 vs 4	1	0.08384591	6.5656284	0.522507	0.034	0.04454545
7 vs 2	1	0.07366048	8.5985064	0.588999	0.027	0.04454545
7 vs 42	1	0.03336466	2.7178432	0.3521506	0.034	0.04454545
7 vs 0.5	1	0.18269757	18.5330078	0.7554315	0.026	0.04454545
14 vs 1	1	0.29545572	9.5998797	0.6153816	0.019	0.04454545
14 vs 4	1	0.065907	4.1459337	0.3719683	0.016	0.04454545
14 vs 2	1	0.06809244	5.5388759	0.4417362	0.027	0.04454545
14 vs 42	1	0.03662085	2.2879538	0.2760577	0.101	0.10876923
14 vs 0.5	1	0.27676428	20.6534764	0.7468673	0.01	0.04454545
1 vs 4	1	0.32163646	9.3642751	0.6519142	0.039	0.04747826
1 vs 2	1	0.26873972	9.1711729	0.6471711	0.03	0.04454545
1 vs 42	1	0.20765583	5.3076981	0.5702482	0.03	0.04454545
1 vs 0.5	1	0.09065953	2.93851	0.3701589	0.145	0.15037037
4 vs 2	1	0.01158527	0.9505391	0.1367576	0.559	0.559
4 vs 42	1	0.05698817	3.4285032	0.4067749	0.03	0.04454545
4 vs 0.5	1	0.25237408	18.7229515	0.7573105	0.031	0.04454545
2 vs 42	1	0.05613006	4.8482631	0.4922963	0.016	0.04454545
2 vs 0.5	1	0.19738708	21.2801937	0.7800602	0.034	0.04454545
42 vs 0.5	1	0.19288631	14.6939632	0.7461151	0.027	0.04454545

Table S1.6: RB-TnSeq PERMANOVA analysis

	Df	SumOfSqs	R2	F	Pr(>F)
Experimental Day	15	23.845	0.45739	15.4931	0.0001
Mouse ID	25	7.071	0.13564	2.7567	0.0001
Experimental Run	3	4.8	0.09207	15.5925	0.0001
Residual	160	16.417	0.3149	NA	NA
Total	203	52.133	1	NA	NA

Table S1.7: Metabolomics internal standards

Panel	ITSD	Vendor	Product Number	Concentration	Mass/Volume for 1L
SCFA	D3-Acetate	CIL	DLM-3126-25	4 mM	340 mg
SCFA	D5-Propionate	CIL	DLM-1601-1	1 mM	101.1 mg
SCFA	D7-Butyrate	CIL	DLM-7616-PK	.5 mM	58.56 mg
SCFA	D9-Valerate	CIL	DLM-572-5	.25 mM	29.60 µL
SCFA	D8-Valine	CIL	DLM-488-0.25	.05 mM	6.26 mg
SCFA	D6-Succinate	CIL	DLM-831-PK	1 mM	124.14 mg
SCFA	D6-Phenol	CIL	DLM-370-PK	.025 mM	2.5 mg
TMS	U13C-Palmitate	CIL	CLM-409-PK	.04 mM	10.9 mg
TMS/SCFA	D7N15-Proline	CIL	DLNM-7562-0.25	.02 mM	2.46 mg
Bile Acids	D4-Cholic Acid	CIL	DLM-2611-0.05	1 ug/mL	1 mL of 1 mg/mL stock
Bile Acids	D4-Deoxycholic Acid	CIL	DLM-2824-0.01	1 ug/mL	1 mL of 1 mg/mL stock

Table S1.7 (cont.): Metabolomics internal standards

Bile Acids	D4-Glycocholic Acid	CIL	DLM-2742-0.01	1 ug/mL	1 mL of 1 mg/mL stock
Bile Acids	D4-Glycodeoxycholic Acid	CIL	DLM-9554-0.01	.5 ug/mL	.5 mL of 1 mg/mL stock
Bile Acids	D4-Litchocholic Acid	CIL	DLM-9560-0.05	5 ug/mL	5 mL of 1 mg/mL stock
Bile Acids	D4-Taurocholic Acid	CIL	DLM-9572-0.01	1 ug/mL	1 mL of 1 mg/mL stock
Bile Acids	D4-Taurodeoxycholic Acid	CIL	DLM-9568-0.01	.5 ug/mL	.5 mL of 1 mg/mL stock
Bile Acids	D5-Alpha-Muricholic Acid	CIL	DLM-10627-PK	3.5 ug/mL	3.5 mL of 1 mg/mL stock
Indoles	13C11-L-Tryptophan	CIL	CLM-4290-H	500 nM	50 µL of 10 mM stock
Indoles	13C9-L-Phenylalanine	CIL	CLM-2250-H	500 nM	50 µL of 10 mM stock
Indoles	13C9-L-Tyrosine	CIL	CLM-2263-H	500 nM	50 µL of 10 mM stock
Indoles	D4-Serotonin	CIL	DLM-11030-0	500 nM	50 µL of 10 mM stock
Indoles	13C6-5-Hydroxyindole-3-acetic acid	CIL	CLM-9936-0	500 nM	50 µL of 10 mM stock
Indoles	D4-Tryptamine	CIL	DLM-6989-0	500 nM	50 µL of 10 mM stock
Indoles	D3-Melatonin	CIL	DLM-7101-0	500 nM	50 µL of 10 mM stock
Indoles	13C6-Niacin	CIL	CLM-9954-0	2 µM	200 µL of 10 mM stock
Indoles	13C10-L-Kynurenine	CIL	CLM-9884-0	500 nM	50 µL of 10 mM stock
Indoles	D5-Kynurenic Acid	CIL	DLM-7374-0	500 nM	50 µL of 10 mM stock
Indoles	Anthranilic Acid, Ring-13C6	CIL	CLM-701-0	500 nM	50 µL of 10 mM stock

Table S1.8: Amino acid PERMANOVA analysis

Metabolite	F	p	R2
Alanine	0.4023	0.6802	0.08207
Asparagine	4.367	0.04727	0.4925
Aspartate	13.58	0.001912	0.7512
Cysteine	3.081	0.09563	0.3772
Glutamate	7.805	0.01082	0.6343
Glutamine	3.075	0.09597	0.406
Glycine	42.77	2.53E-05	0.9048
Isoleucine	8.411	0.008711	0.6515
Leucine	2.616	0.1272	0.3676
Lysine	1.906	0.2042	0.2975
Methionine	0.1456	0.8665	0.03135
Phenylalanine	3.122	0.09338	0.4096
Proline	4.649	0.04104	0.5082
Serine	33.35	6.89E-05	0.8811
Threonine	72.38	2.83E-06	0.9415
Tryptophan	1.924	0.2015	0.2995
Tyrosine	8.562	0.008269	0.6555
Valine	4.271	0.04964	0.4869

Table S1.9: Amino acid PERMANOVA post-hoc analyses

Metabolite	Comparison	Mean Diff.	Discovery?	Individual p value	q value
Asparagine	D1 vs. D7	0.772	Yes	0.0311	0.0163
Asparagine	D1 vs. D14	0.7765	Yes	0.0304	0.0163
Asparagine	D7 vs. D14	0.0045	No	0.9885	0.346
Glutamate	D1 vs. D7	-0.199	Yes	0.0037	0.0039
Glutamate	D1 vs. D14	-0.06575	No	0.2322	0.0813
Glutamate	D7 vs. D14	0.1333	Yes	0.0289	0.0152
Glycine	D1 vs. D7	0.2798	Yes	<0.0001	<0.0001
Glycine	D1 vs. D14	0.3128	Yes	<0.0001	<0.0001
Glycine	D7 vs. D14	0.033	No	0.3976	0.1392
Isoleucine	D1 vs. D7	2.134	Yes	0.0057	0.0035
Isoleucine	D1 vs. D14	2.073	Yes	0.0067	0.0035
Isoleucine	D7 vs. D14	-0.06125	No	0.9199	0.322
Proline	D1 vs. D7	-6.223	Yes	0.0146	0.0307
Proline	D1 vs. D14	-2.283	No	0.2976	0.2083
Proline	D7 vs. D14	3.94	No	0.0887	0.0931
Serine	D1 vs. D7	2.921	Yes	<0.0001	<0.0001
Serine	D1 vs. D14	2.883	Yes	<0.0001	<0.0001
Serine	D7 vs. D14	-0.03775	No	0.9287	0.3251
Threonine	D1 vs. D7	2.073	Yes	<0.0001	<0.0001
Threonine	D1 vs. D14	2.063	Yes	<0.0001	<0.0001
Threonine	D7 vs. D14	-0.0105	No	0.959	0.3356
Tyrosine	D1 vs. D7	0.5433	Yes	0.0112	0.0059
Tyrosine	D1 vs. D14	0.663	Yes	0.0037	0.0039
Tyrosine	D7 vs. D14	0.1198	No	0.5009	0.1753
Valine	D1 vs. D7	0.5643	No	0.0309	0.0528
Valine	D1 vs. D14	0.5535	No	0.0335	0.0528
Valine	D7 vs. D14	-0.01075	No	0.9622	>0.9999

Table S1.10: Supplementary file available at https://github.com/mkennedy21/Btheta. Table includes all pairwise RNAseq comparisons and GSEA analyses.

Table S1.11: ANOVA on RB-Tn mutant growth rates with post-hoc pairwise analyses

one-way ANOVA

F	p	R2
34.34	<0.0001	0.7874

Post-hoc follow-up:

Comparison	Mean Diff.	Discovery?	Individual P Value	q value
WT vs. Tn_BT1874	-0.5516	Yes	<0.0001	<0.0001
WT vs. *Tn_BT1876	-0.566	Yes	<0.0001	<0.0001
WT vs. *Tn_BT1872/73	-0.595	Yes	<0.0001	<0.0001
WT vs. Tn_BT1872	-0.6356	Yes	<0.0001	<0.0001
WT vs. Tn_BT1872	-0.6643	Yes	<0.0001	<0.0001
WT vs. Tn_BT1872/73	-0.6337	Yes	<0.0001	<0.0001
WT vs. Tn_BT1874/BT3132	-0.4423	Yes	<0.0001	<0.0001
WT vs. Tn_BT3133	-0.4574	Yes	<0.0001	<0.0001
WT vs. Tn_BT3133	-0.6113	Yes	<0.0001	<0.0001
WT vs. Tn_BT3133	-0.6037	Yes	<0.0001	<0.0001
WT vs. WT_BT1871OE	-0.2917	Yes	<0.0001	<0.0001

Table S1.12: Comparison of a-gal expression in WT and RB-Tn mutants.

Gene	Comparison	P value	Mean of WT	Mean of Tn Mut.	Difference	SE of diff.	t ratio	df
BT1871	WT vs Tn_BT1872	<0.000001	70.46	1847	-1777	7.109	249.9	5
BT1871	WT vs Tn_BT3133	0.032341	70.46	53.78	16.68	5.679	2.938	5
BT3131	WT vs Tn_BT1872	0.014004	9.628	6.528	3.1	0.838	3.7	5
BT3131	WT vs Tn_BT3133	0.000002	9.628	1585	-1575	64.83	24.29	5
BT2851	WT vs Tn_BT1872	0.651401	14.92	16.19	-1.272	2.65	0.4801	5
BT2851	WT vs Tn_BT3133	0.945557	14.92	14.82	0.1033	1.439	0.07178	5

Table S1.13: ANOVA comparison of raffinose abundances in mouse chow and cecal contents at different days of colonization with post-hoc pairwise comparisons.

one-way ANOVA

F	p	R2
69.36	<0.0001	0.9487

Post-hoc follow-up:

Comparison	Mean Diff.	Discovery?	Individual P Value	q value
Food vs. D0	-54.66	Yes	<0.0001	<0.0001
Food vs. D1	-60.54	Yes	<0.0001	<0.0001
Food vs. D7	28.23	Yes	0.0008	0.0026
Food vs. D14	20.04	Yes	0.0057	0.0219
D0 vs. D1	-5.874	No	0.0854	0.4068
D0 vs. D7	82.9	Yes	<0.0001	<0.0001
D0 vs. D14	74.7	Yes	<0.0001	<0.0001
D1 vs. D7	88.77	Yes	<0.0001	<0.0001
D1 vs. D14	80.58	Yes	<0.0001	<0.0001
D7 vs. D14	-8.195	No	0.0645	0.2763

Table S1.14: ANOVA comparisons of WT and RB-Tn mutant growth rates on minimal media with the indicated carbon substrate; post-hoc follow-up analyses where applicable.

Raffinose one-way ANOVA			
F	**p**	**R2**	
45.49	<0.0001	0.8835	
Raffinose Post-hoc follow-up:			
Comparison	**Mean Diff.**	**Individual P Value**	**q value**
WT vs. Tn_BT1872	-0.1025	<0.0001	<0.0001
WT vs. Tn_BT3133	-0.00427	0.2647	0.7562
Tn_BT1872 vs. Tn_BT3133	0.09828	<0.0001	<0.0001
Melibiose one-way ANOVA			
F	**p**	**R2**	
146.4	<0.0001	0.9513	
Melibiose Post-hoc follow-up:			
Comparison	**Mean Diff.**	**Individual P Value**	**q value**
WT vs. Tn_BT1872	-0.5122	<0.0001	<0.0001
WT vs. Tn_BT3133	-0.4557	<0.0001	<0.0001
Tn_BT1872 vs. Tn_BT3133	0.05651	0.037	0.1057
Sucrose one-way ANOVA			
F	**p**	**R2**	
0.05349	0.9481	0.007082	
Galactose one-way ANOVA			
F	**p**	**R2**	
2.627	0.1074	0.2729	
Glucose one-way ANOVA			
F	**p**	**R2**	
0.01702	0.9831	0.002264	

Table S1.15: ANOVA comparison of melibiose abundances in mouse chow and cecal contents at different days of colonization with post-hoc pairwise comparisons.

one-way ANOVA

F	p	R2
9.917	0.0004	0.7256

Post-hoc follow-up:

Comparison	Mean Diff.	Discovery?	Individual P Value	q value
Food vs. PBS	-1.938	Yes	0.0194	0.0278
Food vs. D1	-3.392	Yes	0.0014	0.001
Food vs. D7	0.01984	No	0.4121	0.9813
Food vs. D14	0.7756	No	0.1708	0.3659
PBS vs. D1	-1.455	Yes	0.039	0.0651
PBS vs. D7	1.958	Yes	0.0144	0.0172
PBS vs. D14	2.714	Yes	0.0022	0.0021
D1 vs. D7	3.412	Yes	0.001	0.0005
D1 vs. D14	4.168	Yes	0.0003	<0.0001
D7 vs. D14	0.7558	No	0.1708	0.342

Table S1.16: ANOVA comparison of sucrose abundances in mouse chow and cecal contents at different days of colonization with post-hoc pairwise comparisons.

one-way ANOVA

F	p	R2
63.48	<0.0001	0.9442

Post-hoc follow-up:

Comparison	Mean Diff.	Discovery?	Individual P Value	q value
Food vs. PBS	28.14	Yes	<0.0001	<0.0001
Food vs. D1	27.88	Yes	<0.0001	<0.0001
Food vs. D7	28.38	Yes	<0.0001	<0.0001
Food vs. D14	28.34	Yes	<0.0001	<0.0001
PBS vs. D1	-0.263	No	0.8915	0.6213
PBS vs. D7	0.2399	No	0.9009	0.6213
PBS vs. D14	0.2048	No	0.9154	0.6213
D1 vs. D7	0.5029	No	0.8046	0.6213
D1 vs. D14	0.4678	No	0.818	0.6213
D7 vs. D14	-0.03509	No	0.9862	0.6213

APPENDIX 2: SUPPLEMENTAL FIGURES AND TABLES FOR CHAPTER 2

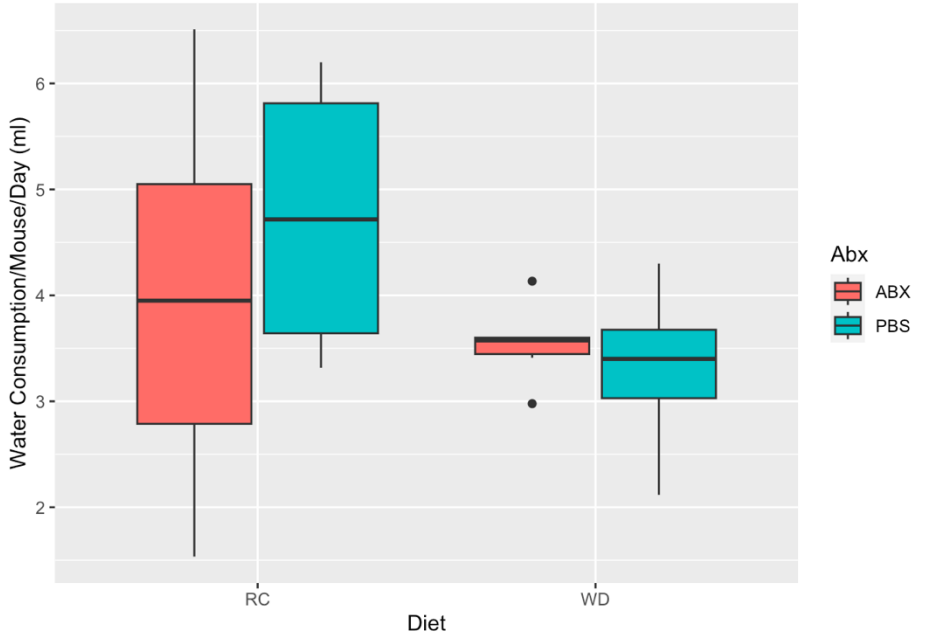

Figure S2.1: Water consumption of mice on each dietary and antibiotic treatment. Measurements collected during the 72 hours when antibiotics were being administered. No statistically significant differences between any groups were identified.

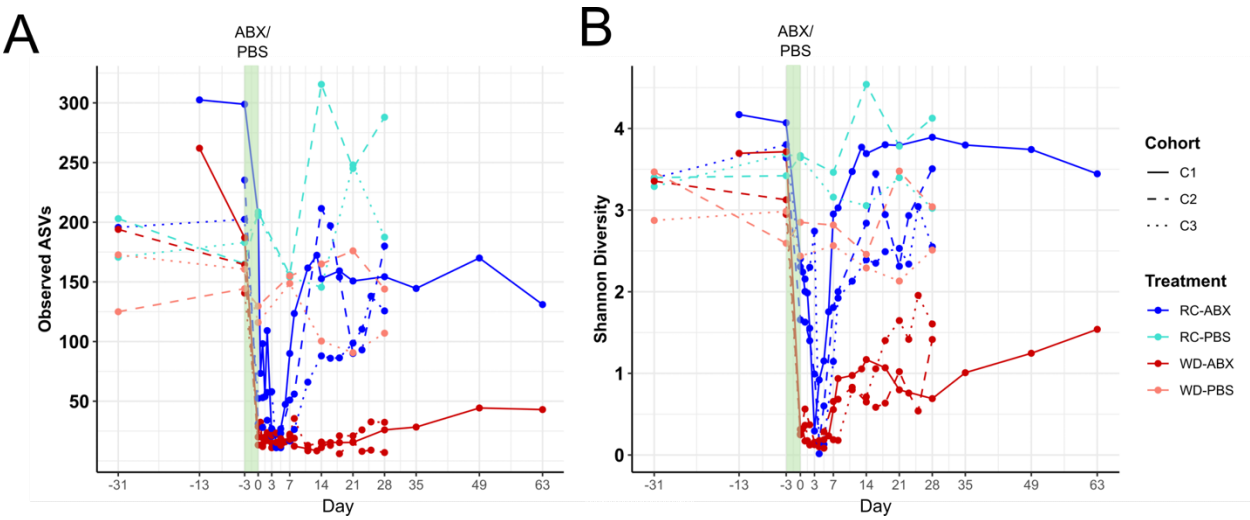

Figure S2.2: Alpha diversity by treatment group and cohort. (A) ASV richness, (B) Shannon Diversity.

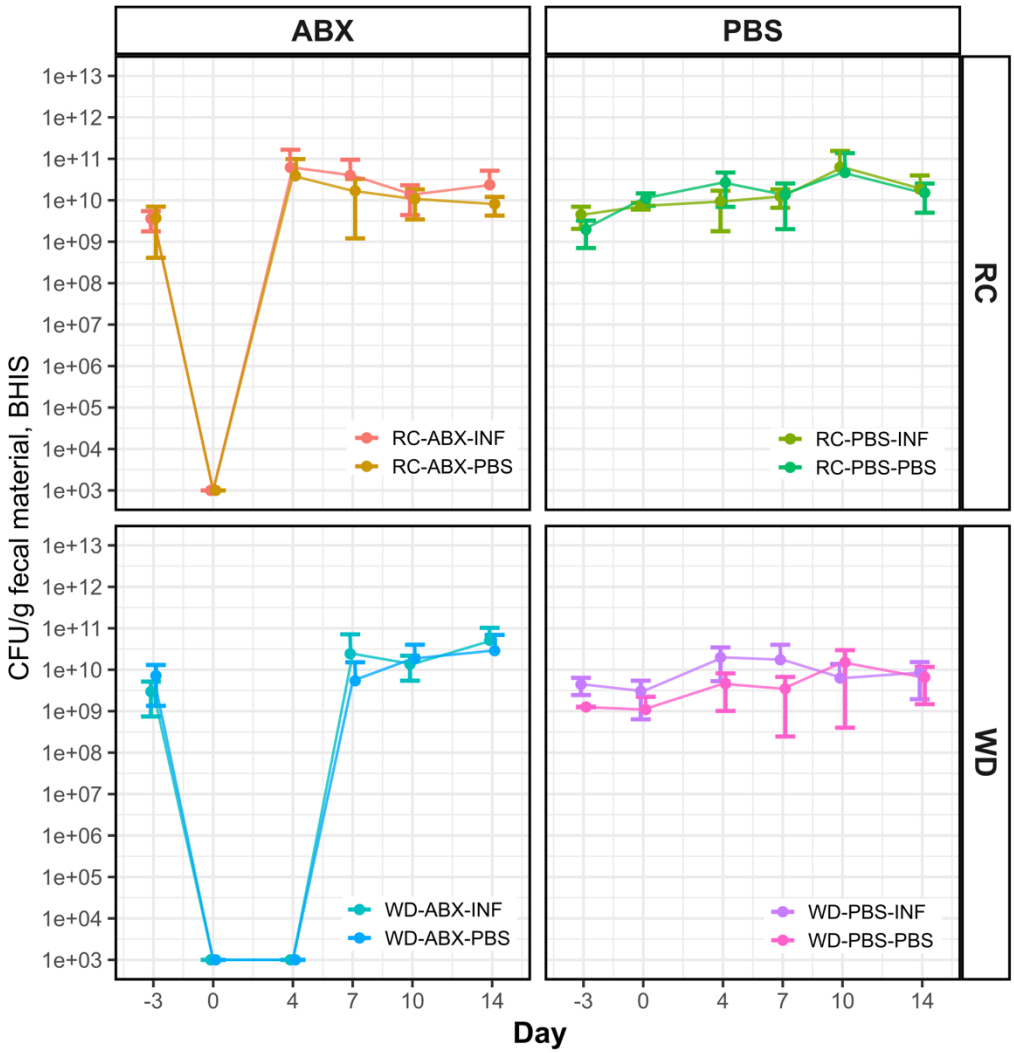

Figure S2.3: Bacterial biomass (CFUs/g fecal material) for all treatment groups in colonization resistance experiments. n=3-9/group.

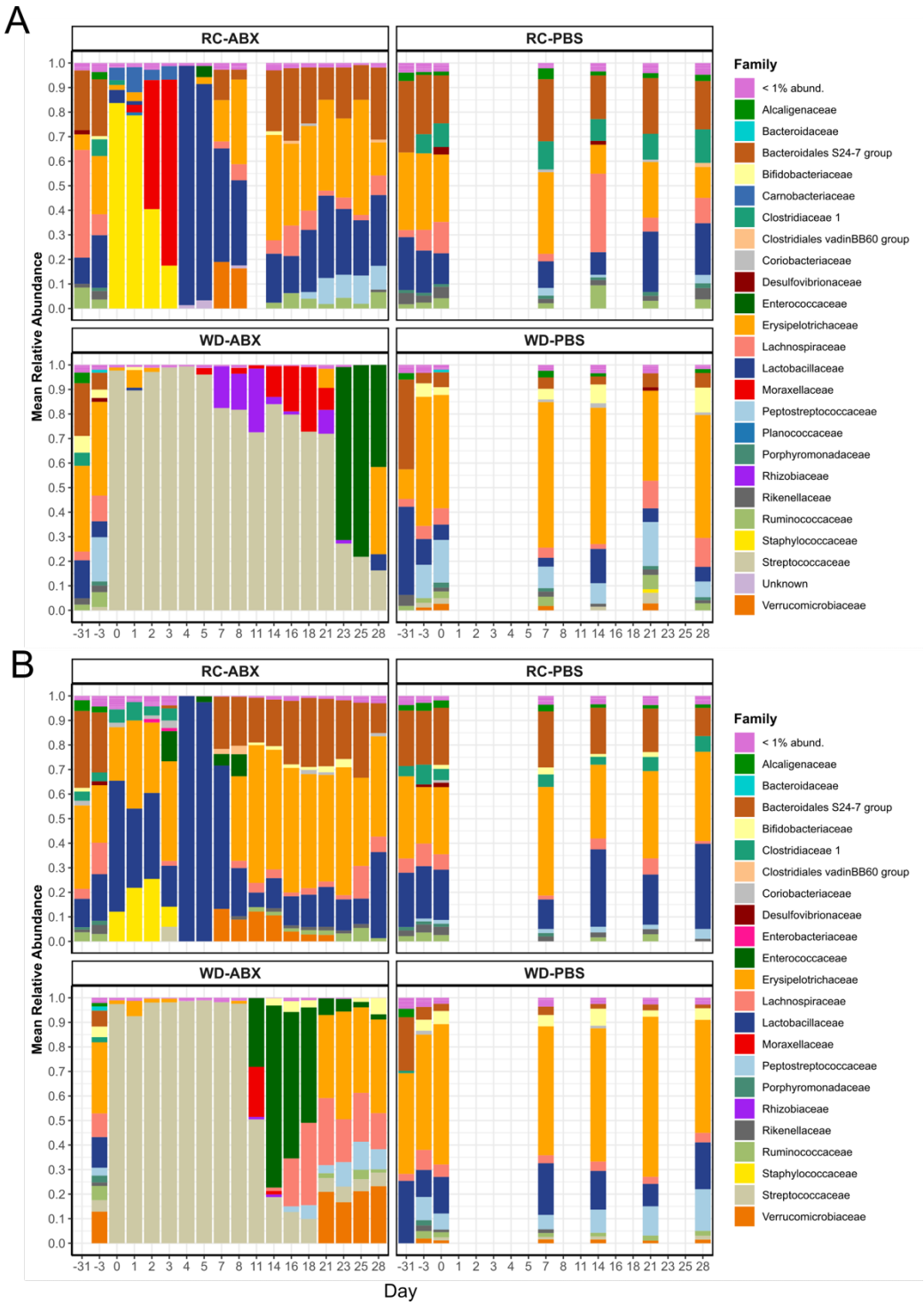

Figure S2.4: Mean relative abundances of different microbial families for mice from Cohorts 2 and 3. n=1-4/group.

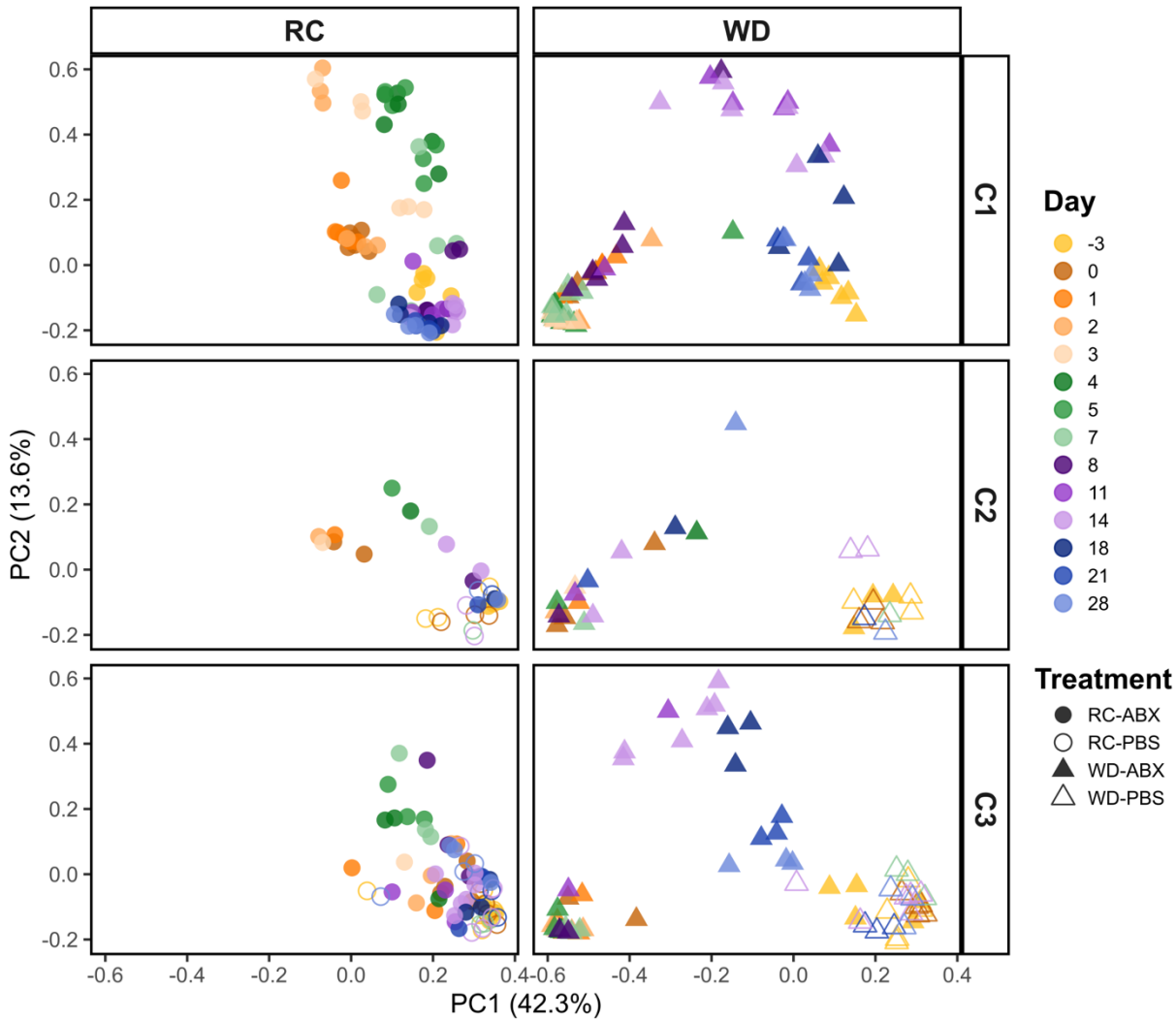

Figure S2.5: PCoA of 16S-based microbiome taxonomic composition at the genus level using Bray-Curtis dissimilarity for samples from all treatment groups and cohorts through D28.

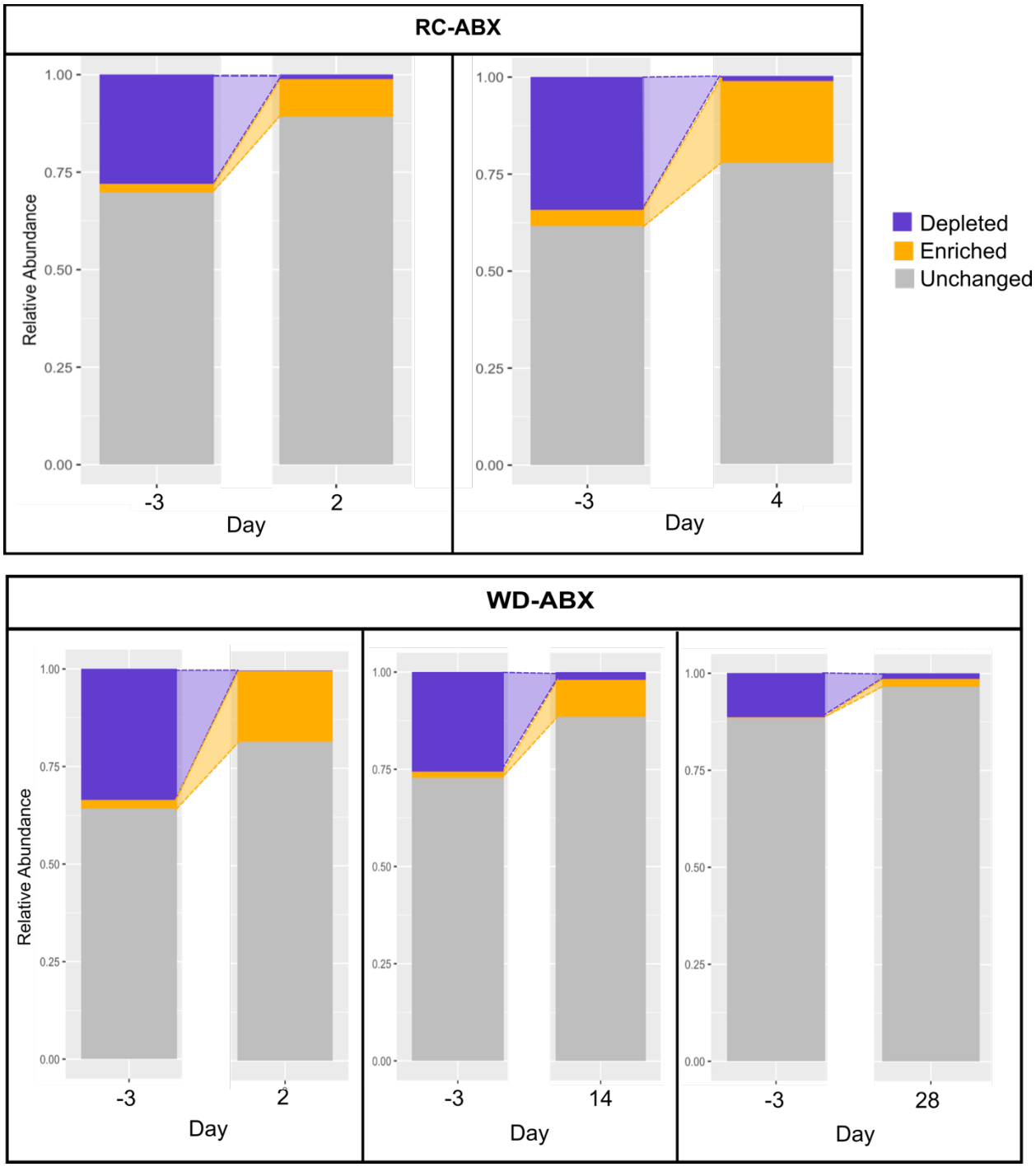

Figure S2.6: Relative abundances of KOs that become depleted or enriched after D-3. Each paired plot represents the change in relative abundance of KOs that were identified as significantly differentially abundant between D-3 and the indicated day.

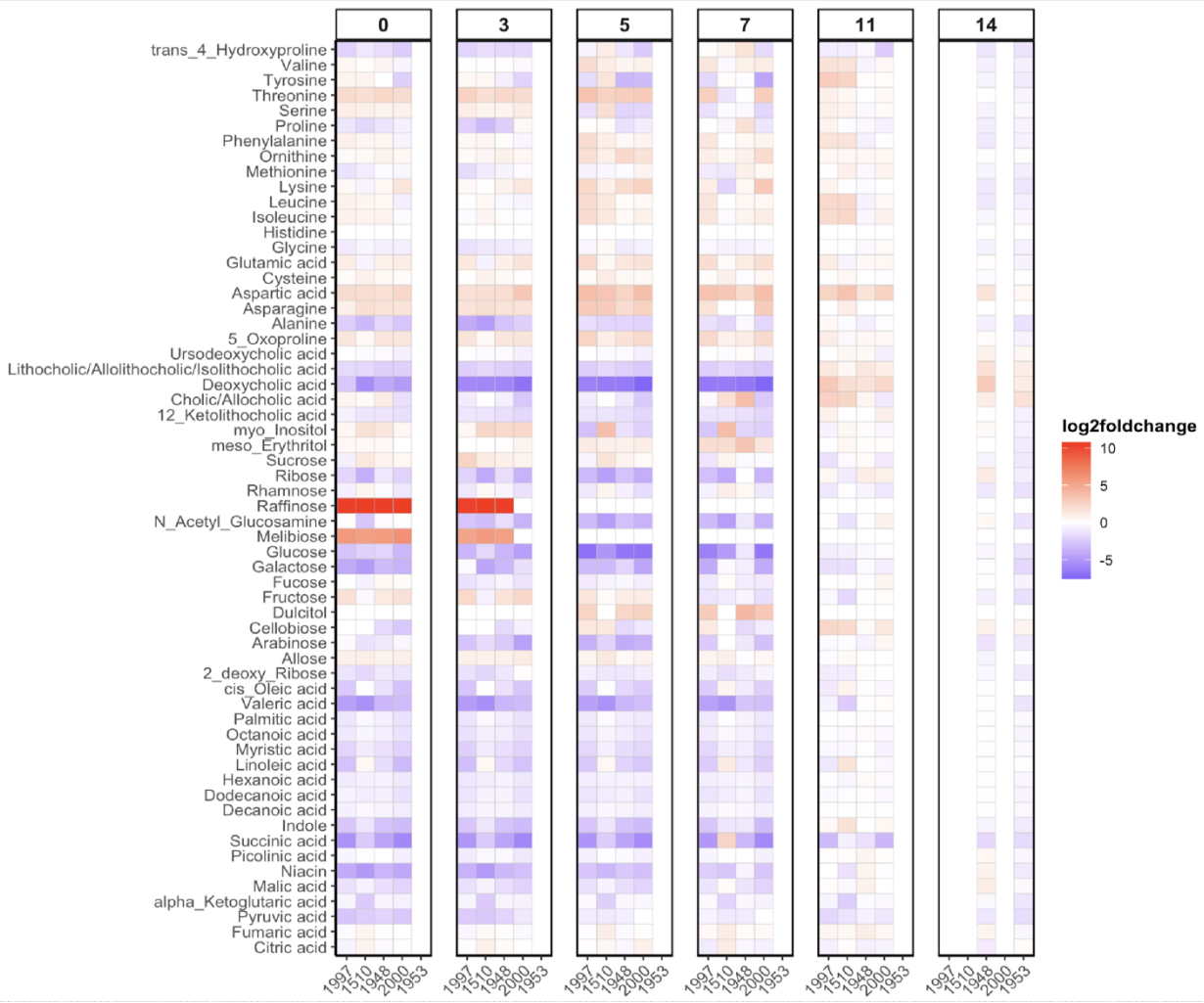

Figure S2.7: Normalized metabolite abundances for mice on RC-ABX at different timepoints are consistent across mice. Each vertical block represents a different day of recovery. Each column within a block represents samples from a different mouse. Abundances are normalized to D-3 (pre-ABX) for each mouse.

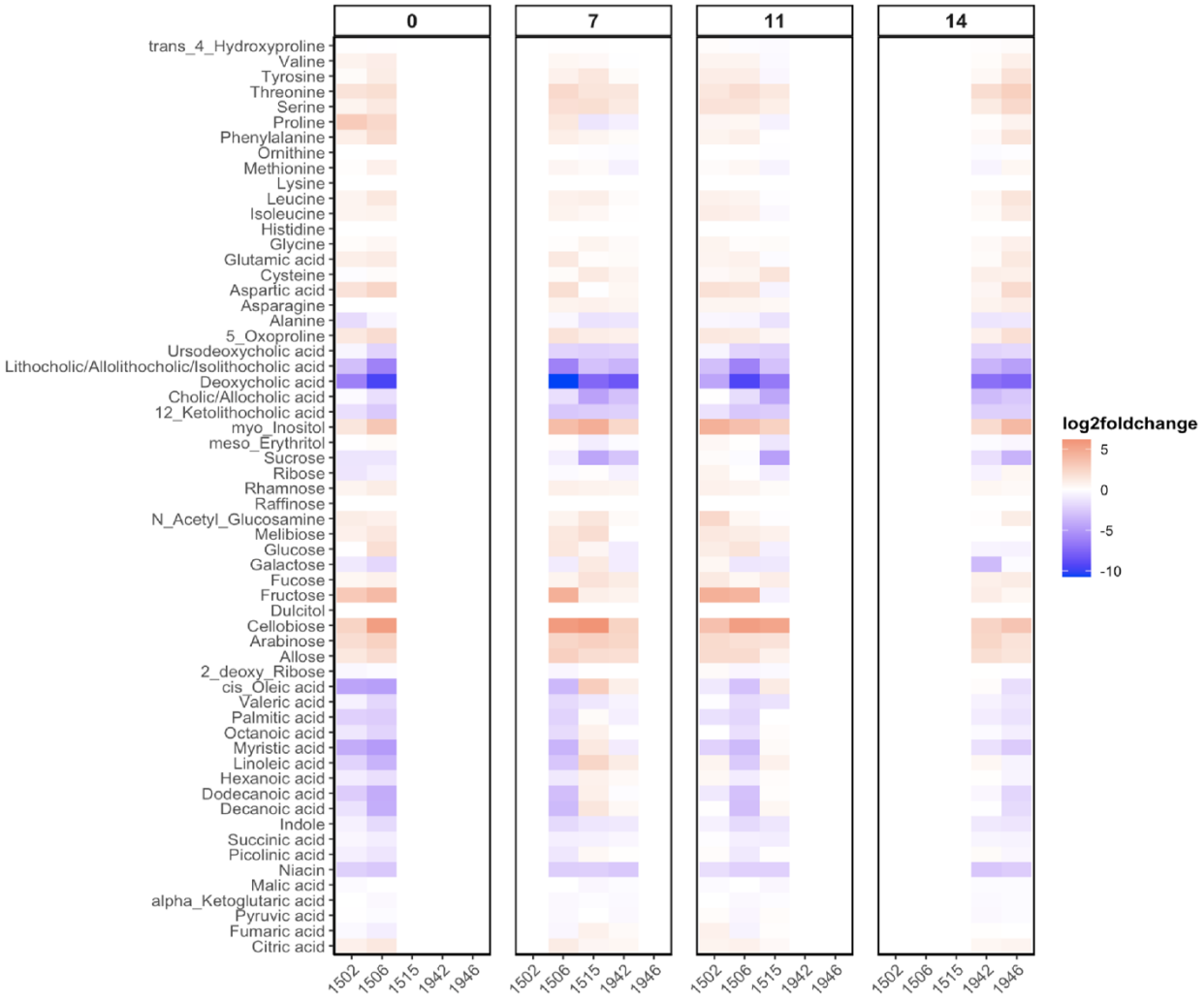

Figure S2.8: Normalized metabolite abundances for mice on WD-ABX at different timepoints are consistent across mice. Each vertical block represents a different day of recovery. Each column within a block represents samples from a different mouse. Abundances are normalized to D-3 (pre-ABX) for each mouse.

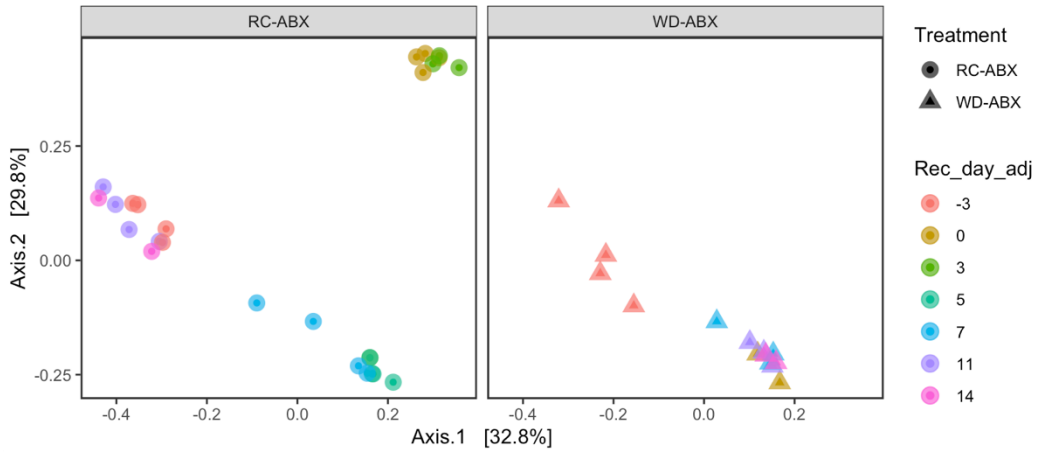

Figure S2.9: PCoA plot using Bray-Curtis dissimilarity on fecal metabolomic profile for mice on RC-ABX and WD-ABX. See Table S2.8.

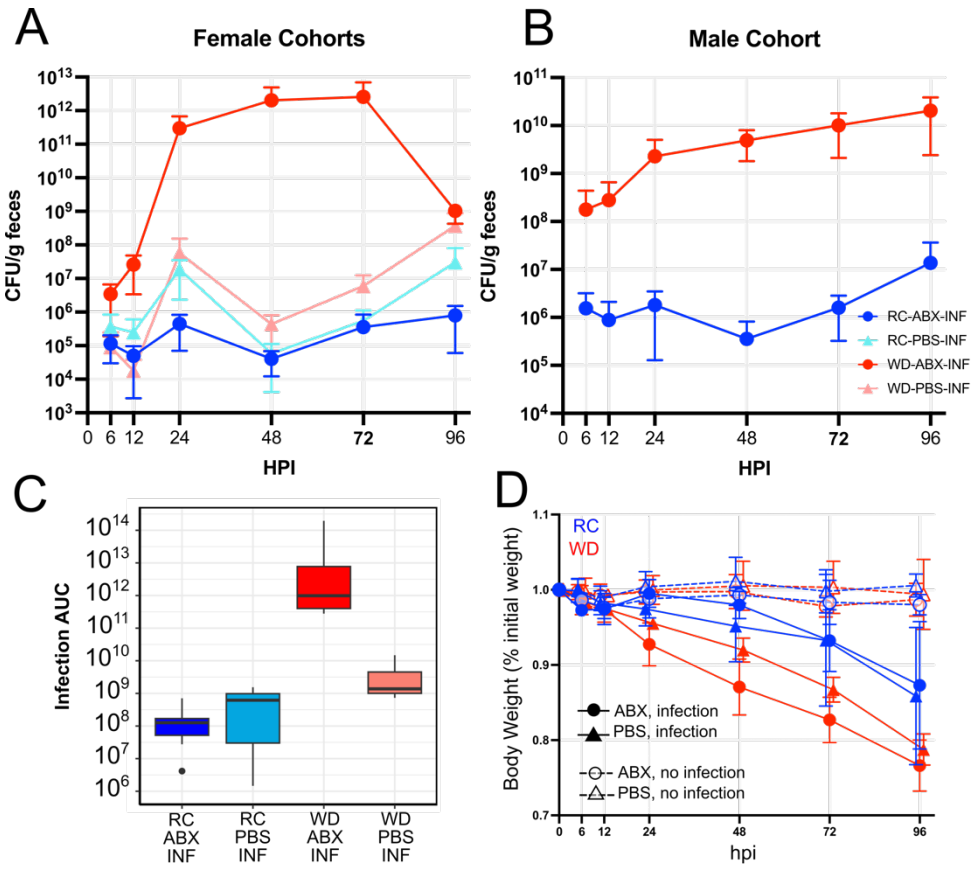

Figure S2.10: Supplemental information regarding colonization resistance experiments. CFU counts from (A) Female and (B) male cohorts. (C) Infection AUC for all infected treatment groups. See Table S2.13. (D) Body weight after infection as a percentage of pre-infection body weight for all treatment groups. See Table S2.14.

Table S2.1: Metabolomics internal standards

Panel	ITSD	Vendor	Product Number	Concentration	Mass/Volume for 1L
SCFA	D3-Acetate	CIL	DLM-3126-25	4 mM	340 mg
SCFA	D5-Propionate	CIL	DLM-1601-1	1 mM	101.1 mg
SCFA	D7-Butyrate	CIL	DLM-7616-PK	.5 mM	58.56 mg
SCFA	D9-Valerate	CIL	DLM-572-5	.25 mM	29.60 µL
SCFA	D8-Valine	CIL	DLM-488-0.25	.05 mM	6.26 mg
SCFA	D6-Succinate	CIL	DLM-831-PK	1 mM	124.14 mg
SCFA	D6-Phenol	CIL	DLM-370-PK	.025 mM	2.5 mg
TMS	U13C-Palmitate	CIL	CLM-409-PK	.04 mM	10.9 mg
TMS/SCFA	D7N15-Proline	CIL	DLNM-7562-0.25	.02 mM	2.46 mg
Bile Acids	D4-Cholic Acid	CIL	DLM-2611-0.05	1 ug/mL	1 mL of 1 mg/mL stock
Bile Acids	D4-Deoxycholic Acid	CIL	DLM-2824-0.01	1 ug/mL	1 mL of 1 mg/mL stock
Bile Acids	D4-Glycocholic Acid	CIL	DLM-2742-0.01	1 ug/mL	1 mL of 1 mg/mL stock
Bile Acids	D4-Glycodeoxycholic Acid	CIL	DLM-9554-0.01	.5 ug/mL	.5 mL of 1 mg/mL stock
Bile Acids	D4-Litchocholic Acid	CIL	DLM-9560-0.05	5 ug/mL	5 mL of 1 mg/mL stock
Bile Acids	D4-Taurocholic Acid	CIL	DLM-9572-0.01	1 ug/mL	1 mL of 1 mg/mL stock
Bile Acids	D4-Taurodeoxycholic Acid	CIL	DLM-9568-0.01	.5 ug/mL	.5 mL of 1 mg/mL stock
Bile Acids	D5-Alpha-Muricholic Acid	CIL	DLM-10627-PK	3.5 ug/mL	3.5 mL of 1 mg/mL stock

Table S2.1 (cont.): Metabolomics internal standards

Indoles	13C11-L-Tryptophan	CIL	CLM-4290-H	500 nM	50 µL of 10 mM stock
Indoles	13C9-L-Phenylalanine	CIL	CLM-2250-H	500 nM	50 µL of 10 mM stock
Indoles	13C9-L-Tyrosine	CIL	CLM-2263-H	500 nM	50 µL of 10 mM stock
Indoles	D4-Serotonin	CIL	DLM-11030-0	500 nM	50 µL of 10 mM stock
Indoles	13C6-5-Hydroxyindole-3-acetic acid	CIL	CLM-9936-0	500 nM	50 µL of 10 mM stock
Indoles	D4-Tryptamine	CIL	DLM-6989-0	500 nM	50 µL of 10 mM stock
Indoles	D3-Melatonin	CIL	DLM-7101-0	500 nM	50 µL of 10 mM stock
Indoles	13C6-Niacin	CIL	CLM-9954-0	2 µM	200 µL of 10 mM stock
Indoles	13C10-L-Kynurenine	CIL	CLM-9884-0	500 nM	50 µL of 10 mM stock
Indoles	D5-Kynurenic Acid	CIL	DLM-7374-0	500 nM	50 µL of 10 mM stock
Indoles	Anthranilic Acid, Ring-13C6	CIL	CLM-701-0	500 nM	50 µL of 10 mM stock

Table S2.2: qPCR primers for host immune response to St infection. Derived from Devlin et al., 2022.

Species	Target	Primer pairs
Mus Musculus	*Actb*	5'-GGCTGTATTCCCCTCCATCG-3'
		5'-CCAGTTGGTAACAATGCCATGT-3'
Mus Musculus	*Duox2*	5'-GCACTGTGCAGAACAGCTAGGACAAC-3'
		5'-ACCTCATCACCTTCTTGCGGGAG-3'
Mus Musculus	*Cxcl1*	5'-TGCACCCAAACCGAAGTCAT-3'
		5'-TTGTCAGAAGCCAGCGTTCAC-3'
Mus Musculus	*Ifng*	5'-TCAAGTGGCATAGATGTGGAAGAA-3'
		5'-TGGCTCTGCAGGATTTTCATG-3'
Mus Musculus	*Nos2*	5'-TTGGGTCTTGTTCACTCCACGG-3'
		5'-CCTCTTTCAGGTCACTTTGGTAGG-3'
Mus Musculus	*Il22*	5'-GGCCAGCCTTGCAGATAACA-3'
		5'-GCTGATGTGACAGGAGCTGA-3'
Mus Musculus	*Il1b*	5'-GCAACTGTTCCTGAACTCAACT-3'
		5'-ATCTTTTGGGGTCCGTCCAACT-3'
Mus Musculus	*S100a9*	5'-GGTGGAAGCACAGTTGGCA-3'
		5'-GTGTCCAGGTCCTCCATGATG-3'
Mus Musculus	*Tnf*	5'-ATGGCCTCCCTCTCATCAGT-3'
		5'-CTTGGTGGTTTGCTACGACG-3'
Mus Musculus	*Lcn2*	5'-ACATTTGTTCCAAGCTCCAGGGC-3'
		5'-CATGGCGAACTGGTTGTAGTCCG-3'

Table S2.3: Statistical comparison of bacterial biomass measurements for aerobes and anaerobes in mice on RC-ABX and WD-ABX. Post-hoc comparisons performed where appropriate comparing all timepoints to the pre-ABX timepoint (D-3). Available at https://github.com/mkennedy21/WD-abx.

Table S2.4: ANOVA and post-hoc multiple hypothesis tests comparing ASV richness across treatment groups and timepoints. Available at https://github.com/mkennedy21/WD-abx.

Table S2.5: ANOVA and post-hoc pairwise comparisons of functional richness across timepoints with RC-ABX and WD-ABX treatment groups. Analyses performed at the gene call, KO, and KCat level. n=2-8/group. Available at https://github.com/mkennedy21/WD-abx.

Table S2.6: ANOVA and post-hoc pairwise comparisons of functional redundancy across timepoints with RC-ABX and WD-ABX treatment groups. n=2-8/group. Available at https://github.com/mkennedy21/WD-abx.

Table S2.7: Linear regression results for functional redundancy at D-3 and D28 across RC-ABX and WD-ABX. Datasets were filtered to include only KOs that recovered to at least some extent (i.e. D28 FR was > 0). Model formula: FR_d28 ~ FR_d-3.

RC: including only KOs with > 0 count at D28				
	Estimate	**Std. Error**	**t**	**P value**
Intercept	0.561205	0.22637	2.479	0.0132
D-3	0.646653	0.002618	246.996	< 2e-16

R2	**F**	**DF**	**P value**
0.8543	6.10E+04	10407	< 2e-16

WD: including only KOs with > 0 count at D28				
	Estimate	**Std. Error**	**t**	**P value**
Intercept	0.46143	0.138182	3.359	0.000786
D-3	0.172492	0.001755	98.272	< 2e-16

R2	**F**	**DF**	**P value**
0.5613	9657	7546	< 2.2 e -16

Table S2.8: PERMANOVA analysis of fecal metabolomics TMS panel using Bray-Curtis dissimilarity.

PERMANOVA: BC_dist ~ Day*Treatment					
	Df	SumOfSqs	R2	F	Pvalue
Day	6	3.271585	0.419371	9.087366	1.00E-04
Treatment	1	1.307543	0.167609	21.79149	1.00E-04
Day*Treatment	4	1.541969	0.197659	6.424609	1.00E-04
Residual	28	1.680069	0.215361		
Total	39	7.801166	1		

Table S2.9: ANOVA and post-hoc comparisons of SCFA levels for mice on RC-ABX or WD-ABX. n=2-3/group. Available at https://github.com/mkennedy21/WD-abx.

Table S2.10: ANOVA and post-hoc comparisons of genes of interest for mice on RC-ABX and WD-ABX. Includes data for a-gal genes, SCFA genes, bile acid transformation genes, and complex polysaccharide metabolism genes. Available at https://github.com/mkennedy21/WD-abx.

Table S2.11: ANOVA and post-hoc comparisons of ASV richness across timepoints for all treatment groups, and across treatment groups at D14. Available at https://github.com/mkennedy21/WD-abx.

Table S2.12: PERMANOVA and post-hoc pairwise comparisons of all treatment groups based on Bray-Curtis dissimilarity. Available at https://github.com/mkennedy21/WD-abx.

Table S2.13: ANOVA and post-hoc comparison of infection AUC across treatment groups for colonization resistance experiments. n=3-9/group Available at https://github.com/mkennedy21/WD-abx.

Table S2.14: ANOVA and post-hoc comparisons of body weight across infected and uninfected treatment groups at t=96 hpi. Available at https://github.com/mkennedy21/WD-abx.

Table S2.15: Kruskal-Wallis test and post-hoc comparisons of St infection load across treatment groups for all body tissues. Available at https://github.com/mkennedy21/WD-abx.

Table S2.16: ANOVA and post-hoc comparisons of immune gene expression across treatment groups. Available at https://github.com/mkennedy21/WD-abx.

REFERENCES

Adamberg, Kaarel, Signe Adamberg, Karin Ernits, Anneli Larionova, Tiia Voor, Madis Jaagura, Triinu Visnapuu, and Tiina Alamäe. 2018. "Composition and Metabolism of Fecal Microbiota from Normal and Overweight Children Are Differentially Affected by Melibiose, Raffinose and Raffinose-Derived Fructans." *Anaerobe* 52 (August): 100–110. https://doi.org/10.1016/j.anaerobe.2018.06.009.

Albenberg, LG, and GD Wu. 2014. "Diet and the Intestinal Microbiome: Associations, Functions, and Implications for Health and Disease." *Gastroenterology* 146 (6): 1564–72. https://doi.org/10.1053/J.GASTRO.2014.01.058.

Allesina, Stefano, Antonio Bodini, and Mercedes Pascual. 2009. "Functional Links and Robustness in Food Webs." *Philosophical Transactions of the Royal Society B: Biological Sciences* 364 (1524): 1701–9. https://doi.org/10.1098/rstb.2008.0214.

Altschul, Stephen F., Warren Gish, Webb Miller, Eugene W. Myers, and David J. Lipman. 1990. "Basic Local Alignment Search Tool." *Journal of Molecular Biology* 215 (3): 403–10. https://doi.org/10.1016/S0022-2836(05)80360-2.

Anitha, Mallappa, François Reichardt, Sahar Tabatabavakili, Behtash Ghazi Nezami, Benoit Chassaing, Simon Mwangi, Matam Vijay-Kumar, Andrew Gewirtz, and Shanthi Srinivasan. 2016. "Intestinal Dysbiosis Contributes to the Delayed Gastrointestinal Transit in High-Fat Diet Fed Mice." *Cellular and Molecular Gastroenterology and Hepatology* 2 (3): 328–39. https://doi.org/10.1016/j.jcmgh.2015.12.008.

Aramaki, Takuya, Romain Blanc-Mathieu, Hisashi Endo, Koichi Ohkubo, Minoru Kanehisa, Susumu Goto, and Hiroyuki Ogata. 2020. "KofamKOALA: KEGG Ortholog Assignment Based on Profile HMM and Adaptive Score Threshold." *Bioinformatics* 36 (7): 2251–52. https://doi.org/10.1093/BIOINFORMATICS/BTZ859.

Asnicar, Francesco, Sarah E. Berry, Ana M. Valdes, Long H. Nguyen, Gianmarco Piccinno, David A. Drew, Emily Leeming, et al. 2021. "Microbiome Connections with Host Metabolism and Habitual Diet from 1,098 Deeply Phenotyped Individuals." *Nature Medicine* 27 (2): 321–32. https://doi.org/10.1038/s41591-020-01183-8.

Bäckhed, Fredrik, Claire M. Fraser, Yehuda Ringel, Mary Ellen Sanders, R. Balfour Sartor, Philip M. Sherman, James Versalovic, Vincent Young, and B. Brett Finlay. 2012. "Defining a Healthy Human Gut Microbiome: Current Concepts, Future Directions, and Clinical Applications." *Cell Host and Microbe* 12 (5): 611–22. https://doi.org/10.1016/j.chom.2012.10.012.

Bäckhed, Fredrik, Josefine Roswall, Yangqing Peng, Qiang Feng, Huijue Jia, Petia Kovatcheva-Datchary, Yin Li, et al. 2015. "Dynamics and Stabilization of the Human Gut Microbiome during the First Year of Life." *Cell Host & Microbe* 17 (5): 690–703. https://doi.org/10.1016/j.chom.2015.04.004.

Barroso-Batista, João, Miguel F. Pedro, Joana Sales-Dias, Catarina J.G. Pinto, Jessica A. Thompson, Helena Pereira, Jocelyne Demengeot, Isabel Gordo, and Karina B. Xavier. 2020. "Specific Eco-Evolutionary Contexts in the Mouse Gut Reveal Escherichia Coli

Metabolic Versatility." *Current Biology* 30 (6): 1049-1062.e7. https://doi.org/10.1016/j.cub.2020.01.050.

Barroso-Batista, João, Ana Sousa, Marta Lourenço, Marie-Louise Bergman, Daniel Sobral, Jocelyne Demengeot, Karina B. Xavier, and Isabel Gordo. 2014. "The First Steps of Adaptation of Escherichia Coli to the Gut Are Dominated by Soft Sweeps." *PLoS Genetics* 10 (3): e1004182. https://doi.org/10.1371/journal.pgen.1004182.

Barthel, Manja, Siegfried Hapfelmeier, Leticia Quintanilla-Martínez, Marcus Kremer, Manfred Rohde, Michael Hogardt, Klaus Pfeffer, Holger Rüssmann, and Wolf Dietrich Hardt. 2003. "Pretreatment of Mice with Streptomycin Provides a Salmonella Enterica Serovar Typhimurium Colitis Model That Allows Analysis of Both Pathogen and Host." *Infection and Immunity* 71 (5): 2839. https://doi.org/10.1128/IAI.71.5.2839-2858.2003.

Bateman, Alex, Lachlan Coin, Richard Durbin, Robert D. Finn, Volker Hollich, Sam Griffiths-Jones, Ajay Khanna, et al. 2004. "The Pfam Protein Families Database." *Nucleic Acids Research* 32 (suppl_1): D138–41. https://doi.org/10.1093/NAR/GKH121.

Baumgartner, Michael, Katia R. Pfrunder-Cardozo, and Alex R. Hall. 2021. "Microbial Community Composition Interacts with Local Abiotic Conditions to Drive Colonization Resistance in Human Gut Microbiome Samples." *Proceedings of the Royal Society B: Biological Sciences* 288 (1947): 20203106. https://doi.org/10.1098/rspb.2020.3106.

Becattini, Simone, Matthew T. Sorbara, Sohn G. Kim, Eric L. Littmann, Qiwen Dong, Gavin Walsh, Roberta Wright, et al. 2021. "Rapid Transcriptional and Metabolic Adaptation of Intestinal Microbes to Host Immune Activation." *Cell Host & Microbe* 29 (3): 378-393.e5. https://doi.org/10.1016/j.chom.2021.01.003.

Bell, Michael. 2014. "Antibiotic Misuse: A Global Crisis." *JAMA Internal Medicine* 174 (12): 1920–21. https://doi.org/10.1001/jamainternmed.2014.3289.

Bisanz, Jordan E., Vaibhav Upadhyay, Jessie A. Turnbaugh, Kimberly Ly, and Peter J. Turnbaugh. 2019. "Meta-Analysis Reveals Reproducible Gut Microbiome Alterations in Response to a High-Fat Diet." *Cell Host & Microbe* 26 (2): 265-272.e4. https://doi.org/10.1016/J.CHOM.2019.06.013.

Bolger, Anthony M., Marc Lohse, and Bjoern Usadel. 2014. "Trimmomatic: A Flexible Trimmer for Illumina Sequence Data." *Bioinformatics* 30 (15): 2114–20. https://doi.org/10.1093/bioinformatics/btu170.

Buffie, Charlie G., and Eric G. Pamer. 2013. "Microbiota-Mediated Colonization Resistance against Intestinal Pathogens." *Nature Reviews Immunology* 13 (11): 790–801. https://doi.org/10.1038/nri3535.

Bunker, Jeffrey J., Steven A. Erickson, Theodore M. Flynn, Carole Henry, Jason C. Koval, Marlies Meisel, Bana Jabri, Dionysios A. Antonopoulos, Patrick C. Wilson, and Albert Bendelac. 2017. "Natural Polyreactive IgA Antibodies Coat the Intestinal Microbiota." *Science* 358 (6361): eaan6619. https://doi.org/10.1126/science.aan6619.

Carmody, Rachel N., Georg K. Gerber, Jesus M. Luevano, Daniel M. Gatti, Lisa Somes, Karen L. Svenson, and Peter J. Turnbaugh. 2015. "Diet Dominates Host Genotype in Shaping the

Murine Gut Microbiota." *Cell Host and Microbe* 17 (1): 72–84. https://doi.org/10.1016/j.chom.2014.11.010.

Chandler, Michael, Olivier Fayet, Philippe Rousseau, Bao Ton Hoang, and Guy Duval-Valentin. 2015. "Copy-out-Paste-in Transposition of IS911: A Major Transposition Pathway." *Microbiology Spectrum* 3 (4). https://doi.org/10.1128/MICROBIOLSPEC.MDNA3-0031-2014.

Chng, Kern Rei, Tarini Shankar Ghosh, Yi Han Tan, Tannistha Nandi, Ivor Russel Lee, Amanda Hui Qi Ng, Chenhao Li, et al. 2020. "Metagenome-Wide Association Analysis Identifies Microbial Determinants of Post-Antibiotic Ecological Recovery in the Gut." *Nature Ecology and Evolution* 4 (9): 1256–67. https://doi.org/10.1038/s41559-020-1236-0.

Cohen, Nathaniel Aviv, and Nitsan Maharshak. 2017. "Novel Indications for Fecal Microbial Transplantation: Update and Review of the Literature." *Digestive Diseases and Sciences* 62 (5): 1131–45. https://doi.org/10.1007/s10620-017-4535-9.

Coyne, Michael J., Maria Chatzidaki-Livanis, Lawrence C. Paoletti, and Laurie E. Comstock. 2008. "Role of Glycan Synthesis in Colonization of the Mammalian Gut by the Bacterial Symbiont Bacteroides Fragilis." *Proceedings of the National Academy of Sciences* 105 (35): 13099–104. https://doi.org/10.1073/pnas.0804220105.

Crook, Nathan, Aura Ferreiro, Andrew J. Gasparrini, Mitchell W. Pesesky, Molly K. Gibson, Bin Wang, Xiaoqing Sun, et al. 2019. "Adaptive Strategies of the Candidate Probiotic E. Coli Nissle in the Mammalian Gut." *Cell Host & Microbe* 25 (4): 499. https://doi.org/10.1016/J.CHOM.2019.02.005.

Dapa, Tanja, Ricardo Serotte Ramiro, Miguel Filipe Pedro, Isabel Gordo, and Karina Bivar Xavier. 2022. "Diet Leaves a Genetic Signature in a Keystone Member of the Gut Microbiota." *Cell Host & Microbe* 30 (2): 183-199.e10. https://doi.org/10.1016/J.CHOM.2022.01.002.

David, Lawrence A., Corinne F. Maurice, Rachel N. Carmody, David B. Gootenberg, Julie E. Button, Benjamin E. Wolfe, Alisha V. Ling, et al. 2014. "Diet Rapidly and Reproducibly Alters the Human Gut Microbiome." *Nature* 505 (7484): 559–63. https://doi.org/10.1038/nature12820.

Desai, Mahesh S, Anna M Seekatz, Nicole M Koropatkin, Nobuhiko Kamada, Christina A Hickey, Mathis Wolter, Nicholas A Pudlo, et al. 2016. "A Dietary Fiber-Deprived Gut Microbiota Degrades the Colonic Mucus Barrier and Enhances Pathogen Susceptibility." *Cell* 167 (5): 1339-1353.e21. https://doi.org/10.1016/j.cell.2016.10.043.

Dethlefsen, Les, and David A. Relman. 2011. "Incomplete Recovery and Individualized Responses of the Human Distal Gut Microbiota to Repeated Antibiotic Perturbation." *Proceedings of the National Academy of Sciences of the United States of America* 108 (SUPPL. 1): 4554–61. https://doi.org/10.1073/pnas.1000087107.

Devkota, Suzanne, Yunwei Wang, Mark W. Musch, Vanessa Leone, Hannah Fehlner-Peach, Anuradha Nadimpalli, Dionysios A. Antonopoulos, Bana Jabri, and Eugene B. Chang.

2012. “Dietary-Fat-Induced Taurocholic Acid Promotes Pathobiont Expansion and Colitis in Il10-/- Mice.” *Nature* 487 (7405): 104–8. https://doi.org/10.1038/nature11225.

Devlin, Jason R., William Santus, Jorge Mendez, Wenjing Peng, Aiying Yu, Junyao Wang, Xiomarie Alejandro-Navarreto, et al. 2022. “Salmonella Enterica Serovar Typhimurium Chitinases Modulate the Intestinal Glycome and Promote Small Intestinal Invasion.” *PLOS Pathogens* 18 (4): e1010167. https://doi.org/10.1371/JOURNAL.PPAT.1010167.

Diaz-Ochoa, Vladimir E., Diana Lam, Carlin S. Lee, Suzi Klaus, Judith Behnsen, Janet Z. Liu, Nicholas Chim, et al. 2016. “Salmonella Mitigates Oxidative Stress and Thrives in the Inflamed Gut by Evading Calprotectin-Mediated Manganese Sequestration.” *Cell Host & Microbe* 19 (6): 814–25. https://doi.org/10.1016/j.chom.2016.05.005.

Donaldson, Gregory P., Wen Chi Chou, Abigail L. Manson, Peter Rogov, Thomas Abeel, James Bochicchio, Dawn Ciulla, et al. 2020. “Spatially Distinct Physiology of Bacteroides Fragilis within the Proximal Colon of Gnotobiotic Mice.” *Nature Microbiology* 5 (5): 746–56. https://doi.org/10.1038/s41564-020-0683-3.

Douglas, Angela E. 2020. “The Microbial Exometabolome: Ecological Resource and Architect of Microbial Communities.” *Philosophical Transactions of the Royal Society B: Biological Sciences* 375 (1798): 20190250. https://doi.org/10.1098/rstb.2019.0250.

Drula, Elodie, Marie-Line Garron, Suzan Dogan, Vincent Lombard, Bernard Henrissat, and Nicolas Terrapon. 2022. “The Carbohydrate-Active Enzyme Database: Functions and Literature.” *Nucleic Acids Research* 50 (D1): D571–77. https://doi.org/10.1093/nar/gkab1045.

Earle, Kristen A., Gabriel Billings, Michael Sigal, Joshua S. Lichtman, Gunnar C. Hansson, Joshua E. Elias, Manuel R. Amieva, Kerwyn Casey Huang, and Justin L. Sonnenburg. 2015. “Quantitative Imaging of Gut Microbiota Spatial Organization.” *Cell Host & Microbe* 18 (4): 478–88. https://doi.org/10.1016/J.CHOM.2015.09.002.

Eddy, Sean R. 2011. “Accelerated Profile HMM Searches.” *PLOS Computational Biology* 7 (10): e1002195. https://doi.org/10.1371/JOURNAL.PCBI.1002195.

Eisenstein, Michael. 2020. “The Hunt for a Healthy Microbiome.” *Nature* 577 (7792): S6–8. https://doi.org/10.1038/d41586-020-00193-3.

Eren, A. Murat, Özcan C. Esen, Christopher Quince, Joseph H. Vineis, Hilary G. Morrison, Mitchell L. Sogin, and Tom O. Delmont. 2015. “Anvi’o: An Advanced Analysis and Visualization Platform for ’omics Data.” *PeerJ* 3: e1319. https://doi.org/10.7717/peerj.1319.

Eren, A. Murat, Evan Kiefl, Alon Shaiber, Iva Veseli, Samuel E. Miller, Matthew S. Schechter, Isaac Fink, et al. 2020. “Community-Led, Integrated, Reproducible Multi-Omics with Anvi’o.” *Nature Microbiology 2020 6:1* 6 (1): 3–6. https://doi.org/10.1038/s41564-020-00834-3.

Eren, A. Murat, Joseph H. Vineis, Hilary G. Morrison, and Mitchell L. Sogin. 2013. “A Filtering Method to Generate High Quality Short Reads Using Illumina Paired-End Technology.” *PLOS ONE* 8 (6): e66643. https://doi.org/10.1371/journal.pone.0066643.

Fang, Xin, Jonathan M. Monk, Sergey Nurk, Margarita Akseshina, Qiyun Zhu, Christopher Gemmell, Connor Gianetto-Hill, et al. 2018. "Metagenomics-Based, Strain-Level Analysis of Escherichia Coli From a Time-Series of Microbiome Samples From a Crohn's Disease Patient." *Frontiers in Microbiology* 9. https://www.frontiersin.org/articles/10.3389/fmicb.2018.02559.

Ford, Alexander C., Lucinda A. Harris, Brian E. Lacy, Eamonn M. M. Quigley, and Paul Moayyedi. 2018. "Systematic Review with Meta-Analysis: The Efficacy of Prebiotics, Probiotics, Synbiotics and Antibiotics in Irritable Bowel Syndrome." *Alimentary Pharmacology & Therapeutics* 48 (10): 1044–60. https://doi.org/10.1111/apt.15001.

Francino, M. P. 2016. "Antibiotics and the Human Gut Microbiome: Dysbioses and Accumulation of Resistances." *Frontiers in Microbiology* 6. https://www.frontiersin.org/articles/10.3389/fmicb.2015.01543.

Frazão, N., A. Konrad, M. Amicone, E. Seixas, D. Güleresi, M. Lässig, and I. Gordo. 2022. "Two Modes of Evolution Shape Bacterial Strain Diversity in the Mammalian Gut for Thousands of Generations." *Nature Communications* 13 (1): 5604. https://doi.org/10.1038/s41467-022-33412-8.

Garud, Nandita R., Benjamin H. Good, Oskar Hallatschek, and Katherine S. Pollard. 2019. "Evolutionary Dynamics of Bacteria in the Gut Microbiome within and across Hosts." *PLoS Biology* 17 (1): e3000102. https://doi.org/10.1371/journal.pbio.3000102.

Gensollen, Thomas, Shankar S Iyer, Dennis L Kasper, and Richard S Blumberg. 2016. "How Colonization by Microbiota in Early Life Shapes the Immune System." *Science (New York, N.Y.)* 352 (6285): 539–44. https://doi.org/10.1126/science.aad9378.

Ghalayini, Mohamed, Adrien Launay, Antoine Bridier-Nahmias, Olivier Clermont, Erick Denamur, Mathilde Lescat, and Olivier Tenaillon. 2018. "Evolution of a Dominant Natural Isolate of Escherichia Coli in the Human Gut over the Course of a Year Suggests a Neutral Evolution with Reduced Effective Population Size." *Applied and Environmental Microbiology* 84 (6): e02377-17. https://doi.org/10.1128/AEM.02377-17.

Gilbert, Jack A., and Susan V. Lynch. 2019. "Community Ecology as a Framework for Human Microbiome Research." *Nature Medicine* 25 (6): 884–89. https://doi.org/10.1038/s41591-019-0464-9.

Goodman, Andrew L., Nathan P. McNulty, Yue Zhao, Douglas Leip, Robi D. Mitra, Catherine A. Lozupone, Rob Knight, and Jeffrey I. Gordon. 2009. "Identifying Genetic Determinants Needed to Establish a Human Gut Symbiont in Its Habitat." *Cell Host and Microbe* 6 (3): 279–89. https://doi.org/10.1016/j.chom.2009.08.003.

Guo, Yijie, Sho Kitamoto, and Nobuhiko Kamada. 2020. "Microbial Adaptation to the Healthy and Inflamed Gut Environments." *Gut Microbes* 12 (1): 1857505. https://doi.org/10.1080/19490976.2020.1857505.

Hapfelmeier, Siegfried, Melissa A. E. Lawson, Emma Slack, Jorum K. Kirundi, Maaike Stoel, Mathias Heikenwalder, Julia Cahenzli, et al. 2010. "Reversible Microbial Colonization of

Germ-Free Mice Reveals the Dynamics of IgA Immune Responses." *Science* 328 (5986): 1705–9. https://doi.org/10.1126/science.1188454.

Hayase, Eiko, Tomo Hayase, Mohamed A. Jamal, Takahiko Miyama, Chia-Chi Chang, Miriam R. Ortega, Saira S. Ahmed, et al. 2022. "Mucus-Degrading Bacteroides Link Carbapenems to Aggravated Graft-versus-Host Disease." *Cell* 185 (20): 3705-3719.e14. https://doi.org/10.1016/j.cell.2022.09.007.

Hibbing, Michael E, Clay Fuqua, Matthew R Parsek, and S Brook Peterson. 2010. "Bacterial Competition: Surviving and Thriving in the Microbial Jungle." *Nature Reviews. Microbiology* 8 (1): 15–25. https://doi.org/10.1038/nrmicro2259.

Hildebrand, Falk, Toni I. Gossmann, Clémence Frioux, Ezgi Özkurt, Pernille Neve Myers, Pamela Ferretti, Michael Kuhn, Mohammad Bahram, Henrik Bjørn Nielsen, and Peer Bork. 2021. "Dispersal Strategies Shape Persistence and Evolution of Human Gut Bacteria." *Cell Host & Microbe* 29 (7): 1167-1176.e9. https://doi.org/10.1016/j.chom.2021.05.008.

Howe, Adina, Daina L. Ringus, Ryan J. Williams, Zi-Ning Choo, Stephanie M. Greenwald, Sarah M. Owens, Maureen L. Coleman, Folker Meyer, and Eugene B. Chang. 2016. "Divergent Responses of Viral and Bacterial Communities in the Gut Microbiome to Dietary Disturbances in Mice." *The ISME Journal* 10 (5): 1217–27. https://doi.org/10.1038/ismej.2015.183.

Human Microbiome Project Consortium. 2012. "Structure, Function and Diversity of the Healthy Human Microbiome." *Nature* 486 (7402): 207–14. https://doi.org/10.1038/nature11234.

Huus, Kelsey E., Kylynda C. Bauer, Eric M. Brown, Tahereh Bozorgmehr, Sarah E. Woodward, Antonio Serapio-Palacios, Rozlyn C. T. Boutin, Charisse Petersen, and B. Brett Finlay. 2020. "Commensal Bacteria Modulate Immunoglobulin A Binding in Response to Host Nutrition." *Cell Host & Microbe* 27 (6): 909-921.e5. https://doi.org/10.1016/j.chom.2020.03.012.

Hyatt, Doug, Gwo Liang Chen, Philip F. LoCascio, Miriam L. Land, Frank W. Larimer, and Loren J. Hauser. 2010. "Prodigal: Prokaryotic Gene Recognition and Translation Initiation Site Identification." *BMC Bioinformatics* 11 (1): 1–11. https://doi.org/10.1186/1471-2105-11-119/TABLES/5.

Ianiro, Gianluca, Michal Punčochář, Nicolai Karcher, Serena Porcari, Federica Armanini, Francesco Asnicar, Francesco Beghini, et al. 2022. "Variability of Strain Engraftment and Predictability of Microbiome Composition after Fecal Microbiota Transplantation across Different Diseases." *Nature Medicine* 28 (9): 1913–23. https://doi.org/10.1038/s41591-022-01964-3.

Irving, Sophie E., Naznin R. Choudhury, and Rebecca M. Corrigan. 2021. "The Stringent Response and Physiological Roles of (Pp)PGpp in Bacteria." *Nature Reviews Microbiology* 19 (4): 256–71. https://doi.org/10.1038/s41579-020-00470-y.

Ivanov, Ivaylo I., Koji Atarashi, Nicolas Manel, Eoin L. Brodie, Tatsuichiro Shima, Ulas Karaoz, Dongguang Wei, et al. 2009. "Induction of Intestinal Th17 Cells by Segmented Filamentous Bacteria." *Cell* 139 (3): 485–98. https://doi.org/10.1016/j.cell.2009.09.033.

Jerison, Elizabeth R, and Michael M Desai. 2015. "Genomic Investigations of Evolutionary Dynamics and Epistasis in Microbial Evolution Experiments." *Current Opinion in Genetics & Development*, Genomes and evolution, 35 (December): 33–39. https://doi.org/10.1016/j.gde.2015.08.008.

Joglekar, Payal, Hua Ding, Pablo Canales-Herrerias, Pankaj Jay Pasricha, Justin L. Sonnenburg, and Daniel A. Peterson. 2019. "Intestinal IgA Regulates Expression of a Fructan Polysaccharide Utilization Locus in Colonizing Gut Commensal Bacteroides Thetaiotaomicron." *MBio* 10 (6): e02324-19. https://doi.org/10.1128/mBio.02324-19.

Johansson, Malin E. V., Hedvig E. Jakobsson, Jessica Holmén-Larsson, André Schütte, Anna Ermund, Ana M. Rodríguez-Piñeiro, Liisa Arike, et al. 2015. "Normalization of Host Intestinal Mucus Layers Requires Long-Term Microbial Colonization." *Cell Host & Microbe* 18 (5): 582–92. https://doi.org/10.1016/j.chom.2015.10.007.

Johansson, Malin E. V., Henrik Sjövall, and Gunnar C. Hansson. 2013. "The Gastrointestinal Mucus System in Health and Disease." *Nature Reviews Gastroenterology & Hepatology* 10 (6): 352–61. https://doi.org/10.1038/nrgastro.2013.35.

Johansson, Malin E.V., Mia Phillipson, Joel Petersson, Anna Velcich, Lena Holm, and Gunnar C. Hansson. 2008. "The Inner of the Two Muc2 Mucin-Dependent Mucus Layers in Colon Is Devoid of Bacteria." *Proceedings of the National Academy of Sciences of the United States of America* 105 (39): 15064–69. https://doi.org/10.1073/pnas.0803124105.

Kanehisa, Minoru, and Susumu Goto. 2000. "KEGG: Kyoto Encyclopedia of Genes and Genomes." *Nucleic Acids Research* 28 (1): 27. https://doi.org/10.1093/NAR/28.1.27.

Kaoutari, Abdessamad El, Fabrice Armougom, Jeffrey I. Gordon, Didier Raoult, and Bernard Henrissat. 2013. "The Abundance and Variety of Carbohydrate-Active Enzymes in the Human Gut Microbiota." *Nature Reviews Microbiology* 11 (7): 497–504. https://doi.org/10.1038/nrmicro3050.

Knights, Dan, Kara G. Lassen, and Ramnik J. Xavier. 2013. "Advances in Inflammatory Bowel Disease Pathogenesis: Linking Host Genetics and the Microbiome." *Gut* 62 (10): 1505–10. https://doi.org/10.1136/gutjnl-2012-303954.

Koenig, Jeremy E., Aymé Spor, Nicholas Scalfone, Ashwana D. Fricker, Jesse Stombaugh, Rob Knight, Largus T. Angenent, and Ruth E. Ley. 2011. "Succession of Microbial Consortia in the Developing Infant Gut Microbiome." *Proceedings of the National Academy of Sciences* 108 (Supplement 1): 4578–85. https://doi.org/10.1073/PNAS.1000081107.

Kolmogorov, Mikhail, Jeffrey Yuan, Yu Lin, and Pavel A. Pevzner. 2019. "Assembly of Long, Error-Prone Reads Using Repeat Graphs." *Nature Biotechnology 2019 37:5* 37 (5): 540–46. https://doi.org/10.1038/s41587-019-0072-8.

Kuwahara, Tomomi, Atsushi Yamashita, Hideki Hirakawa, Haruyuki Nakayama, Hidehiro Toh, Natsumi Okada, Satoru Kuhara, Masahira Hattori, Tetsuya Hayashi, and Yoshinari Ohnishi. 2004. "Genomic Analysis of Bacteroides Fragilis Reveals Extensive DNA Inversions Regulating Cell Surface Adaptation." *Proceedings of the National Academy of Sciences* 101 (41): 14919–24. https://doi.org/10.1073/pnas.0404172101.

Langmead, Ben, and Steven L. Salzberg. 2012. “Fast Gapped-Read Alignment with Bowtie 2.” *Nature Methods 2012 9:4* 9 (4): 357–59. https://doi.org/10.1038/nmeth.1923.

Laubitz, Daniel, Katri Typpo, Monica Midura-Kiela, Clairessa Brown, Albert Barberán, Fayez K. Ghishan, and Pawel R. Kiela. 2021. “Dynamics of Gut Microbiota Recovery after Antibiotic Exposure in Young and Old Mice (A Pilot Study).” *Microorganisms* 9 (3): 1–12. https://doi.org/10.3390/microorganisms9030647.

Lee, Jee Yon, Stephanie A. Cevallos, Mariana X. Byndloss, Connor R. Tiffany, Erin E. Olsan, Brian P. Butler, Briana M. Young, et al. 2020. “High-Fat Diet and Antibiotics Cooperatively Impair Mitochondrial Bioenergetics to Trigger Dysbiosis That Exacerbates Pre-Inflammatory Bowel Disease.” *Cell Host & Microbe* 28 (2): 273-284.e6. https://doi.org/10.1016/J.CHOM.2020.06.001.

Lee, Jee-Yon, Renée M. Tsolis, and Andreas J. Bäumler. 2022. “The Microbiome and Gut Homeostasis.” *Science* 377 (6601): eabp9960. https://doi.org/10.1126/science.abp9960.

Lee, Michael D. 2019. “GToTree: A User-Friendly Workflow for Phylogenomics.” *Bioinformatics* 35 (20): 4162–64. https://doi.org/10.1093/BIOINFORMATICS/BTZ188.

Lee, Mirae, and Eugene B. Chang. 2021. “Inflammatory Bowel Diseases (IBD) and the Microbiome—Searching the Crime Scene for Clues.” *Gastroenterology*, The Gut microbiome: Reaching the Promise through Discovery, 160 (2): 524–37. https://doi.org/10.1053/j.gastro.2020.09.056.

Lenski, Richard E. 2017. “Experimental Evolution and the Dynamics of Adaptation and Genome Evolution in Microbial Populations.” *The ISME Journal* 11 (10): 2181–94. https://doi.org/10.1038/ismej.2017.69.

Leone, Vanessa, Sean M Gibbons, Kristina Martinez, Alan L Hutchison, Edmond Y Huang, Candace M Cham, Joseph F Pierre, et al. 2015. “Effects of Diurnal Variation of Gut Microbes and High-Fat Feeding on Host Circadian Clock Function and Metabolism.” *Cell Host & Microbe* 17 (5): 681–89. https://doi.org/10.1016/j.chom.2015.03.006.

Levy, Maayan, Aleksandra A. Kolodziejczyk, Christoph A. Thaiss, and Eran Elinav. 2017. “Dysbiosis and the Immune System.” *Nature Reviews Immunology 2017 17:4* 17 (4): 219–32. https://doi.org/10.1038/nri.2017.7.

Li, Dinghua, Chi-Man Liu, Ruibang Luo, Kunihiko Sadakane, and Tak-Wah Lam. 2015. “MEGAHIT: An Ultra-Fast Single-Node Solution for Large and Complex Metagenomics Assembly via Succinct de Bruijn Graph.” *Bioinformatics (Oxford, England)* 31 (10): 1674–76. https://doi.org/10.1093/bioinformatics/btv033.

Li, Heng. 2018. “Minimap2: Pairwise Alignment for Nucleotide Sequences.” *Bioinformatics* 34 (18): 3094–3100. https://doi.org/10.1093/BIOINFORMATICS/BTY191.

Li, Heng, Bob Handsaker, Alec Wysoker, Tim Fennell, Jue Ruan, Nils Homer, Gabor Marth, Goncalo Abecasis, and Richard Durbin. 2009. “The Sequence Alignment/Map Format and SAMtools.” *Bioinformatics (Oxford, England)* 25 (16): 2078–79. https://doi.org/10.1093/BIOINFORMATICS/BTP352.

Liu, Hualan, Anthony L. Shiver, Morgan N. Price, Hans K. Carlson, Valentine V. Trotter, Yan Chen, Veronica Escalante, et al. 2021. "Functional Genetics of Human Gut Commensal Bacteroides Thetaiotaomicron Reveals Metabolic Requirements for Growth across Environments." *Cell Reports* 34 (9). https://doi.org/10.1016/j.celrep.2021.108789.

Love, Michael I., Wolfgang Huber, and Simon Anders. 2014. "Moderated Estimation of Fold Change and Dispersion for RNA-Seq Data with DESeq2." *Genome Biology* 15 (12): 550. https://doi.org/10.1186/s13059-014-0550-8.

Macpherson, Andrew J., and Nicola L. Harris. 2004. "Interactions between Commensal Intestinal Bacteria and the Immune System." *Nature Reviews Immunology* 4 (6): 478–85. https://doi.org/10.1038/nri1373.

Mahowald, Michael A, Federico E Rey, Henning Seedorf, Peter J Turnbaugh, Robert S Fulton, Aye Wollam, Neha Shah, et al. 2009. "Characterizing a Model Human Gut Microbiota Composed of Members of Its Two Dominant Bacterial Phyla." *Proceedings of the National Academy of Sciences of the United States of America* 106 (14): 5859–64. https://doi.org/10.1073/pnas.0901529106.

Maldonado-Gómez, María X., Inés Martínez, Francesca Bottacini, Amy O'Callaghan, Marco Ventura, Douwe van Sinderen, Benjamin Hillmann, et al. 2016. "Stable Engraftment of Bifidobacterium Longum AH1206 in the Human Gut Depends on Individualized Features of the Resident Microbiome." *Cell Host & Microbe* 20 (4): 515–26. https://doi.org/10.1016/J.CHOM.2016.09.001.

Martens, Eric C, Herbert C Chiang, and Jeffrey I Gordon. 2008. "Mucosal Glycan Foraging Enhances Fitness and Transmission of a Saccharolytic Human Gut Bacterial Symbiont." *Cell Host & Microbe* 4 (5): 447–57. https://doi.org/10.1016/j.chom.2008.09.007.

Mazmanian, Sarkis K., June L. Round, and Dennis L. Kasper. 2008. "A Microbial Symbiosis Factor Prevents Intestinal Inflammatory Disease." *Nature* 453 (7195): 620–25. https://doi.org/10.1038/nature07008.

McFarland, Lynne V., Charlesnika T. Evans, and Ellie J. C. Goldstein. 2018. "Strain-Specificity and Disease-Specificity of Probiotic Efficacy: A Systematic Review and Meta-Analysis." *Frontiers in Medicine* 5. https://www.frontiersin.org/articles/10.3389/fmed.2018.00124.

McMurdie, Paul J., and Susan Holmes. 2013. "Phyloseq: An R Package for Reproducible Interactive Analysis and Graphics of Microbiome Census Data." *PLOS ONE* 8 (4): e61217. https://doi.org/10.1371/JOURNAL.PONE.0061217.

Miyoshi, Jun, Alexandria M Bobe, Sawako Miyoshi, Yong Huang, Nathaniel Hubert, Tom O Delmont, A Murat Eren, Vanessa Leone, and Eugene B Chang. 2017. "Peripartum Antibiotics Promote Gut Dysbiosis, Loss of Immune Tolerance, and Inflammatory Bowel Disease in Genetically Prone Offspring." *Cell Reports* 20 (2): 491–504. https://doi.org/10.1016/j.celrep.2017.06.060.

Miyoshi, Jun, Vanessa Leone, Kentaro Nobutani, Mark W. Musch, Kristina Martinez-Guryn, Yunwei Wang, Sawako Miyoshi, Alexandria M. Bobe, A. Murat Eren, and Eugene B.

Chang. 2018. “Minimizing Confounders and Increasing Data Quality in Murine Models for Studies of the Gut Microbiome.” *PeerJ* 6 (7): e5166. https://doi.org/10.7717/PEERJ.5166.

Nakajima, Akira, Alexis Vogelzang, Mikako Maruya, Michio Miyajima, Megumi Murata, Aoi Son, Tomomi Kuwahara, et al. 2018. “IgA Regulates the Composition and Metabolic Function of Gut Microbiota by Promoting Symbiosis between Bacteria.” *Journal of Experimental Medicine* 215 (8): 2019–34. https://doi.org/10.1084/jem.20180427.

Ng, Katharine M., Jessica A. Ferreyra, Steven K. Higginbottom, Jonathan B. Lynch, Purna C. Kashyap, Smita Gopinath, Natasha Naidu, et al. 2013. “Microbiota-Liberated Host Sugars Facilitate Post-Antibiotic Expansion of Enteric Pathogens.” *Nature* 502 (7469): 96–99. https://doi.org/10.1038/nature12503.

Ng, Katherine Michelle, Andrés Aranda-Díaz, Carolina Tropini, Matthew Ryan Frankel, William Van Treuren, Colleen T. O’Laughlin, Bryan Douglas Merrill, et al. 2019. “Recovery of the Gut Microbiota after Antibiotics Depends on Host Diet, Community Context, and Environmental Reservoirs.” *Cell Host and Microbe* 26 (5): 650-665.e4. https://doi.org/10.1016/j.chom.2019.10.011.

NHANES. 2009. *NHANES - What We Eat in America: Nutrient Intakes from Food by Gender and Age*. Vol. National Health and Nutrition Examination Survey Data. Hyattsville, MD: U.S. Department of Health and Human Services, Centers for Disease Control and Prevention. https://www.ars.usda.gov/ARSUserFiles/80400530/pdf/0910/table_1_nin_gen_09.pdf.

Nieuwdorp, Max, Pim W. Gilijamse, Nikhil Pai, and Lee M. Kaplan. 2014. “Role of the Microbiome in Energy Regulation and Metabolism.” *Gastroenterology*, The Gut Microbiome in Health and Disease, 146 (6): 1525–33. https://doi.org/10.1053/j.gastro.2014.02.008.

Oksanen, Jari, G Simpson, F Blanchet, R Kindt, P Legendre, P Minchin, R O’Hara, et al. 2022. “Vegan: Community Ecology Package.”

O’Malley, Maureen A. 2007. “The Nineteenth Century Roots of ‘Everything Is Everywhere.’” *Nature Reviews Microbiology 2007 5:8* 5 (8): 647–51. https://doi.org/10.1038/nrmicro1711.

O’Toole, Paul W., Julian R. Marchesi, and Colin Hill. 2017. “Next-Generation Probiotics: The Spectrum from Probiotics to Live Biotherapeutics.” *Nature Microbiology* 2 (5): 1–6. https://doi.org/10.1038/nmicrobiol.2017.57.

Palleja, Albert, Kristian H. Mikkelsen, Sofia K. Forslund, Alireza Kashani, Kristine H. Allin, Trine Nielsen, Tue H. Hansen, et al. 2018. “Recovery of Gut Microbiota of Healthy Adults Following Antibiotic Exposure.” *Nature Microbiology* 3 (11): 1255–65. https://doi.org/10.1038/s41564-018-0257-9.

Palmer, Alexander D., and James M. Slauch. 2017. “Mechanisms of Salmonella Pathogenesis in Animal Models.” *Human and Ecological Risk Assessment : HERA* 23 (8): 1877. https://doi.org/10.1080/10807039.2017.1353903.

Palmer, Chana, Elisabeth M. Bik, Daniel B. DiGiulio, David A. Relman, and Patrick O. Brown. 2007. "Development of the Human Infant Intestinal Microbiota." *PLOS Biology* 5 (7): e177. https://doi.org/10.1371/journal.pbio.0050177.

Peterson, Daniel A., Nathan P. McNulty, Janaki L. Guruge, and Jeffrey I. Gordon. 2007. "IgA Response to Symbiotic Bacteria as a Mediator of Gut Homeostasis." *Cell Host and Microbe* 2 (5): 328–39. https://doi.org/10.1016/j.chom.2007.09.013.

Porter, Nathan T., Pablo Canales, Daniel A. Peterson, and Eric C. Martens. 2017. "A Subset of Polysaccharide Capsules in the Human Symbiont Bacteroides Thetaiotaomicron Promote Increased Competitive Fitness in the Mouse Gut." *Cell Host & Microbe* 22 (4): 494-506.e8. https://doi.org/10.1016/J.CHOM.2017.08.020.

Prach, Karel, and Lawrence R. Walker. 2011. "Four Opportunities for Studies of Ecological Succession." *Trends in Ecology & Evolution* 26 (3): 119–23. https://doi.org/10.1016/J.TREE.2010.12.007.

Qin, Junjie, Ruiqiang Li, Jeroen Raes, Manimozhiyan Arumugam, Kristoffer Solvsten Burgdorf, Chaysavanh Manichanh, Trine Nielsen, et al. 2010. "A Human Gut Microbial Gene Catalog Established by Metagenomic Sequencing." *Nature* 464 (7285): 59. https://doi.org/10.1038/NATURE08821.

Raymond, Frédéric, Maxime Déraspe, Maurice Boissinot, Michel G. Bergeron, and Jacques Corbeil. 2016. "Partial Recovery of Microbiomes after Antibiotic Treatment." *Https://Doi.Org/10.1080/19490976.2016.1216747* 7 (5): 428–34. https://doi.org/10.1080/19490976.2016.1216747.

Read, Mark N., and Andrew J. Holmes. 2017. "Towards an Integrative Understanding of Diet–Host–Gut Microbiome Interactions." *Frontiers in Immunology* 8. https://www.frontiersin.org/articles/10.3389/fimmu.2017.00538.

Reese, Aspen T, Eugenia H Cho, Bruce Klitzman, Scott P Nichols, Natalie A Wisniewski, Max M Villa, Heather K Durand, et al. 2018. "Antibiotic-Induced Changes in the Microbiota Disrupt Redox Dynamics in the Gut." Edited by Lora V Hooper. *ELife* 7 (June): e35987. https://doi.org/10.7554/eLife.35987.

Reinisch, Walter. 2017. "Fecal Microbiota Transplantation in Inflammatory Bowel Disease." *Digestive Diseases* 35 (1–2): 123–26. https://doi.org/10.1159/000449092.

Ridlon, Jason M., Dae J. Kang, Phillip B. Hylemon, and Jasmohan S. Bajaj. 2014. "Bile Acids and the Gut Microbiome." *Current Opinion in Gastroenterology* 30 (3): 332–38. https://doi.org/10.1097/MOG.0000000000000057.

Ritchie, Marina L., and Tamara N. Romanuk. 2012. "A Meta-Analysis of Probiotic Efficacy for Gastrointestinal Diseases." Edited by Markus M. Heimesaat. *PLoS ONE* 7 (4): e34938. https://doi.org/10.1371/journal.pone.0034938.

Rivera-Chávez, Fabian, Lillian F. Zhang, Franziska Faber, Christopher A. Lopez, Mariana X. Byndloss, Erin E. Olsan, Gege Xu, et al. 2016. "Depletion of Butyrate-Producing Clostridia from the Gut Microbiota Drives an Aerobic Luminal Expansion of Salmonella." *Cell Host and Microbe* 19 (4): 443–54. https://doi.org/10.1016/j.chom.2016.03.004.

Robinson, James T., Helga Thorvaldsdóttir, Wendy Winckler, Mitchell Guttman, Eric S. Lander, Gad Getz, and Jill P. Mesirov. 2011. "Integrative Genomics Viewer." *Nature Biotechnology* 29 (1): 24. https://doi.org/10.1038/NBT.1754.

Roodgar, Morteza, Benjamin H. Good, Nandita R. Garud, Stephen Martis, Mohan Avula, Wenyu Zhou, Samuel M. Lancaster, et al. 2021. "Longitudinal Linked-Read Sequencing Reveals Ecological and Evolutionary Responses of a Human Gut Microbiome during Antibiotic Treatment." *Genome Research* 31 (8): 1433–46. https://doi.org/10.1101/gr.265058.120.

Santos, Renato L., Shuping Zhang, Renée M. Tsolis, Robert A. Kingsley, L. Garry Adams, and Andreas J. Bäumler. 2001. "Animal Models of Salmonella Infections: Enteritis versus Typhoid Fever." *Microbes and Infection* 3 (14): 1335–44. https://doi.org/10.1016/S1286-4579(01)01495-2.

Schlomann, Brandon H, and Raghuveer Parthasarathy. 2019. "Timescales of Gut Microbiome Dynamics." *Current Opinion in Microbiology*, Microbiota, 50 (August): 56–63. https://doi.org/10.1016/j.mib.2019.09.011.

Schofield, Whitman B., Maria Zimmermann-Kogadeeva, Michael Zimmermann, Natasha A. Barry, and Andrew L. Goodman. 2018. "The Stringent Response Determines the Ability of a Commensal Bacterium to Survive Starvation and to Persist in the Gut." *Cell Host & Microbe* 24 (1): 120-132.e6. https://doi.org/10.1016/J.CHOM.2018.06.002.

Sergushichev, Alexey A. 2016. "An Algorithm for Fast Preranked Gene Set Enrichment Analysis Using Cumulative Statistic Calculation." bioRxiv. https://doi.org/10.1101/060012.

Shaw, Liam P., Hassan Bassam, Chris P. Barnes, A. Sarah Walker, Nigel Klein, and Francois Balloux. 2019. "Modelling Microbiome Recovery after Antibiotics Using a Stability Landscape Framework." *The ISME Journal* 13 (7): 1845–56. https://doi.org/10.1038/s41396-019-0392-1.

Shepherd, Elizabeth Stanley, William C. Deloache, Kali M. Pruss, Weston R. Whitaker, and Justin L. Sonnenburg. 2018. "An Exclusive Metabolic Niche Enables Strain Engraftment in the Gut Microbiota." *Nature* 557 (7705): 434–38. https://doi.org/10.1038/s41586-018-0092-4.

Shreiner, Andrew B., John Y. Kao, and Vincent B. Young. 2015. "The Gut Microbiome in Health and in Disease." *Current Opinion in Gastroenterology* 31 (1): 69–75. https://doi.org/10.1097/MOG.0000000000000139.

Siguier, Patricia, Jonathan Filée, and Michael Chandler. 2006. "Insertion Sequences in Prokaryotic Genomes." *Current Opinion in Microbiology*, Antimicrobials/Genomics, 9 (5): 526–31. https://doi.org/10.1016/j.mib.2006.08.005.

Sonnenburg, Erica D., Samuel A. Smits, Mikhail Tikhonov, Steven K. Higginbottom, Ned S. Wingreen, and Justin L. Sonnenburg. 2016. "Diet-Induced Extinction in the Gut Microbiota Compounds over Generations." *Nature* 529 (7585): 212–15. https://doi.org/10.1038/nature16504.

Sonnenburg, Erica D., and Justin L. Sonnenburg. 2014. "Starving Our Microbial Self: The Deleterious Consequences of a Diet Deficient in Microbiota-Accessible Carbohydrates." *Cell Metabolism* 20 (5): 779–86. https://doi.org/10.1016/j.cmet.2014.07.003.

Sonnenburg, Justin L., Christina T. L. Chen, and Jeffrey I. Gordon. 2006. "Genomic and Metabolic Studies of the Impact of Probiotics on a Model Gut Symbiont and Host." *PLOS Biology* 4 (12): e413. https://doi.org/10.1371/journal.pbio.0040413.

Sonnenburg, Justin L., Jian Xu, Douglas D. Leip, Chien Huan Chen, Benjamin P. Westover, Jeremy Weatherford, Jeremy D. Buhler, and Jeffrey I. Gordon. 2005. "Glycan Foraging in Vivo by an Intestine-Adapted Bacterial Symbiont." *Science (New York, N.Y.)* 307 (5717): 1955–59. https://doi.org/10.1126/SCIENCE.1109051.

Springael, Dirk, and Eva M. Top. 2004. "Horizontal Gene Transfer and Microbial Adaptation to Xenobiotics: New Types of Mobile Genetic Elements and Lessons from Ecological Studies." *Trends in Microbiology* 12 (2): 53–58. https://doi.org/10.1016/j.tim.2003.12.010.

Stewart, Christopher J., Nadim J. Ajami, Jacqueline L. O'Brien, Diane S. Hutchinson, Daniel P. Smith, Matthew C. Wong, Matthew C. Ross, et al. 2018. "Temporal Development of the Gut Microbiome in Early Childhood from the TEDDY Study." *Nature* 562 (7728): 583–88. https://doi.org/10.1038/s41586-018-0617-x.

Suez, Jotham, and Eran Elinav. 2017. "The Path towards Microbiome-Based Metabolite Treatment." *Nature Microbiology* 2 (6): 1–5. https://doi.org/10.1038/nmicrobiol.2017.75.

Tanes, Ceylan, Kyle Bittinger, Yuan Gao, Elliot S. Friedman, Lisa Nessel, Unmesha Roy Paladhi, Lillian Chau, et al. 2021. "Role of Dietary Fiber in the Recovery of the Human Gut Microbiome and Its Metabolome." *Cell Host & Microbe* 29 (3): 394-407.e5. https://doi.org/10.1016/j.chom.2020.12.012.

Tatusov, Roman L., Natalie D. Fedorova, John D. Jackson, Aviva R. Jacobs, Boris Kiryutin, Eugene V. Koonin, Dmitri M. Krylov, et al. 2003. "The COG Database: An Updated Version Includes Eukaryotes." *BMC Bioinformatics* 4 (September). https://doi.org/10.1186/1471-2105-4-41.

Taur, Ying, Katharine Coyte, Jonas Schluter, Elizabeth Robilotti, Cesar Figueroa, Mergim Gjonbalaj, Eric R. Littmann, et al. 2018. "Reconstitution of the Gut Microbiota of Antibiotic-Treated Patients by Autologous Fecal Microbiota Transplant." *Science Translational Medicine* 10 (460): eaap9489. https://doi.org/10.1126/scitranslmed.aap9489.

Tempel, Sebastien, Justin Bedo, and Emmanuel Talla. 2022. "From a Large-Scale Genomic Analysis of Insertion Sequences to Insights into Their Regulatory Roles in Prokaryotes." *BMC Genomics* 23 (1): 451. https://doi.org/10.1186/s12864-022-08678-3.

Thaiss, Christoph A., and Eran Elinav. 2017. "The Remedy within: Will the Microbiome Fulfill Its Therapeutic Promise?" *Journal of Molecular Medicine* 95 (10): 1021–27. https://doi.org/10.1007/s00109-017-1563-z.

The Jackson Laboratory. 2017. "When Are Mice Considered Old?" The Jackson Laboratory. 2017. https://www.jax.org/news-and-insights/jax-blog/2017/November/when-are-mice-considered-old.

Townsend, Guy E., Weiwei Han, Nathan D. Schwalm, Xinyu Hong, Natasha A. Bencivenga-Barry, Andrew L. Goodman, and Eduardo A. Groisman. 2020. "A Master Regulator of Bacteroides Thetaiotaomicron Gut Colonization Controls Carbohydrate Utilization and an Alternative Protein Synthesis Factor." *MBio* 11 (1). https://doi.org/10.1128/MBIO.03221-19.

Trigodet, Florian, Karen Lolans, Emily Fogarty, Alon Shaiber, Hilary G. Morrison, Luis Barreiro, Bana Jabri, and A. Murat Eren. 2022. "High Molecular Weight DNA Extraction Strategies for Long-Read Sequencing of Complex Metagenomes." *Molecular Ecology Resources*. https://doi.org/10.1111/1755-0998.13588.

Tropini, Carolina, Eli Lin Moss, Bryan Douglas Merrill, Katharine Michelle Ng, Steven Kyle Higginbottom, Ellen Pun Casavant, Carlos Gutierrez Gonzalez, et al. 2018. "Transient Osmotic Perturbation Causes Long-Term Alteration to the Gut Microbiota." *Cell* 173 (7): 1742-1754.e17. https://doi.org/10.1016/j.cell.2018.05.008.

Turnbaugh, Peter J., Fredrik Bäckhed, Lucinda Fulton, and Jeffrey I. Gordon. 2008. "Diet-Induced Obesity Is Linked to Marked but Reversible Alterations in the Mouse Distal Gut Microbiome." *Cell Host and Microbe* 3 (4): 213–23. https://doi.org/10.1016/j.chom.2008.02.015.

Turnbaugh, Peter J., Ruth E. Ley, Michael A. Mahowald, Vincent Magrini, Elaine R. Mardis, and Jeffrey I. Gordon. 2006. "An Obesity-Associated Gut Microbiome with Increased Capacity for Energy Harvest." *Nature* 444 (7122): 1027–1131. https://doi.org/10.1038/nature05414.

Van Herreweghen, Florence, Kim De Paepe, Hugo Roume, Frederiek-Maarten Kerckhof, and Tom Van de Wiele. 2018. "Mucin Degradation Niche as a Driver of Microbiome Composition and Akkermansia Muciniphila Abundance in a Dynamic Gut Model Is Donor Independent." *FEMS Microbiology Ecology* 94 (12): fiy186. https://doi.org/10.1093/femsec/fiy186.

Vandecraen, Joachim, Michael Chandler, Abram Aertsen, and Rob Van Houdt. 2017. "The Impact of Insertion Sequences on Bacterial Genome Plasticity and Adaptability." *Critical Reviews in Microbiology* 43 (6): 709–30. https://doi.org/10.1080/1040841X.2017.1303661.

Varel, Vincent H., and Marvin P. Bryant. 1974. "Nutritional Features of Bacteroides Fragilis Subsp. Fragilis." *Applied Microbiology* 28 (2): 251–57.

Vasquez, Kimberly S., Lisa Willis, Nate J. Cira, Katharine M. Ng, Miguel F. Pedro, Andrés Aranda-Díaz, Manohary Rajendram, et al. 2021. "Quantifying Rapid Bacterial Evolution and Transmission within the Mouse Intestine." *Cell Host & Microbe* 29 (9): 1454-1468.e4. https://doi.org/10.1016/j.chom.2021.08.003.

Veseli, Iva, Yiqun T. Chen, Matthew S. Schechter, Chiara Vanni, Emily C. Fogarty, Andrea R. Watson, Bana Jabri, et al. 2023. "Microbes with Higher Metabolic Independence Are Enriched in Human Gut Microbiomes under Stress." bioRxiv. https://doi.org/10.1101/2023.05.10.540289.

Vieira, Marcos Costa, and Mário Almeida-Neto. 2015. "A Simple Stochastic Model for Complex Coextinctions in Mutualistic Networks: Robustness Decreases with Connectance." *Ecology Letters* 18 (2): 144–52. https://doi.org/10.1111/ele.12394.

Walker, Bruce J., Thomas Abeel, Terrance Shea, Margaret Priest, Amr Abouelliel, Sharadha Sakthikumar, Christina A. Cuomo, et al. 2014. "Pilon: An Integrated Tool for Comprehensive Microbial Variant Detection and Genome Assembly Improvement." *PLOS ONE* 9 (11): e112963. https://doi.org/10.1371/JOURNAL.PONE.0112963.

Walter, Jens, María X Maldonado-Gómez, and Inés Martínez. 2018. "To Engraft or Not to Engraft: An Ecological Framework for Gut Microbiome Modulation with Live Microbes." *Current Opinion in Biotechnology* 49 (February): 129–39. https://doi.org/10.1016/J.COPBIO.2017.08.008.

Wang, Jin, Pan Wang, Xinghe Wang, Yingdong Zheng, and Yonghong Xiao. 2014. "Use and Prescription of Antibiotics in Primary Health Care Settings in China." *JAMA Internal Medicine* 174 (12): 1914–20. https://doi.org/10.1001/jamainternmed.2014.5214.

Wang, Qing, Kaicen Wang, Wenrui Wu, Eleni Giannoulatou, Joshua W. K. Ho, and Lanjuan Li. 2019. "Host and Microbiome Multi-Omics Integration: Applications and Methodologies." *Biophysical Reviews* 11 (1): 55–65. https://doi.org/10.1007/s12551-018-0491-7.

Watson, Andrea R., Jessika Füssel, Iva Veseli, Johanna Zaal DeLongchamp, Marisela Silva, Florian Trigodet, Karen Lolans, et al. 2022. "Metabolic Independence Drives Gut Microbial Colonization and Resilience in Health and Disease." bioRxiv. https://doi.org/10.1101/2021.03.02.433653.

———. 2023. "Metabolic Independence Drives Gut Microbial Colonization and Resilience in Health and Disease." *Genome Biology* 24 (1): 78. https://doi.org/10.1186/s13059-023-02924-x.

Wetmore, Kelly M., Morgan N. Price, Robert J. Waters, Jacob S. Lamson, Jennifer He, Cindi A. Hoover, Matthew J. Blow, et al. 2015. "Rapid Quantification of Mutant Fitness in Diverse Bacteria by Sequencing Randomly Bar-Coded Transposons." *MBio* 6 (3): e00306-15. https://doi.org/10.1128/MBIO.00306-15.

Wexler, Aaron G., and Andrew L. Goodman. 2017. "An Insider's Perspective: Bacteroides as a Window into the Microbiome." *Nature Microbiology* 2 (April). https://doi.org/10.1038/nmicrobiol.2017.26.

Wickham, Hadley, Mara Averick, Jennifer Bryan, Winston Chang, Lucy D'Agostino McGowan, Romain François, Garrett Grolemund, et al. 2019. "Welcome to the Tidyverse." *Journal of Open Source Software* 4 (43): 1686. https://doi.org/10.21105/joss.01686.

Wilson, Brooke C., Tommi Vatanen, Wayne S. Cutfield, and Justin M. O'Sullivan. 2019. "The Super-Donor Phenomenon in Fecal Microbiota Transplantation." *Frontiers in Cellular and Infection Microbiology* 9 (JAN): 2. https://doi.org/10.3389/fcimb.2019.00002.

Winter, Sebastian E., Parameth Thiennimitr, Maria G. Winter, Brian P. Butler, Douglas L. Huseby, Robert W. Crawford, Joseph M. Russell, et al. 2010. "Gut Inflammation Provides

a Respiratory Electron Acceptor for Salmonella." *Nature* 467 (7314): 426–29. https://doi.org/10.1038/nature09415.

Wong, Andrea C., and Maayan Levy. 2019. "New Approaches to Microbiome-Based Therapies." *MSystems* 4 (3): 10.1128/msystems.00122-19. https://doi.org/10.1128/msystems.00122-19.

Wotzka, Sandra Y., Markus Kreuzer, Lisa Maier, Markus Arnoldini, Bidong D. Nguyen, Alexander O. Brachmann, Dorothée L. Berthold, et al. 2019. "Escherichia Coli Limits Salmonella Typhimurium Infections after Diet Shifts and Fat-Mediated Microbiota Perturbation in Mice." *Nature Microbiology* 4 (12): 2164–74. https://doi.org/10.1038/s41564-019-0568-5.

Wu, Meng, Nathan P. McNulty, Dmitry A. Rodionov, Matvei S. Khoroshkin, Nicholas W. Griffin, Jiye Cheng, Phil Latreille, et al. 2015. "Genetic Determinants of in Vivo Fitness and Diet Responsiveness in Multiple Human Gut Bacteroides." *Science* 350 (6256). https://doi.org/10.1126/SCIENCE.AAC5992.

Xiao, Yandong, Marco Tulio Angulo, Songyang Lao, Scott T. Weiss, and Yang-Yu Liu. 2020. "An Ecological Framework to Understand the Efficacy of Fecal Microbiota Transplantation." *Nature Communications* 11 (1): 3329. https://doi.org/10.1038/s41467-020-17180-x.

Zaura, Egija, Bernd W. Brandt, M. Joost Teixeira de Mattos, Mark J. Buijs, Martien P.M. Caspers, Mamun Ur Rashid, Andrej Weintraub, et al. 2015. "Same Exposure but Two Radically Different Responses to Antibiotics: Resilience of the Salivary Microbiome versus Long-Term Microbial Shifts in Feces." *MBio* 6 (6). https://doi.org/10.1128/mBio.01693-15.

Zhang, Han, Tanner Yohe, Le Huang, Sarah Entwistle, Peizhi Wu, Zhenglu Yang, Peter K. Busk, Ying Xu, and Yanbin Yin. 2018. "DbCAN2: A Meta Server for Automated Carbohydrate-Active Enzyme Annotation." *Nucleic Acids Research* 46 (W1): W95–101. https://doi.org/10.1093/nar/gky418.

Zhang, Manjing, Megan Kennedy, Orlando DeLeon, Jacie Bissell, Florian Trigodet, Karen Lolans, Sara Temelkova, et al. 2022. "Dynamic Genetic Adaptation of Bacteroides Thetaiotaomicron Murine Gut Colonization." bioRxiv. https://doi.org/10.1101/2022.02.23.481734.

Zhao, Chunhua, Hongjun Dong, Yanping Zhang, and Yin Li. 2019. "Discovery of Potential Genes Contributing to the Biosynthesis of Short-Chain Fatty Acids and Lactate in Gut Microbiota from Systematic Investigation in E. Coli." *Npj Biofilms and Microbiomes* 5 (1): 1–8. https://doi.org/10.1038/s41522-019-0092-7.

Zhao, Shijie, Tami D. Lieberman, Mathilde Poyet, Kathryn M. Kauffman, Sean M. Gibbons, Mathieu Groussin, Ramnik J. Xavier, and Eric J. Alm. 2019. "Adaptive Evolution within Gut Microbiomes of Healthy People." *Cell Host and Microbe* 25 (5): 656-667.e8. https://doi.org/10.1016/j.chom.2019.03.007.

Zmora, Niv, Gili Zilberman-Schapira, Jotham Suez, Uria Mor, Mally Dori-Bachash, Stavros Bashiardes, Eran Kotler, et al. 2018. "Personalized Gut Mucosal Colonization Resistance

to Empiric Probiotics Is Associated with Unique Host and Microbiome Features." *Cell* 174 (6): 1388-1405.e21. https://doi.org/10.1016/j.cell.2018.08.041.